1. Report No.	2. Government Accession No.	3. Recipient's Catalog No.
SWUTC/13/600451-00003-2		

4. Title and Subtitle	5. Report Date
COMPENDIUM OF STUDENT PAPERS: 2013 UNDERGRADUATE TRANSPORTATION SCHOLARS PROGRAM	November 2013
	6. Performing Organization Code
7. Author(s)	8. Performing Organization Report No.
Daniel Bartilson, Adrian Contreras, Kevin Mackan, Mark Membreño, and Parker C. Moore, Authors, and H. Gene Hawkins, Editor	Report 600451-00003-2
9. Performing Organization Name and Address	10. Work Unit No. (TRAIS)
Texas A&M Transportation Institute Texas A&M University System College Station, Texas 77843-3135	11. Contract or Grant No. DTRT12-G-UTC06
12. Sponsoring Agency Name and Address	13. Type of Report and Period Covered
Southwest Region University Transportation Center Texas A&M Transportation Institute Texas A&M University System College Station, Texas 77843-3135	14. Sponsoring Agency Code

15. Supplementary Notes

Program Director: H. Gene Hawkins, Ph.D., P.E.

Participating Students: Daniel Bartilson, Adrian Contreras, Kevin Mackan, Mark Membreño, and Parker C. Moore. Supported by a grant from the U.S. Department of Transportation, University Transportation Centers Program.

16. Abstract

This report is a compilation of research papers written by students participating in the 2013 Undergraduate Transportation Scholars Program. The 10-week summer program, now in its 23nd year, provides undergraduate students in Civil Engineering the opportunity to learn about transportation engineering through participating in sponsored transportation research projects. The program design allows students to interact directly with a Texas A&M University faculty member or Texas Transportation Institute researcher in developing a research proposal, conducting valid research, and documenting the research results through oral presentations and research papers.

The papers in this compendium report on the following topics: 1) Validation of Computer Vision for Structural Vibration Studies; 2) Evaluating Driver Response to Prototype Traffic Control Devices at Access Points; 3) Evaluation of Apparent Capacities through Freeway Lane Closures; 4) Operational Effects of Chevrons on Horizontal Curves Using Speed and Energy Differentials and Speed Profiles; and 5) Preliminary Development of a Trip Generation Manual for Texas.

17. Key Words	18. Distribution Statement
Structural Vibration, Traffic Signal Structure, Access Management, Traffic Control Devices, Work Zone Traffic Control, Highway Capacity, Traffic Signs, Roadway Geometry, Trip Generation	No restrictions. This document is available to the public through NTIS: National Technical Information Service 5285 Port Royal Road Alexandria, Virginia 22312

19. Security Classif.(of this report)	20. Security Classif.(of this page)	21. No. of Pages	22. Price
Unclassified	Unclassified	137	

COMPENDIUM OF STUDENT PAPERS:
2013 UNDERGRADUATE
TRANSPORTATION SCHOLARS PROGRAM

Back Row (left to right): Dr. H. Gene Hawkins (Program Director), Dr. Benjamin Sperry (Mentor), Mr. Bradford K. Brimley (Mentor), Ms. Melisa Finley (Mentor), Mr. Kyle Weighaus, Dr. Gerald Ullman (Mentor) and Dr. Stephan Hurlebaus (Mentor)
Front Row Students (left to right): Parker C. Moore, Mark Membreño, Adrian Contreras, Kevin Mackan, and Daniel Bartilson

Program Sponsored by

Transportation Scholars Program
Southwest Region University Transportation Center
Texas A&M Transportation Institute
Texas A&M University System
College Station, TX 77843-3135

and the

Zachry Department of Civil Engineering
Texas A&M University
College Station, Texas 77843-3136

November 2013

PREFACE

The Southwest Region University Transportation Center (SWUTC), through the Transportation Scholars Program, the Texas A&M Transportation Institute (TTI) and the Zachry Department of Civil Engineering at Texas A&M University, established the Undergraduate Transportation Engineering Fellows Program in 1990. The program design allows students to interact directly with a Texas A&M University faculty member or TTI researcher in developing a research proposal, conducting valid research, and documenting the research results through oral presentations and research papers. The intent of the program is to introduce transportation engineering to students who have demonstrated outstanding academic performance, thus developing capable and qualified future transportation leaders.

In the summer of 2013, the following students and their faculty/staff mentors were:

STUDENTS	**MENTORS**
Daniel Bartilson Texas A&M University, TX	Dr. Stefan Hurlebaus
Adrian Contreras Texas A&M University, TX	Ms. Melisa Finley
Kevin Mackan Texas A&M University, TX	Dr. Gerald Ullman
Mark Membreño Texas A&M University, TX	Mr. Bradford K. Brimley
Parker C. Moore Georgia Southern University	Dr. Benjamin R. Sperry

Sincere appreciation is extended to the following individuals:

- Mrs. Cathy Bryan, who assisted with program administrative matters and Mrs. Barbara Lorenz in the preparation of the final compendium.

The authors recognize that support was provided by a grant from the U. S. Department of Transportation, University Transportation Centers Program to the Southwest Region University Transportation Center.

CONTENTS

DISCLAIMER

The contents of this report reflect the view of the authors, who are responsible for the facts and the accuracy of the information presented herein. This document is disseminated under the sponsorship of the Department of Transportation, University Transportation Centers Program in the interest of information exchange. The U.S. Government assumes no liability for the contents or use thereof.

Validation of Computer Vision for Structural Vibration Studies

Prepared for
Undergraduate Transportation Scholars Program

By

Daniel Bartilson
Junior Civil Engineering Major
Texas A&M University

Professional Mentors:
Dr. Stefan Hurlebaus
Associate Professor, Zachry Department of Civil Engineering
Associate Research Engineer, Texas A&M Transportation Institute
Texas A&M University

Kyle Wieghaus
Ph.D. Candidate, Texas A&M Transportation Institute
Texas A&M University

Program Director
H. Gene Hawkins, Jr., Ph.D., P.E.
Associate Professor, Zachry Department of Civil Engineering
Research Engineer, Texas A&M Transportation Institute
Texas A&M University

Program Sponsored by:
Southwest Region University Transportation Center

August 9, 2013

STUDENT BIOGRAPHY

Daniel Bartilson is a junior at Texas A&M University in the Zachry Department of Civil Engineering. He intends to graduate with a Bachelor of Science in civil engineering with a structural engineering emphasis during August of 2014.

Daniel has been involved with the American Society of Civil Engineers student chapter and the National Student Steel Bridge competition since his freshman year, the latter providing significant experience with the finite element analysis software utilized during his research. Following graduation, he will pursue graduate education in civil or mechanical engineering with the intent of gaining a Ph.D. His research interests lie in computational mechanics and computer modeling.

ACKNOWLEDGMENT

The author wishes to express gratitude towards Texas A&M Transportation Institute (TTI) for funding the following research. The research activities were conducted in support of the Undergraduate Transportation Scholars Program. The findings and recommendations included in this paper are based on the student's summer activities. They should be considered preliminary and not as representative of the findings and recommendations of any parent project. This paper has not been reviewed or approved by the sponsor. The contents of this paper reflect the views of the author, who is responsible for the facts and the accuracy of these data presented herein. The contents do not necessarily reflect the official view or policies of TTI.

Furthermore, the author expresses appreciation for the efforts, time, and knowledge put forth to the success of this research by the author's mentors, Dr. Stefan Hurlebaus and Kyle Wieghaus.

SUMMARY

The presented computer vision method allows for non-contact, target-less determination of structural displacement and modal parameters, including mode shapes. By using an uncalibrated analytical model to relate structural displacement to structural stress, it is shown possible to utilize a rapid set-up and take-down computer vision-based approach to infer structural stresses to a high degree of precision. Using this computer vision method, it is shown possible to determine natural frequencies of the structure with accuracy similar to strain gage and accelerometer instrumentation. Even with structural displacements corresponding to smaller than 1 pixel, excellent mode shape results are obtained. Finally, one-minute stress ranges from ambient wind excitation are found to have high agreement between the inferred stress from strain gage data and stresses calculated from computer vision tied to an analytical stress model. This demonstrates the ability of this method to develop fatigue life estimates using wind velocity data and modest technical means.

This approach provides a method for using low-cost, low-complexity equipment to determine dynamic characteristics and response of a flexible structure undergoing excitation. When coupled with a simple, uncalibrated analytical model, structural stresses may also be inferred accurately.

TABLE OF CONTENTS

LIST OF FIGURES

LIST OF TABLES

INTRODUCTION

Structural vibrations from live loads and environmental loads constitute a mechanism for fatigue failure due to cyclic stresses developed within the vibrating structure. Modal analysis of a structure is used to determine the natural frequencies of the vibrations of the structure, along with the mode shape and damping ratio associated with motion of the structure at each natural frequency. For example, modal analysis may reveal that a structure will exhibit a natural frequency which closely matches that of an excitation mechanism, such as wind. It may then be possible to engineer the structure to eliminate a harmonic response at this frequency or to utilize knowledge of the mode shape to apply reinforcement to points of the structure which exhibit the greatest potential for failure. Alternatively, modal analysis can be utilized to detect structural impairment via determination of changes in dynamic characteristics of a structure for an efficient estimate of remaining lifetime (*1*).

The natural frequency and mode shapes of a built structure may vary from the theoretical finite element results, leading to updates to the model, and possibly to the built structure. In general, experimental modal analysis utilized to validate the outputs of finite element modal analysis involves large, complex arrays of instrumentation placed on the structure under artificial excitation (*2*). Similarly, methods used to determine stress time series generally involve arrays of strain gauges or linear displacement sensors coupled with an analytical stress model. These technologies represent high-quality options for analysis, but costs and difficulty associated with procurement and installation may make these technologies infeasible for broad application.

In order to realize these benefits without the difficulty associated with application of instrumentation to structures, it may be possible to externally infer dynamic characteristics and stress time series of built structures using a robust computer vision-based technique applied to digital video records of structures under natural or artificial excitation.

BACKGROUND INFORMATION

The following sections provide supporting descriptions of the previous research and pertinent concepts.

Computer Vision, Video Analytics, and Videogrammetry

Video analytics, or video content analysis, refers to any automated "extraction of meaningful information from digital video" which is based upon research into artificial intelligence and pattern recognition, and is thus a subset of computer vision (*3*). While motion detection techniques are often used in combination with computer vision, computer vision attempts to quantify the spatial movement of entities in the recording, while the motion detection simply reports a difference in sequential inputs (3). The applications of computer vision extend from surveillance to transportation to fluid mechanics research, with further applications being realized by the proliferation of low-cost, high-quality video recording devices.

Videogrammetry is based on sequential application of photogrammetry, which is the determination of geometric properties of objects captured within images. Videogrammetry is

closely tied to computer vision, but where videogrammetry attempts to quantify real dimensions from captured images, computer vision involves automated pattern recognition. Videogrammetry can be utilized alongside computer vision methods to determine displacement time series of captured structural points.

Combining computer vision-based techniques and videogrammetry is attractive where the application displacement sensors may alter the dynamic properties of the system, such as small-scale models, or where application would be difficult, such as high-deck bridges. As well, a computer vision-based approach may offer significantly more points of analysis because each pixel can be considered a discrete point of analysis (*4*).

Previous Research

A previous study using computer vision methods performed real-time and offline analysis of dynamic characteristics of bridges. The study utilized a sophisticated image capture device and required the application of specialized targets to the structure (*5*). While this provided a strong proof-of-concept, the non-contact benefits of computer vision techniques were negated by the requirement of specialized targets.

Target-less analysis of bridge dynamic responses using consumer-grade video capture equipment has been reported, but relied on the presence and recognition of a unique pattern or geometry on the tested bridge. This approach utilized edge detection and pattern matching algorithms in combination, initially on specialized targets, but noted that without a target, measurement reliability is strongly influenced by the contrast of the bridge geometry (*6*). As well, by utilization of an edge detection algorithm, researchers have been able to analyze damage in structures by determination of mode shapes from computer vision-based studies (4*)*. However, edge detection algorithms are less robust than pattern recognition algorithms (*6*). Previous application of videogrammetry to wind turbines has resulted in effective determination of mode shapes, but required specialized cameras, lights, targets, and software (*7*).

In order to generalize this method for wider application, it is necessary to develop a method which does not depend on the presence of specialized targets or geometry. Through utilization of a robust pattern recognition tool, the application of computer vision-based techniques and videogrammetry will not be limited to analysis of structural displacement in areas amenable to the attachment of specialized targets. The minimum quadratic difference algorithm, which was originally developed for particle image velocimetry of fluid flows, presents a robust method of analysis of structural motion for the determination of dynamic responses.

Particle Image Velocimetry

Particle image velocimetry (PIV) is an approach for the study of fluid motion which utilizes analysis of consecutive images captured of a flow containing illuminated particles. A sample flow visualization analyzed by the MPIV toolbox developed by N. Mori and K. A. Chang is depicted in Figure 1a (*8*). Images are captured with a digital camera by a charge-coupled device (CCD) which converts photon intensity received at each photosensitive bin within the device to a value in the image matrix representing light intensities at each pixel in the image. For the

simplest case of a grey image, the image matrix is composed of a single value which ranges between white and black for each pixel. The images are captured with a known time between images, which allows for the computation of velocities if particle or pattern displacements are discerned. To this end, computers are used to extract displacement information by some form of comparison between one sub-window of the initial image and multiple sub-windows of the succeeding image (Figure 1b) to determine the highest correlation between points or patterns found during each comparison. The displacement is then determined between the sub-window of the initial image and the most highly correlated sub-window of the succeeding image based on grey value distributions in the image matrix or a similar method.

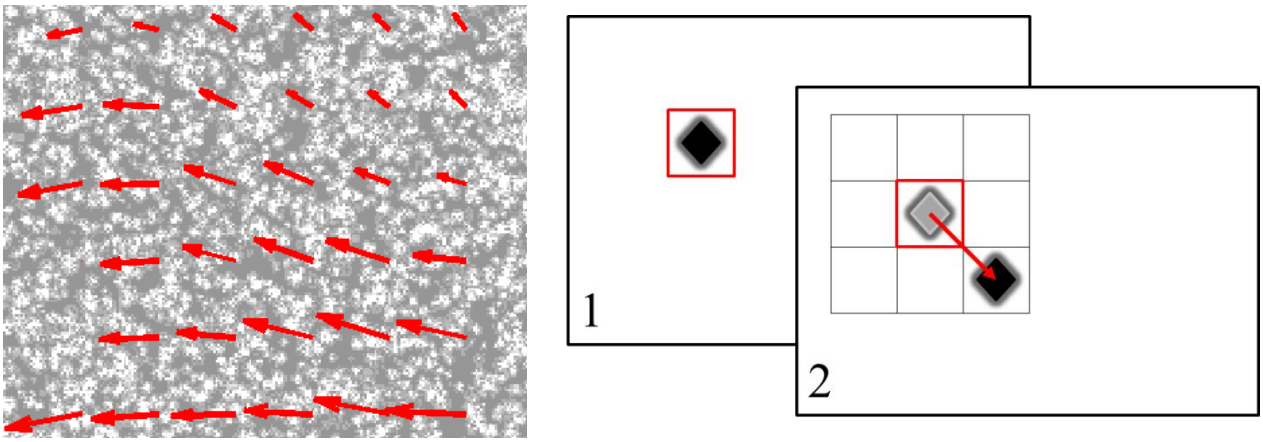

(a) (b)

Figure 1. Examples of (a) flow analysis and (b) image correlation.

The Minimum Quadratic Difference Algorithm

One such algorithm which computes displacements for PIV based on least-square determination of pattern movements is the minimum quadratic difference (MQD) algorithm (*9*).

$$D(m,n) = \frac{1}{M \cdot N} \sum_{i=0}^{M-1} \sum_{j=0}^{N-1} \left[g_1(i,j) - g_2(i+m, j+n) \right]^2 \qquad (1)$$

The MQD algorithm seeks to find the displaced sub-window, $g_2(i+m, j+n)$, which yields the minimum sum of the squared gray value difference, D, relative to the initial image sub-window, $g_1(i, j)$. This algorithm has been shown to lead to root mean square error values less than 0.05 pixel for displacements less than one pixel between images (*8*). The algorithm is thus said to have sub-pixel accuracy (*9*). The MQD algorithm allows for applications that extend beyond fluid motion analysis due to the ability of the algorithm to analyze pattern movement. However, the robustness and accuracy of the MQD algorithm come at the cost of significantly greater computation time than the mainstay cross-correlation algorithm, which has been utilized in other computer vision-based structural vibration studies (*10*, *11*).

Traffic Signal Structures

Due to the long history of research into the dynamic responses of traffic signal structures excited under ambient wind conditions, traffic signal structures are excellent systems for determining the accuracy and applicability of MQD-based computer vision to structures. Traffic signals are generally supported by a vertical pole and horizontal mast arm which jointly constitute a cantilevered traffic signal structure (TSS). The vibrations of these structures are categorized as in-plane (IP) for vertical vibrations (Figure 2) and out-of-plane (OOP) for all other motion, but this essentially means the direction parallel to cars passing under.

Figure 2. In-plane traffic signal structure motion.

PROGRAM DEVELOPMENT

Initially, the MQD algorithm was tested against the more common cross-correlation algorithm to determine inherent benefits and drawbacks associated with utilization of the MQD algorithm. Both algorithms were applied using modified code from the MPIV toolbox (8).

Experimental Setup

A set of 720×480 pixel computer-generated images were created to model displacement between two video frames under analysis. Figure 3a provides the initial image for analysis, and Figure 3b provides the succeeding image for analysis. The images have five rows of eight dots each 20 pixels in diameter. The analysis sub-window size was chosen as 16×16 pixels to ensure accuracy. Each dot was displaced a known magnitude and direction.

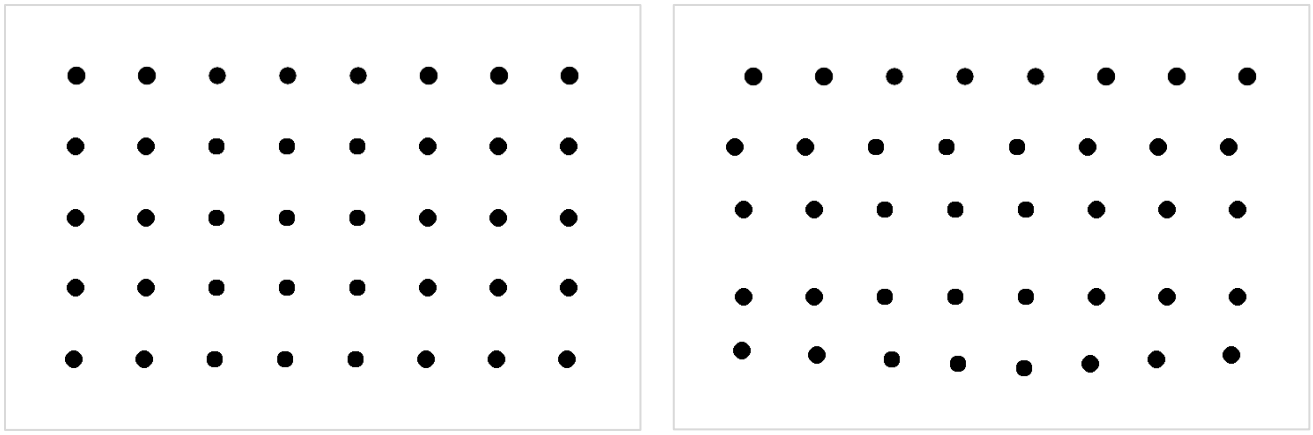

(a) (b)

Figure 3. Computer-generated (a) initial image and (b) succeeding image.

Results and Discussion

The cross-correlation algorithm yielded no results from the displacements shown in Figure 3. This is speculatively due to the nature of the algorithm, which operates by finding the peak value from element-wise multiplication the sub-window matrices from the initial and succeeding images. Due to image matrices representing white as a high value, the peak will be found when particles are lighter than the background. In this instance, the 'moving particle' was darker than the background, leaving the cross-correlation unable to find a valid peak, and thereby displacement. The failure of the cross-correlation algorithm to produce results in this simple analysis led to its exclusion from further testing. The MQD algorithm produced the valid displacement vectors depicted in Figure 4.

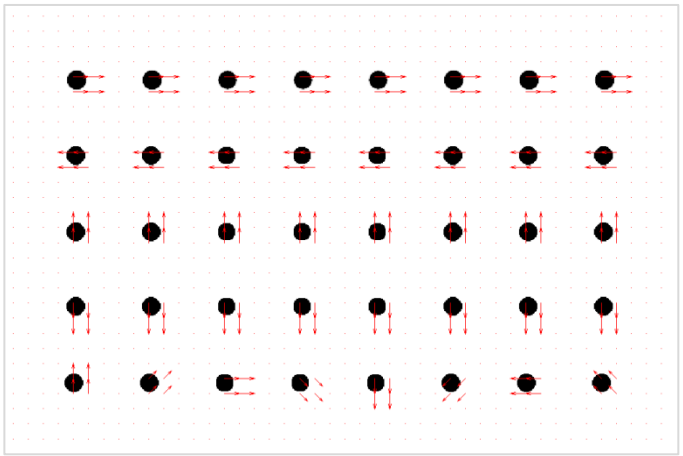

Figure 4. Computer-generated image results from minimum quadratic difference algorithm.

The root mean square errors (RMSE) of the displacement vectors were calculated using Equation (2), where $\hat{x}$ represents the mean of the measurement set, but for this application, $\hat{x}$ represents the known displacement.

$$RMSE = \sqrt{\frac{1}{n}\sum_{i=1}^{n}\left(\hat{x} - x_i\right)^2} \quad (2)$$

Table 1 displays the RMSE of the displacements organized by row. It is noticeable that the first row yielded the same RMSE in both the *X* and *Y* directions, though the *Y* displacement was known to be zero. It was considered likely that the variance in the RMSE according to direction of analysis for each row was a peculiarity of the location of the centers of sub-windows with reference to the locations of the dots in the initial image. In general, an RMS error of less than 0.005 pixels should be expected for displacements greater than 2 pixels measured by the MQD algorithm based on the results shown in Table 1 and the work of Gui and Merzkirch (9).

Table 1. Root Mean Square Error (RMSE) From Dot Grid Analysis

	RMSE of Displacements (pixel)	
Row	***X***	***Y***
1	0.0009	0.0009
2	0.0033	0.0042
3	0.0029	0.0000
4	0.0033	0.0042
5	0.0067	0.0000
All	0.0039	0.0027

FULL-SCALE EXPERIMENTAL VALIDATION ON TRAFFIC SIGNAL STRUCTURE

For authentication of the MQD-based computer vision as a method for determination of displacements and stress change during structural vibration, a snapback free vibration test was performed on the structure. This test involved slowly applying a 600 N load to the tip of the traffic signal structure mast arm, damping all vibrations with the applied load, and rapidly removing the load, which allowed the structure to vibrate freely. This induced large displacement vibrations which occurred predominantly in the first IP mode.

Experimental Structure and Instrumentation

The traffic signal structure utilized (dimensions in Table 2) was located at Texas A&M University's Riverside Campus, and is depicted in Figure 5.

Table 2. Traffic Signal Structure Dimensions

Mast Arm		**Pole**	
Length	13230	**Length**	9140
$D_{Connection}$	279	**D_{Base}**	372
D_{Tip}	127	**D_{Top}**	262
Thickness	6.1	**Thickness**	6.4

NOTE: All dimensions in mm

Figure 5. Traffic signal structure image.

For physical measurement of mast arm tip displacement, a Brüel & Kjær Type 4383 piezoelectric accelerometer was applied to the structure as shown in Figure 6a and connected to a Brüel & Kjær Type 2692-A-0I4 charge conditioning amplifier offering single and double signal integration. The double integration function was utilized to determine displacements with lower and upper filter cutoff frequencies of 0.1 Hz and 1 kHz, respectively. A 10 V/m output scale was chosen for connection to a Tektronix TDS3034B oscilloscope at a sampling rate of 100 Hz.

A strain gage was applied to the base of the pole structure, shown in Figure 6b, and sampled at 100 Hz to measure the strain associated with IP base bending moment caused by IP arm tip displacement. The stress was inferred by using a modulus of elasticity assumed at 200 GPa.

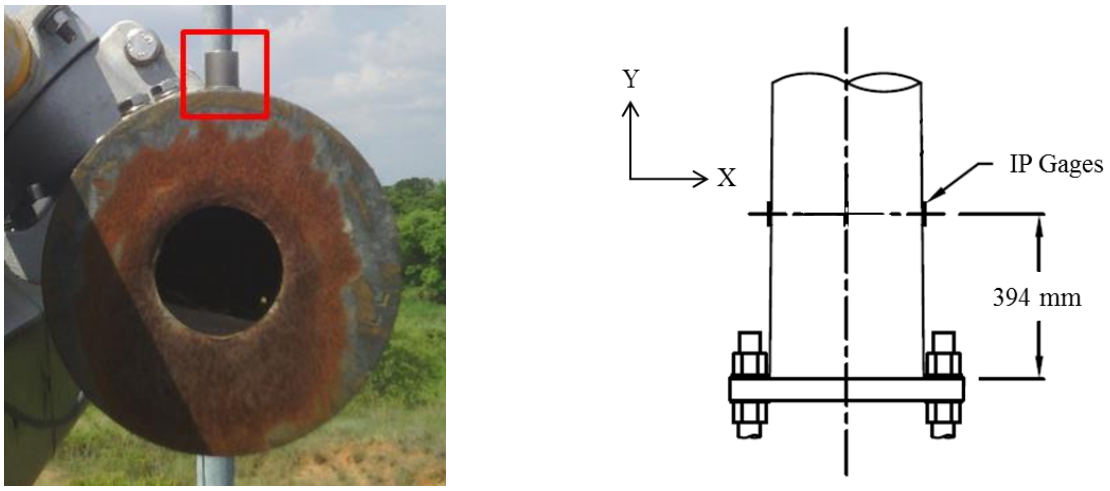

(a) (b)

Figure 6. Location of (a) accelerometer and (b) in-plane (IP) strain gage at pole base

Video was captured with a SONY HDR-CX220 video camera at 1280×720 pixel resolution and a sampling rate of 30 Hz. The camera was securely mounted on a tripod. For analysis, a single 32 pixel square sub-window center was selected within the reference image. A scale factor of 13.2 mm/pixel was chosen based upon the measurement of five geometries in the field of view.

Analytical Model

Figure 7 provides a depiction of the SAP2000 model used for this research. The model utilized 305 mm long prismatic sections with diameters equal to the mean diameter of the non-prismatic section on the true structure. Traffic signal clusters were simulated with 17.2 kg masses applied to nodes 4 and 5 and a 24.5 kg mass applied at node 6. A mast arm tip detail of 0.72 kg and the arm-pole connection of 71.2 kg were modeled as masses applied to nodes 7 and 3, respectively. The section modulus at the base was known to be 638.6×10^3 mm^3 for relating moment to stress.

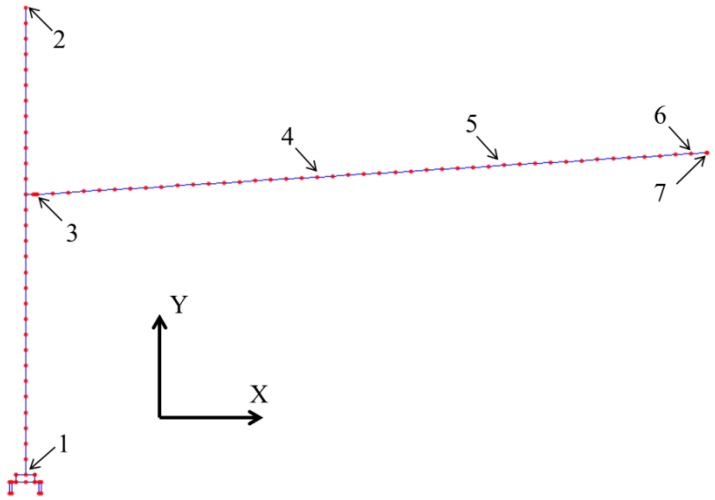

Figure 7. SAP2000 model.

IP base bending moment and IP base bending stress relationships were developed for first IP mode tip displacements because the first IP mode was known to dominate dynamic response of the structure. A fully modeled (full) boundary condition (BC) was utilized to full account for all elements in the pole-foundation connection. For a simpler analysis, node 1 was fixed, with minimal change in moment-displacement and stress-displacement relationships in Figure 8.

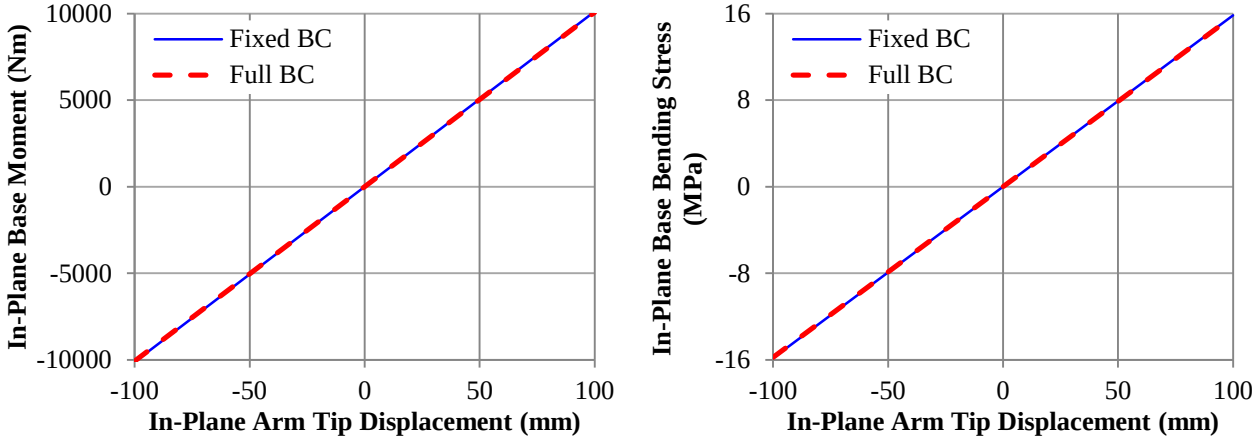

Figure 8. SAP2000 (a) moment-tip displacement and (b) stress-tip displacement.

Free Vibration Test Results

The resulting IP arm tip displacement time series were produced, with a physically measured time series sample in Figure 9a, MQD-based computer vision sample in Figure 9b and direct overlay of the boxed time series in Figure 9c. After resizing the physically measured data from 100 Hz to 30 Hz using nearest-neighbor interpolation, the time series were subtracted directly. A RMS difference value 10.06 mm was obtained from the subtracted time series which corresponds to approximately 5% of the maximum peak-to-peak amplitude of the physical measurement time series. Under visual inspection, it was noted that the physical measurement data provided a similar time series to the results of the computer vision analysis. The time series overlaid in Figure 9c provide a direct visual comparison, displaying the physical measurement time series attaining generally larger magnitude displacements than the computer vision results.

It was noted that the computer vision based results displayed a higher level of noise than the physical measurement data, as shown in the peaks of the overlaid time series in Figure 9c. This suggests a higher RMS error present in the computer vision-based data than in the physical measurement-based data.

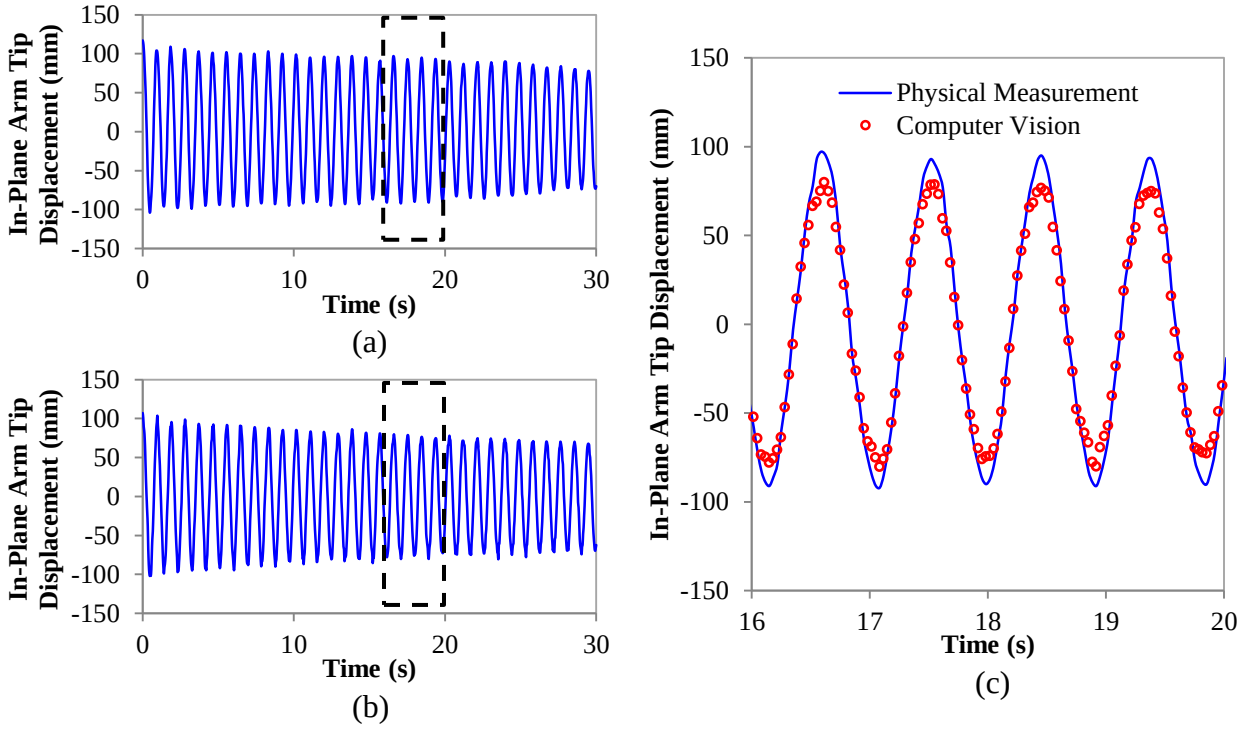

Figure 9. Sample arm tip displacement time series from (a) physical measurement, (b) computer vision, and (c) overlaid results.

Through verification of the MQD-based computer vision method for analysis of structural displacement time histories during vibration, a path was developed to relate the measured displacements to stresses within the structure by application of the SAP2000 analytical stress model. Figure 8b provides the IP base bending stress as a function of IP arm tip displacement for the SAP2000 model, which was shown to be insensitive to boundary conditions. Thus, by developing a relationship between inferred stress from the strain gage and the physically

measured displacement, an experimental model for IP base bending stress as a function of IP arm tip displacement was compared to the SAP2000 stress model. A similar relationship was created and compared based on the computer vision-measured displacements.

The results of this analysis are shown in Figure 10, which shows an approximate 2% error in linear fit coefficient of the computer vision model relative to the fully modeled boundary condition SAP2000 model, and 3% relative to the fixed boundary condition model. Both the developed computer vision model and the physical measurement model exhibited high correlation values ($R^2 \geq 0.98$), with the physical measurement experiencing marginally better correlation likely due to the greater observed smoothness. The physical measurement data shows a more significant deviance from the SAP2000 analytical models and the computer vision results, quantified at an approximate 15% error in the linear fit coefficient relative to the fully modeled boundary condition SAP2000 model. This may suggest that the accelerometer or signal integrator instrumentation experienced a scaling factor error and that the MQD-based computer vision results provided more accurate, though marginally lower precision results than the physical measurement.

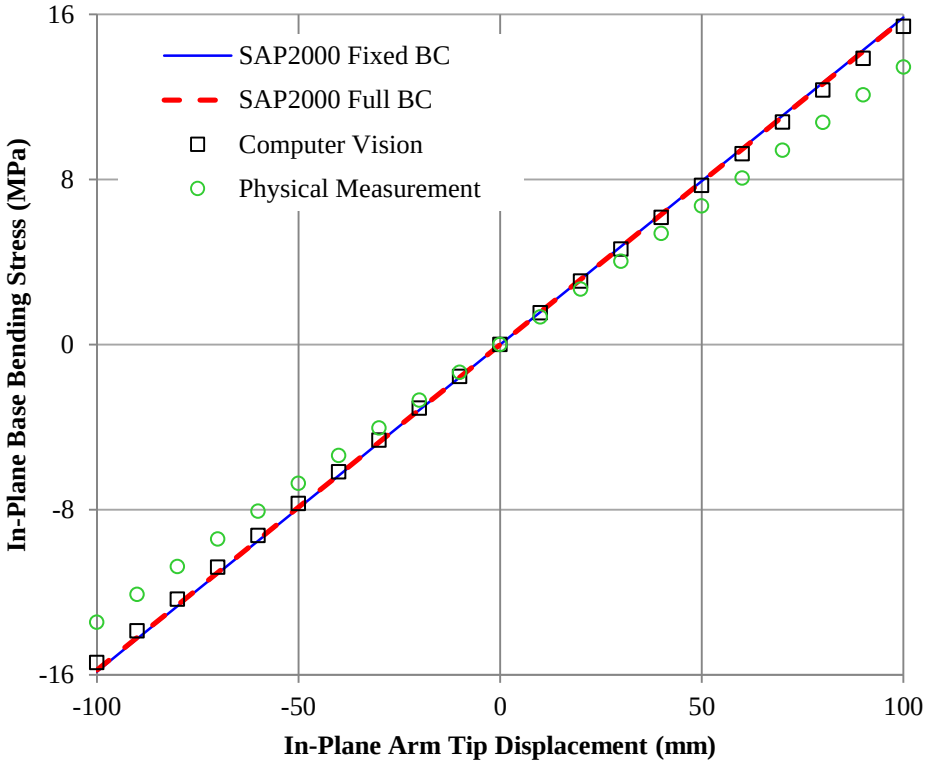

Figure 10. Base stress-tip displacement relationships from model and experiment.

Stress Analysis Validation

With agreement between the SAP2000 stress-displacement model and computer vision coupled with strain gage stress-displacement model, a method was developed to directly compare time series of inferred stress. The method is depicted in Figure 11.

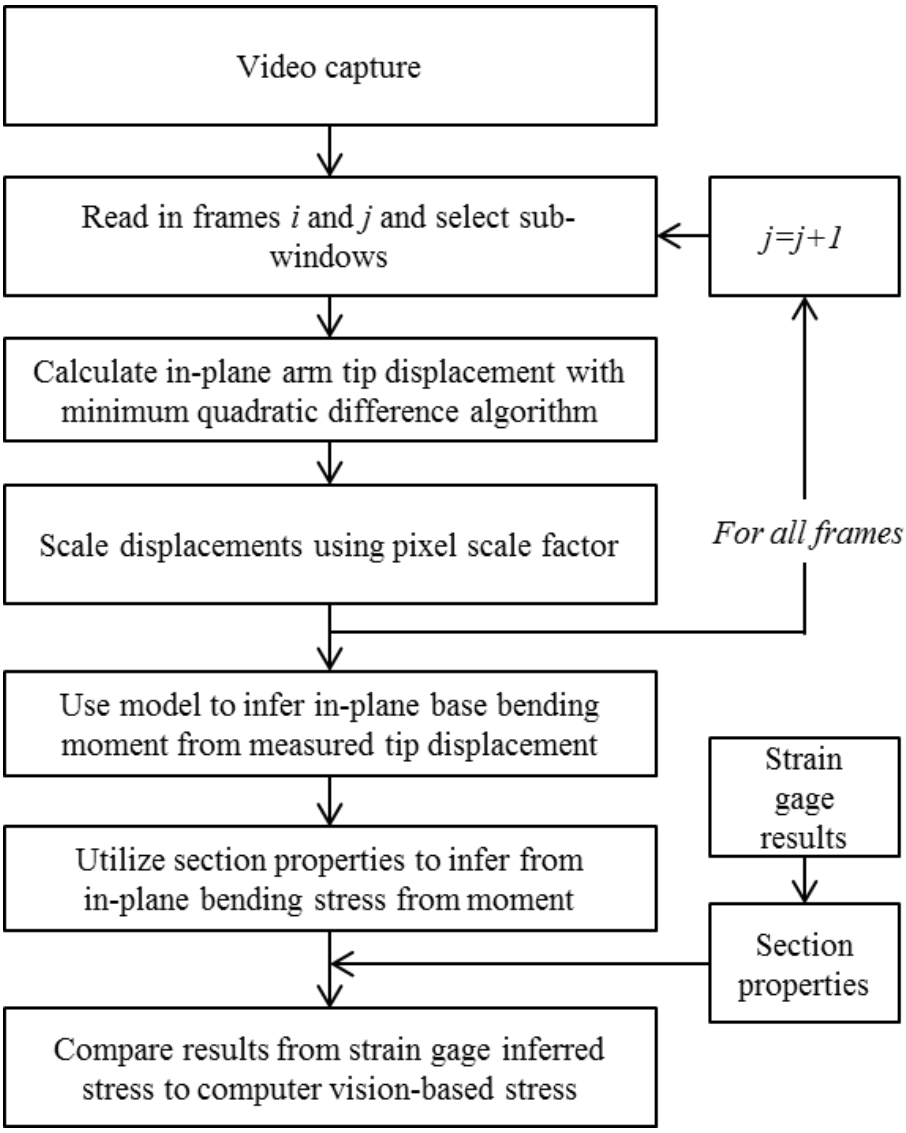

Figure 11. Stress time series development and comparison method.

Figure 12a displays the IP base bending stress time series as inferred from the strain gage and Figure 12b displays the inferred stress time series obtained from combining the fixed boundary condition SAP2000 model with the computer vision measured tip displacements. Figure 12c provides an overlaid time series for direct comparison. The strain gage data was resized from 100 Hz to 30 Hz using nearest neighbor interpolation to allow for direct subtraction of the time series. The RMS difference was computed at 1.05 MPa, which corresponds to approximately 4% of the maximum peak-to-peak amplitude of the time series. Figure 12a shows higher mode interaction in the first few vibrations, which would not be realized in the computer vision output because the SAP2000 relationship between IP arm tip deflection and IP base bending stress is only valid for first IP mode vibration.

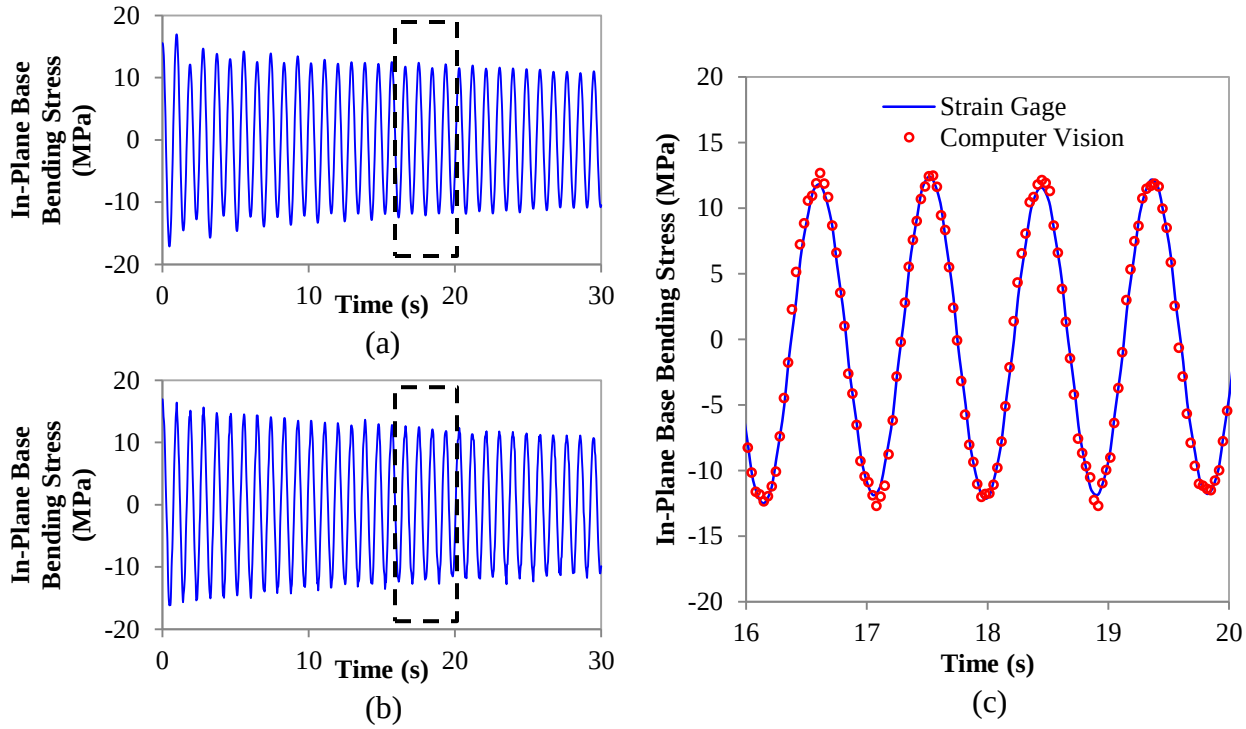

Figure 12. Sample stress time series from (a) strain gage, (b) computer vision, and (c) overlaid results.

Discussion

MQD-based computer vision using a consumer-grade camcorder effectively determined structural displacement during vibration by direct comparison against measured displacements. Similarly, computer vision was validated by producing an IP base bending stress-IP arm tip displacement relationship which agreed well with the analytical models.

Computer vision-measured IP arm tip displacement coupled with the SAP2000 stress-displacement model for a fixed modeled boundary condition allowed for an accurate method of determining stress time series compared to strain gage output. A significant result is the approximate 3% error in linear coefficients of the experimental computer vision model relative to the fixed boundary condition SAP2000 model for stress-displacement relationships. While the fully modeled boundary condition offers a higher degree of accuracy, this model required advanced knowledge of the elements comprising the pole-foundation connection. This is impractical for fast development of stress time series based on computer vision-measured displacements. The presented method provides a method for non-contact, target-less determination of stress time histories during structural vibration using a robust algorithm which does not rely on the presence of specific geometry.

For higher accuracy, a greater number of pixels may be used to represent the displacement by using a higher resolution video capture device (4). Similarly, to obtain a smoother time series, a higher frame rate video capture device may be utilized.

DETERMINATION OF TRAFFIC SIGNAL STRUCTURE DYNAMIC PROPERTIES

Vibrating structures generally exhibit multiple natural frequencies and shapes of deformation corresponding to each frequency, called mode shapes. While one mode may dominate the vibrational response of a structure under excitation, the total vibration is most commonly a superposition of multiple modes. The dynamic characteristics of natural frequencies, mode shapes, and damping ratios are dependent upon the inertial and elastic properties of each structure, and through determination of these characteristics by modal analysis, mitigation of detrimental vibration is made efficient and feasible.

Applications for modal analysis of structures include high mast illumination poles, bridges, overhead sign supports, and other lightweight steel structures such as wind turbines, which may exhibit detrimental vibration and fatigue due to excitation by live loads or environmental loads (2). By determination of the dynamic characteristics, the properties of the structure may be altered to inhibit vibration at certain points or at certain frequencies. Thus, modal analysis is a valuable tool, but is often difficult or costly to employ. In general, the results of finite element-based modal analysis are largely influenced by boundary conditions. In order to allow for analysis using these models, the finite element model is updated using the results of experimental modal analysis performed on built structures, but current methods for experimental modal analysis involve large arrays of instrumentation (2). The cost and difficulty associated with current instrumentation limit the applications of experimental modal analysis to small-scale applications.

As examples of flexible structures which are excited by natural wind, traffic signal structures are easily undergo vibration, with a damping ratio generally less than one percent and an IP fundamental frequency of approximately 1 Hz (*15*). The low IP fundamental frequency coupled with an abundance of wind speeds capable of exciting the structure at this frequency corresponds to large displacement vibrations, while limited damping allows vibrations from a single excitation to continue for minutes before completely dissipating.

The combination of a wealth of previous research into traffic signal structure dynamic responses and the relatively large displacements realized during vibration makes traffic signal structures excellent candidates for the application for testing a computer vision-based approach to dynamic characteristic determination.

MQD-based Computer Vision Mode Shape Determination

In many image processing applications, a region of interest (ROI) is defined for usage and emphasis by the processing tasks. In this approach, a sub-window is defined in the initial image for the comparison and should enclose the geometry of interest. For a task such as determination of displacement time series, damping ratios, or natural frequencies, a single ROI exemplified in Figure 13a may suffice, while mode shape determination depends on the measurement of displacement for multiple points, as shown in Figure 13b, with higher resolution preferred. The benefit of a computer vision-based approach is the large number of pixels available as discrete points of analysis while only requiring a single video capture device (4).

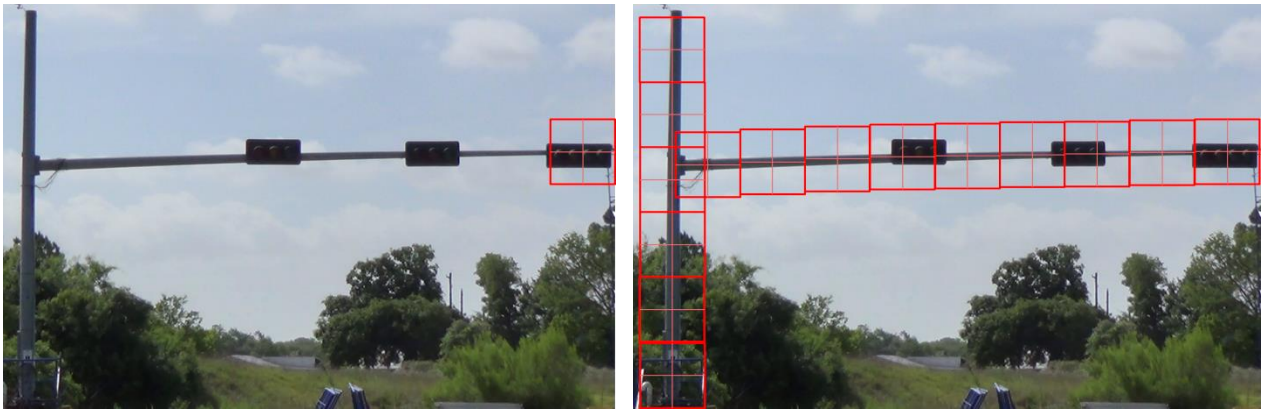

(a) (b)

Figure 13. Example regions of interest for (a) frequency and (b) mode shape analyses.

For mode shape determination, each point of analysis on the structure had a corresponding time series of displacement which was filtered to determine time series of displacements for modes corresponding to the natural frequencies determined in a frequency analysis of a single point on the structure. To realize a valid time series for points of analysis along simple geometry, such as the bare pole or mast arm, it was necessary to apply digital gridlines in the direction of motion for analysis. This forced the MQD algorithm to realize higher correlation between sub-windows that were aligned with the gridlines. Therefore, for mast arm analysis, vertical gridlines were applied on the boundaries of the sub-windows in the vertical direction, and for pole analysis, horizontal gridlines were similarly applied. Once the time series were obtained, it was necessary to develop a parameter to describe the relative displacement of points on the structure, where each time series had approximately a zero mean. Therefore, the RMS displacement was used to quantify displacement associated with each point of analysis. The relative sign of the displacement was inferred by the sign of the mean of the displacement time series for each point. While the mean was near zero, a small bias was introduced by the alternating decrease in peak height resulting from damping, which allowed for the mean to be used as an efficient predictor of relative displacement sign. The results were then checked to ensure that all of the signs were appropriate for a smooth mode shape. Finally, the modal displacements were normalized.

Experimental Approach

To determine the dynamic properties of the structure, three artificial excitations were applied to the structure: snapback, forced vibrations (in the first and second IP modes), and broadband excitation. For each excitation method, three trials were performed, leading to nine total instances of excitation. For each of the nine excitations, data was collected using computer vision, physical measurement, and a strain gage instruments as previously described.

Snapback

The snapback involved slowly applying a 600 N load to the tip of the traffic signal structure mast arm, damping all vibrations with the applied load, and then rapidly removing the load. This induced primarily first IP mode vibration which dissipates over time, which allowed for the determination of modal damping ratios in addition to natural frequencies and mode shapes.

Second IP mode vibrations were also induced, but had displacements at least an order-of-magnitude smaller than the first IP mode vibrations.

Forced Vibrations

Forced vibrations involve manual application of a periodic force at a known natural frequency of the structure. Ideally, this excitation reduces the influence of all other modes and the vibration occurs primarily in the desired mode. This type of excitation leads to greater structural displacements in higher modes than realized under free vibration tests.

Broadband Excitation

To excite multiple modes simultaneously, it is often desirable to use a striking instrument to impose an impact load. Impact loads are comprised of a wide range of frequencies. This may allow for the determination of several natural frequencies and modes, but the smaller structural displacements associated with this method may also reduce signal-to-noise ratio of the analysis. A mallet was used to strike the end of the mast arm to induce broadband excitation.

Results

The following sections detail the results of the experimental modal analysis performed for each of the three excitation methods.

Natural Frequencies

The first and second IP natural frequencies of the traffic signal structure were determined by computer vision-based measurement of IP arm tip displacements, by physical measurement of IP arm tip displacements, and strain gage measurement associated with IP base bending stress. Vibration time series and fast Fourier transforms (FFTs) of the vibration for the results of a sample snapback test are given from computer vision (Figure 14a), physical measurement (Figure 14b), and strain gage (Figure 14c). The FFT changes the analysis from the time domain to the frequency domain, allowing for the inference of natural frequencies of the time-space motion. Each vibration and FFT is depicted in the natural units of measure for each measurement device. Note that the strain gage time series and FFT in Figure 14c shows significantly higher magnitude second IP mode vibration, which is explained by the higher interaction of the pole in the second IP mode shape, and was expected.

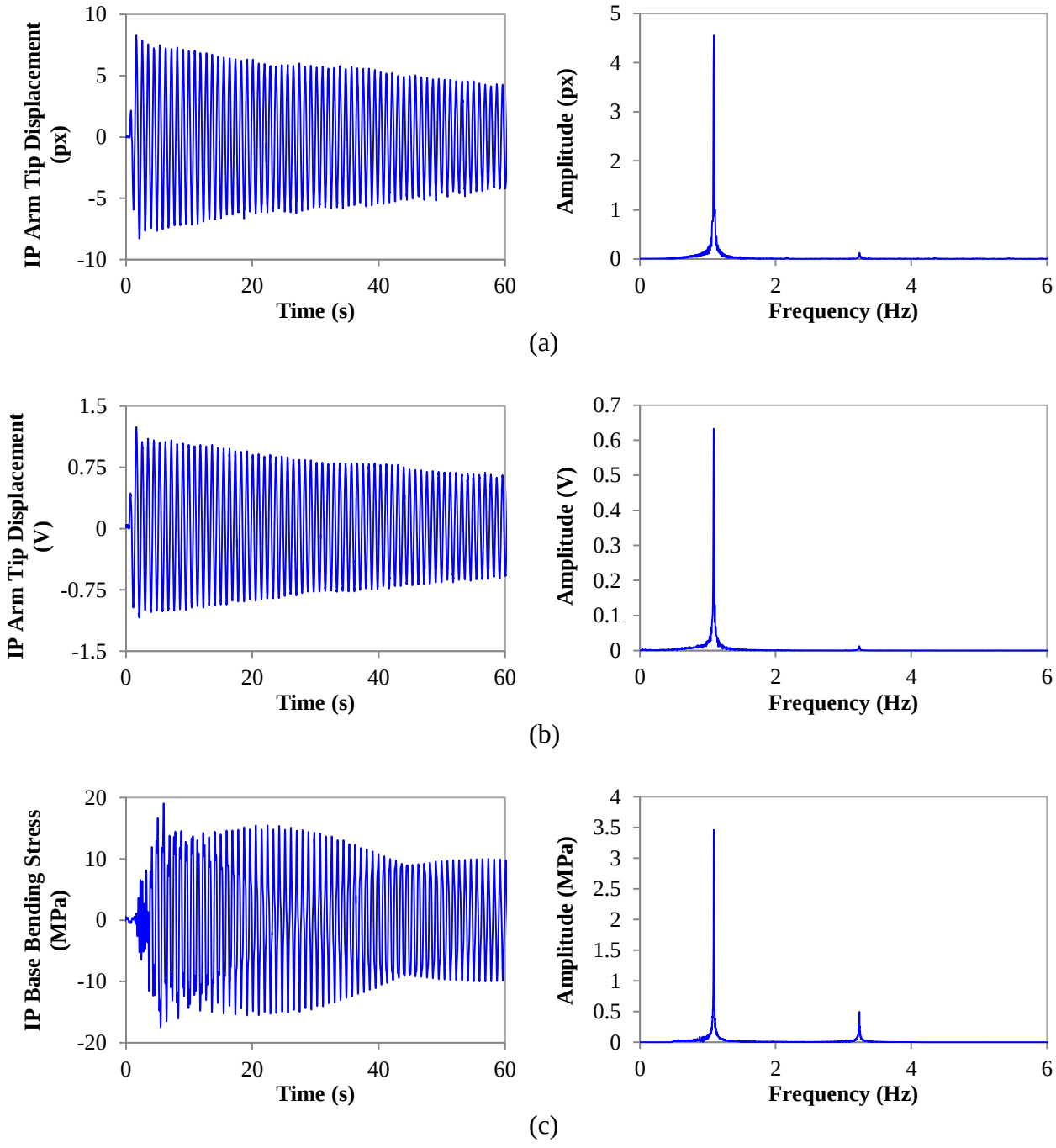

Figure 14. Sample time series and frequency analyses for (a) computer vision, (b) physical measurement, and (c) strain gage readings.

The results of the experimental natural frequency determination are included in Table 3 for each of the 27 combinations of measurement device, excitation technique, and trial number. The results vary minimally across all tests and measurement devices.

Table 3. Experimental First and Second In-Plane (IP) Natural Frequency (*f*) Results

		Computer Vision		Physical Measurement		Strain Gage	
Test	**#**	**f_1 (Hz)**	**f_2 (Hz)**	**f_1 (Hz)**	**f_2 (Hz)**	**f_1 (Hz)**	**f_2 (Hz)**
Snapback	1	1.090	3.234	1.086	3.235	1.088	3.235
	2	1.090	3.237	1.086	3.235	1.088	3.236
	3	1.090	3.237	1.086	3.235	1.089	3.232
	Mean	1.090	3.236	1.086	3.235	1.088	3.234
Forced Vibration IP Mode 1	1	1.090		1.086		1.086	
	2	1.090		1.086		1.086	
	3	1.090		1.086		1.088	
	Mean	1.090		1.086		1.087	
Forced Vibration IP Mode 2	1		3.227		3.223		3.223
	2		3.227		3.223		3.226
	3		3.227		3.223		3.223
	Mean		3.227		3.223		3.224
Broadband Excitation	1	1.083	3.219	1.099	3.223	1.086	3.235
	2	1.083	3.219	1.099	3.223	1.090	3.235
	3	1.083	3.219	1.099	3.223	1.090	3.232
	Mean	1.083	3.219	1.099	3.223	1.088	3.234
Totals	**Mean**	**1.088**	**3.228**	**1.090**	**3.229**	**1.088**	**3.234**

Table 4 provides the first and second IP natural frequency results obtained from modal analysis in SAP2000 for both the fixed and fully modeled boundary conditions. It can be seen that the natural frequencies of the structure were sensitive to boundary condition, with noticeable disagreement between the models on the second IP natural frequency. Therefore, it can be seen that the fully modeled BC led to closer first and second natural frequencies to the measured natural frequencies of the structure in Table 3.

Table 4. SAP2000 First and Second In-Plane Natural Frequency (*f*) Results

SAP2000	**f_1 (Hz)**	**f_2 (Hz)**
Fixed BC	1.105	3.501
Full BC	1.092	3.324

Damping Ratios

To determine the damping ratios, each snapback time series obtained from computer vision, physical measurement, and strain gage was filtered with parameters defined by the previously determined first and second IP natural frequencies. The first IP mode filter was a bandpass filter with a lower pass frequency of 0.5 Hz and an upper pass frequency of 2 Hz. The second IP mode

filter was a bandpass filter with a lower pass frequency of 2 Hz and an upper pass frequency of 4 Hz. A sample total signal with first and second mode filtered signals are included in Figure 15.

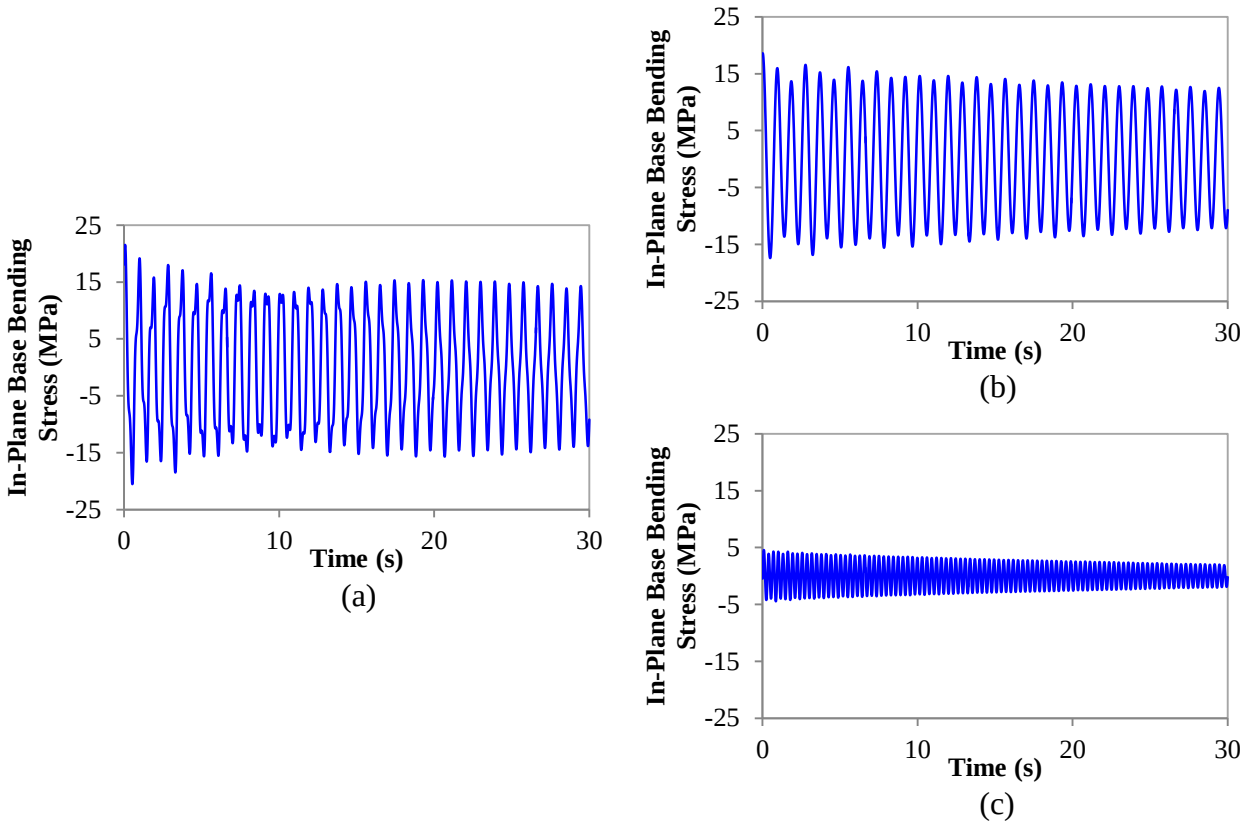

Figure 15. Sample damping ratio analysis (a) total signal, (b) filtered first in-plane mode, and (c) filtered second in-plane mode.

Modal damping ratio, ζ, was determined by incorporating the logarithmic decrement of each signal over a 30 second period between the maximal peak and final peak of the 30 second period (*12*). The modal damping ratio is expressed as a percentage of the critical damping value.

$$\zeta = \frac{1}{2\pi j} \ln\left(\frac{u_i}{u_{i+j}}\right) \tag{3}$$

The results of the damping ratio analysis are included in Table 5, with general agreement between the means for first and second IP mode damping ratios as determined by the three measurement methods.

Table 5. Damping Ratios (ζ) of the First and Second In-Plane Mode

		Computer Vision		Physical Measurement		Strain Gage	
Test	**#**	ζ_1 **(%)**	ζ_2 **(%)**	ζ_1 **(%)**	ζ_2 **(%)**	ζ_1 **(%)**	ζ_2 **(%)**
Snapback	1	0.200	0.030	0.215	0.099	0.197	0.145
	2	0.248	0.356	0.271	0.123	0.257	0.186
	3	0.199	0.065	0.237	0.152	0.212	0.140
	Mean	**0.216**	**0.150**	**0.241**	**0.124**	**0.222**	**0.157**

Mode Shapes

For mode shape determination, it was necessary to use different filtering parameters. The first IP mode filter was defined as a bandpass filter with a lower pass frequency of 1 Hz and an upper pass frequency of 1.2 Hz. The second IP mode filter was defined as a bandpass filter with a lower pass frequency of 3.2 Hz and an upper pass frequency of 3.7 Hz. Following filtering, the last half of the time series was used to eliminate the bias of the RMS operator towards low values possibly induced by filter windowing.

The mode shape is displayed at 1000× normalized displacements with respect to a structure scaled in mm (i.e. the largest displayed displacement in each mode shape is 1000 mm). The results for the first and second IP mode shapes determined from each of the three trials for each excitation technique are shown in Figure 16. For numerical comparison between the SAP2000 fixed BC model mode shape vectors, φ_A, and the computer vision determined mode shape vectors, φ_X, the modal assurance criterion (MAC) was utilized (*13*).

$$MAC(X,A) = \frac{\left(\{\varphi_X\}^T\{\varphi_A\}\right)^2}{\left(\{\varphi_X\}^T\{\varphi_X\}\right)\left(\{\varphi_A\}^T\{\varphi_A\}\right)} \tag{4}$$

MAC values range between 0 and 1, with values above 0.9 are generally considered acceptable if mode shape orthogonality can be shown (*13*). First and second IP mode shape orthogonality was determined using the full-size first and second IP modal displacement vectors and mass matrix from SAP2000, thus orthogonality was assumed in the experimentally determined modal displacement vectors which exhibited MAC correlation to the SAP2000 mode shapes (*14*). Alternatively, a MAC value near zero, which was observed between all sets of first and second IP mode shapes, may be used as an approximation of an orthogonality check (*13*). This suggests that the exhibited mode shapes were indeed orthogonal.

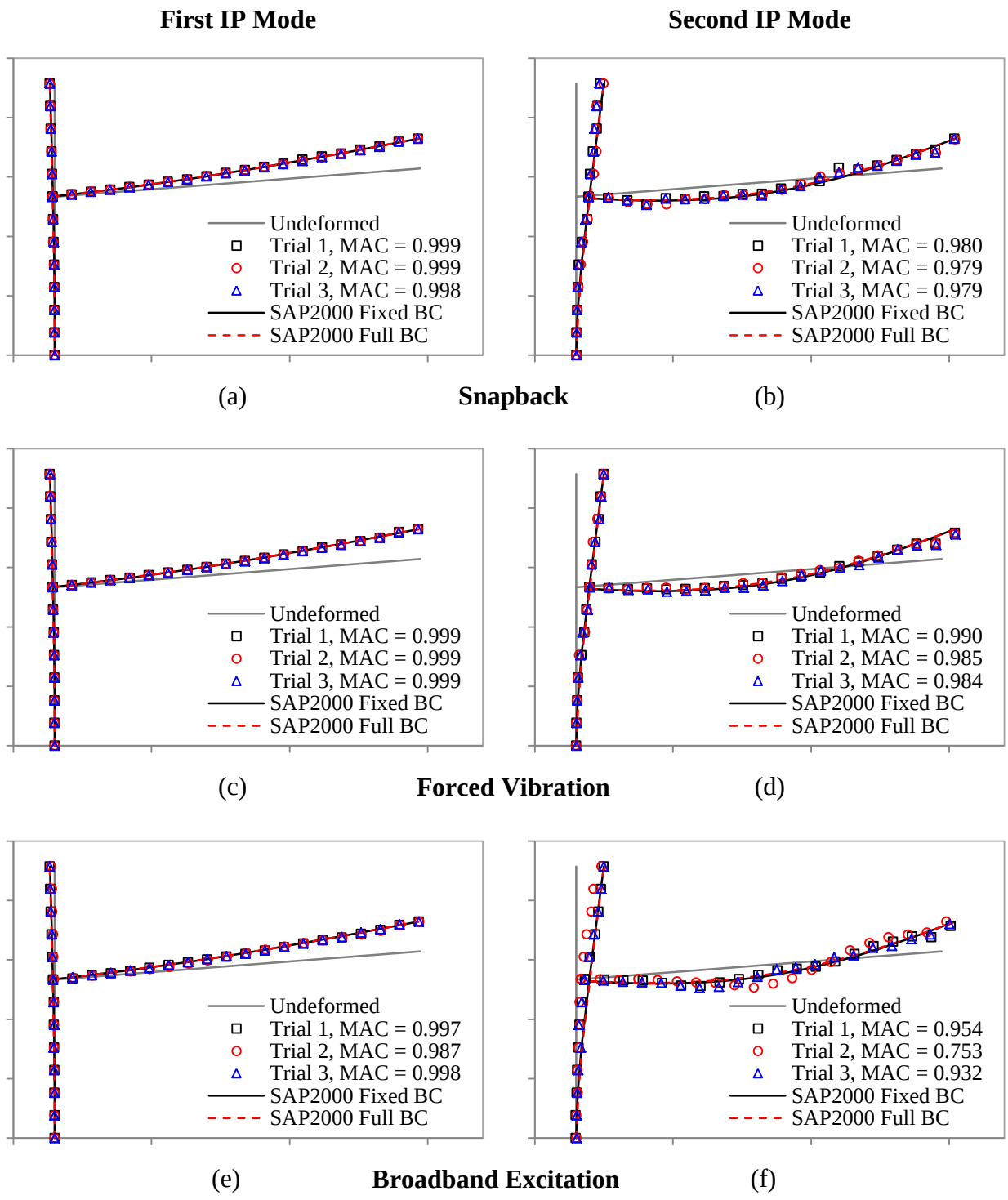

Figure 16. First and second in-plane mode shape results.

Each method for inducing vibration allowed for accurate determination of the first IP mode shape with respect to the modeled mode shape, as shown in Figure 16a, Figure 16c, and Figure 16e. The SAP2000 mode shapes varied minimally with respect to the boundary condition modeling, and the computer vision experimental results concurred with the modeled mode

shapes. The second IP mode shapes, shown in Figure 16b, Figure 16d, and Figure 16f, displayed lower MAC values, indicating marginally lower agreement between the experimentally determined and modeled second IP mode shapes. This occurred due to the higher influence of algorithm error in the computation of mode shape, where the second IP mode displacements were at least an order-of-magnitude smaller than the first IP mode displacements. Therefore, the RMSE associated with MQD analysis became a significant factor when the displacements were on the order-of-magnitude of the MQD RMSE. Despite this, the experimentally determined second IP mode shapes were above the valid criterion for the MAC except for one broadband excitation test. This suggests that computer vision offers a robust, sensitive method for determination of mode shape, even with sub-pixel modal displacement amplitudes.

Figure 17 provides the relationship between the maximum RMS displacement, generally found at the tip of the mast arm or top of the pole, and the MAC value. Inspection of this relationship suggests that valid mode shapes could be determined using a computer vision method for modal displacements which exhibit a maximum RMS displacement of 0.5 pixel.

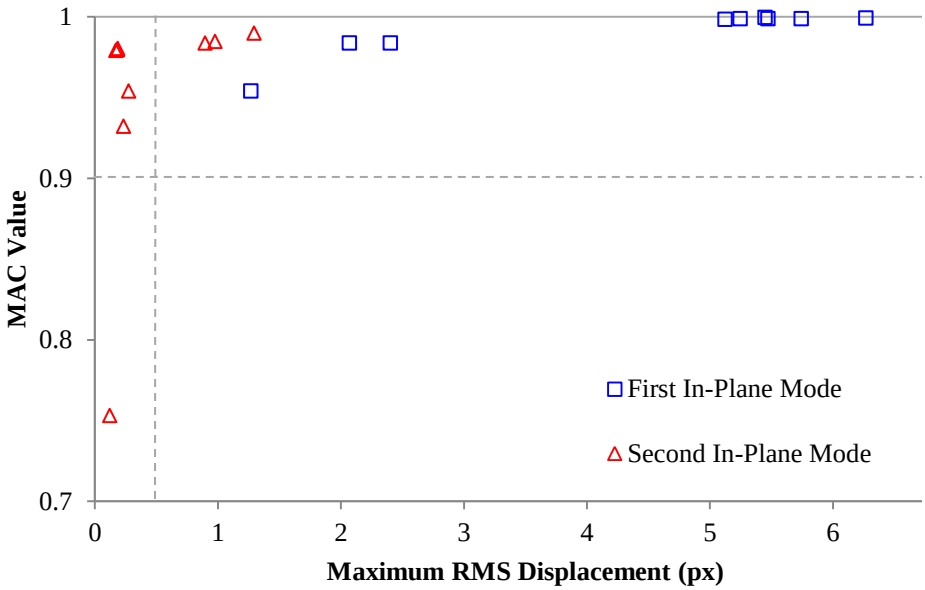

Figure 17. Modal assurance criterion (MAC) value vs. maximum root mean square (RMS) displacement for mode shape analysis.

Discussion

Natural frequency was well agreed upon by the results of the various test techniques and instrumentation, which shows that inherently target-less MQD-based computer vision offers a valid method for determination of structural natural frequencies under artificial excitation.

Damping ratio values showed greater variance among the instrumentation used and snapback trial number. For lower displacements, which correspond to lower pixel displacements for a fixed field of view, the RMSE of displacements determined from the MQD algorithm increases and may account for the higher degree of variance in the determination of logarithmic decrement

of the second IP mode. For small damping ratios, as exhibited by the tested structure, the logarithmic decrement is sensitive to the smoothness of the vibration signal. Computer vision determined displacements, as shown in Figure 9c and Figure 12c, displayed rougher resolution at the peaks of the displacement time signal. While this may explain some of the variance, the obtained small damping ratios (less than 0.5%) are excellent results for low pixel amplitude vibrations, as were experienced in snapback and broadband excitation second IP mode tests. All three excitation techniques were shown to provide mode shapes which satisfy the MAC criterion for similarity to the modeled mode shapes. Indeed, most of the MAC values for the first IP mode shapes were near-perfect, and only one second IP mode shape experiencing less than the 0.9 MAC value criterion. This establishes MQD-based computer vision using consumer-grade cameras as a viable method for determining mode shapes of flexible structures, with the quality of results depending on RMSE pixel displacement magnitude. In general, for this structure, it was noted that a maximum RMSE pixel displacement of 0.5 leads to acceptable results, with near-perfect results obtained for any mode shapes with a 1 pixel or greater maximum RMSE displacement.

AMBIENT WIND RESPONSE ANALYSIS

Cyclic strains are observed at the connections of traffic signal structures due to wind-induced excitation. Such vibrations occur both vertically and horizontally as a result of vortex shedding, natural gusts, truck-induced gusts, and other effects (*15*). As a result of these repetitive strains, connections within the structure exhibit a reduced fatigue life. While fatigue failure of traffic signal support structures does not realize a significant portion of traffic accidents or deaths, concern is highlighted due to the apparent unpredictability of this hazard to motorists and the economics of replacing fatigued traffic signal structures (*16*). Current technology available for the analysis of motion within traffic signal structures has included infrared camera-emitter systems and fixed linear displacement sensors, but most commonly strain gauge output is coupled with an analytical model. Since all points in the time series may be used for analysis rather than only the peak stresses, the inferred one-minute constant amplitude stress range, S_R, may be calculated by

$$S_{R,\,1\,min} = 2\sqrt{2}\sigma_{1\,min} \tag{5}$$

where the standard deviation of stress, σ, is taken over a one-minute moving window. The collection of stress and wind velocity data allows for the determination of relationships between wind speed or direction and the stress range induced in the structure, which allows for the estimation of fatigue lifetimes based on wind velocity data.

The presented research has shown that MQD-based computer vision offers a non-contact, target-less method for determining displacements of traffic signal structures undergoing induced vibration. It has also been shown that it is valid to utilize an analytical model to relate measured structural displacement to structural stress, allowing for the determination of stress time histories. This technique was then validated for ambient wind-induced vibration using a different perspective of the structure.

Full-scale Experimental Approach

Ambient wind velocity and TSS excitation was measured on the dates of July 23, 2013 for approximately one hour and July 29, 2013 for approximately three hours. The wind speeds ranged between 2 and 9 m/s and predominantly approached the structure from its back side, as shown in Figure 18a. An anemometer was affixed to the top of the pole of the structure to determine wind speed.

To improve accuracy under ambient vibrations, the camcorder was moved closer to the structure at a different location to reduce the scaling factor, thereby reducing the magnitude of the MQD algorithm RMSE when scaled into real-world distances. Scale factors between 0.9 and 1.1 mm/pixel were utilized for four instances of video capture of the mast arm tip motion during ambient wind excitation for a total of four hours of video capture. Figure 18b displays the view obtained from the camcorder setup as well as the convention of IP and OOP motion. For this analysis, only IP motion and bending stresses were considered.

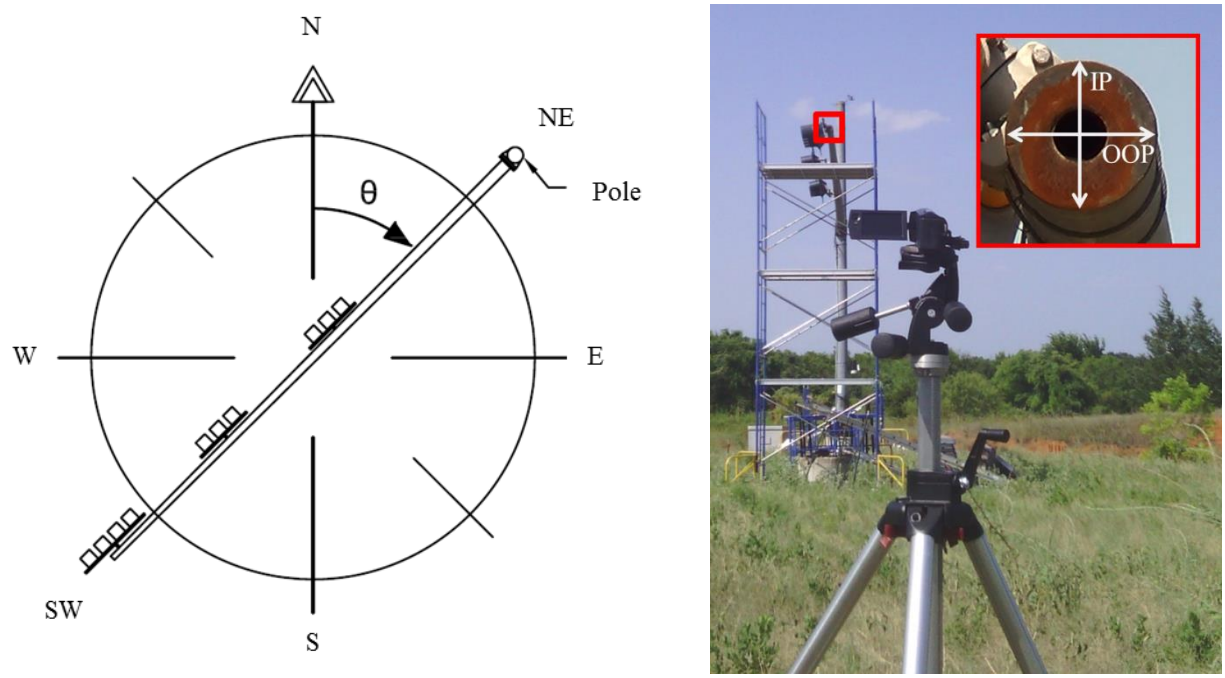

(a) (b)

Figure 18. Ambient wind excitation (a) site plan and (b) video capture setup.

The same IP base bending stress strain gage setup was utilized as in previous experiments. The data was originally sampled at 100 Hz and known section properties were used to infer stress.

Results

Both the computer vision displacement time series and the strain gage inferred stress time series were filtered using a highpass filter with a cutoff frequency of 0.5 Hz to allow for simple alignment of the time series prior to further analysis. This process eliminated the presence of a

mean stress found from the strain gage data, but quantification of the stress range does not depend upon the mean stress.

The pixel displacements from computer vision analysis were scaled into actual displacements using an averaged scale factor. Using the fixed BC stress-deflection relationship developed in Figure 8b, the displacements were then corresponded to stresses for first IP mode motion. Using Equation (5), the stress time series was converted to one-minute constant-amplitude stress ranges from both the strain gage data and the inferred stress using computer vision and the SAP2000 model. The results of this analysis for the 4 instances of video capture are shown in Figure 19.

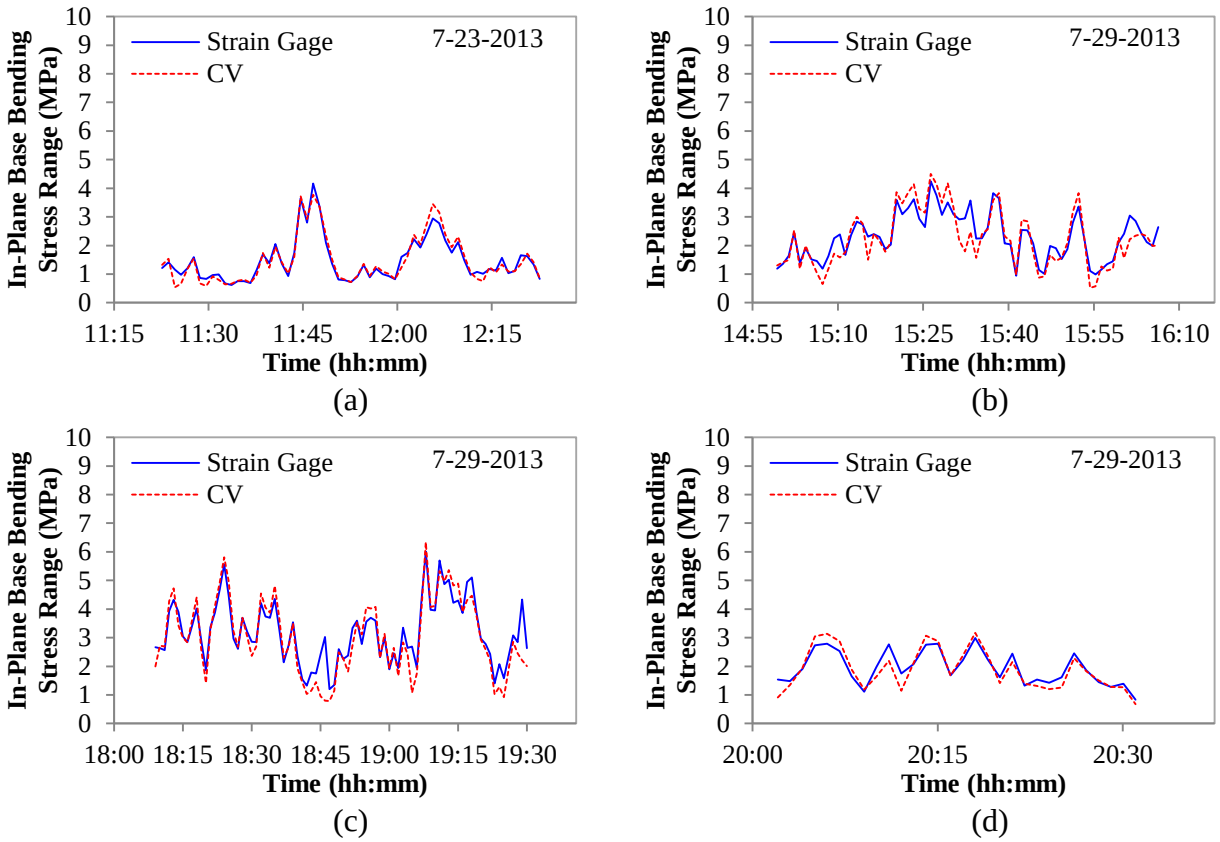

Figure 19. Ambient wind one-minute in-plane bending stress range time series from strain gage and computer vision (CV).

Using the wind speed data, it was possible to develop relationships between IP stress range and wind speed based on the strain gage data and the computer vision inferred stresses. The results are shown in Figure 20.

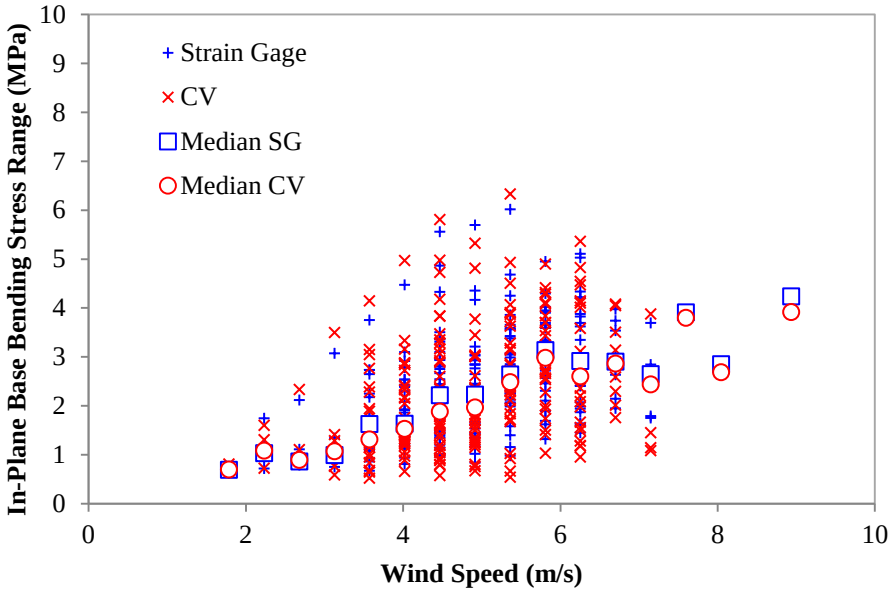

Figure 20. One-minute in-plane base bending stress range-ambient wind speed relationships for computer vision (CV) and strain gage (SG) data.

Discussion

By comparison of the inferred stresses in Figure 19, it can be seen that the computer vision-derived stress ranges provide excellent matching to the features given from the strain gage data. Deviation between the strain gage and computer vision results may be explained by the greater influence of the second IP mode at the base of the pole, which is the point of measurement for the strain gage, than the tip of the mast arm, which was the point of analysis for the computer vision approach. As well, the linear relationship developed for base bending stress as a function of tip displacement was only valid for first IP mode motion, therefore second IP mode stresses was not properly reflected in the computer vision-based stress data.

It can be seen that the median stress range from the computer vision model is marginally lower than the median stress range from the strain gage for the same wind speed. Despite the bias towards a lower inferred stress range, the computer vision model follows the behavior of the strain gage relationship, which suggests that computer vision is a viable method for development of stress range-wind velocity relationship estimates. This may provide a fast technique for the estimation of stress range relationships as a function of ambient wind velocity, as this analysis may be performed for both IP and OOP motion as a function of wind speed and direction.

CONCLUSIONS

The presented MQD-based computer vision method allows for non-contact, target-less determination of structural displacement and therefore modal parameters, including mode shapes. By using an analytical model to correspond structural displacements to stresses during vibrations, structural stress time histories were inferred to a RMSE of 4% maximum stress amplitude. Similarly, the development of an experimental relationship between the computer

vision-measured displacement and the strain gage-inferred stress led to only 3% variance in linear terms relative to the uncalibrated analytical model, which represents a high degree of agreement.

Using this method, it was shown possible to accurately determine natural frequencies of the structure, with accuracy similar to strain gage and accelerometer output. Utilization of time series filtering allowed for determination of modal damping ratios, but determination of second IP mode damping and shape required higher modal displacement to realize reliable results. Even with the maximum observed RMS displacement on the structure reaching only 0.5 pixel, acceptable MAC values were obtained. This proves that even modest modal displacements, on the order of a pixel, may provide excellent experimental mode shape results.

Finally, one-minute inferred stress ranges found to have high agreement between the inferred stress from strain gage data and using computer vision with the uncalibrated model between structural displacement and stress. By developing a relationship between the measured wind speed and the median stress range, it was shown that the computer vision model produced marginally lower values for median stress at a wind speed than the strain gage suggested. Despite the error, the developed relationships agreed well, which suggests that computer vision is viable as a method for determining stress range time series for development of ambient wind excitation relationships or connection fatigue analysis.

The benefits of this method are the inherently non-contact approach and the low-complexity, low-cost instrumentation. Hard-to-access structures such as high mast illumination poles or high span bridges can be analyzed. Similar benefits apply in situations where the dynamic study of the structure is short term and the costs associated with application of traditional instrumentation may make the study infeasible. This study obtained excellent results using a low-cost, consumer-grade camcorder, which suggests that quality may be increased further by the utilization of higher resolution cameras for structural vibration studies.

REFERENCES

1. Pandey, A. K., M. Biswas, and M. M. Samman. Damage detection from changes in curvature mode shapes. *Journal of sound and vibration*, Vol. 145, No. 2, 1991, pp. 321-332.
2. Cunha, Á., and E. Caetano. Experimental modal analysis of civil engineering structures. *Sound and Vibration*, Vol. 40, No. 6, 2006, pp. 12-20.
3. Gagvani, N. Challenges in Video Analytics. *Embedded Computer Vision*, Vol. 1, 2009, pp. 237.
4. Patsias, S., and W. J. Staszewski. Damage detection using optical measurements and wavelets. *Structural Health Monitoring*, Vol. 1, No. 1, 2002, pp. 5-22.
5. Olaszek, P. Investigation of the dynamic characteristic of bridge structures using a computer vision method. *Measurement*, Vol. 25, No. 3, 1999, pp. 227-236.
6. Cigada, A., P. Mazzoleni, M. Tarabini, and E. Zappa. Static and Dynamic Monitoring of Bridges by Means of Vision-Based Measuring System. *Topics in Dynamics of Bridges*, Vol. 3, 2013, pp. 83-92.

7. Paulsen, U. S., T. Schmidt, and O. Erne. Developments in Large Wind Turbine Modal Analysis Using Point Tracking Videogrammetry. *Structural Dynamics and Renewable Energy*, Vol. 1, 2011, pp. 187-198.
8. Mori, N., and K. A. Chang. *Introduction to MPIV*. http://www.oceanwave.jp/softwares/mpiv/. Accessed July 9, 2013.
9. Gui, L., and W. Merzkirch. A comparative study of the MQD method and several correlation-based PIV evaluation algorithms. *Experiments in Fluids*, Vol. 28, No. 1, 2000, pp. 36-44.
10. Chang, C. C., and Y. F. Ji. Flexible videogrammetric technique for three-dimensional structural vibration measurement. *Journal of Engineering Mechanics,* Vol. 133, No. 6, 2007, pp. 656-664.
11. Kim, S, and N. Kim. Dynamic Characteristics of Suspension Bridge Hanger Cables Using Digital Image Processing. *NDT & E International*, Vol. 59, 2013, pp. 25-33.
12. Chopra, A. K. *Dynamics of Structures, 3/E*. Pearson Education India, 2007.
13. Pastor, M., M. Binda, and T. Harčarik. Modal Assurance Criterion. *Procedia Engineering*, Vol. 48, No. 0, 2012, pp. 543-548.
14. Allemang, R. J. The Modal Assurance criterion–twenty Years of use and Abuse. *Sound and Vibration*, Vol. 37, No. 8, 2003, pp. 14-23.
15. Zuo, D., and C. W. Letchford. Wind-induced vibration of a traffic-signal-support structure with cantilevered tapered circular mast arm. *Engineering Structures*, Vol. 32, No. 10, 2010, pp. 3171-3179.
16. Dexter, R. J., and M. J. Ricker. *Fatigue-resistant design of cantilevered signal, sign, and light supports.* Report 469. Transportation Research Board, 2002.

Evaluating Driver Response to Prototype Traffic Control Devices at Access Points

Prepared for
Undergraduate Transportation Scholars Program

by

Adrian Contreras
Senior, Civil Engineering
Texas A&M University

Professional Mentor:
Melisa D. Finley, P.E.
Associate Research Engineer
Texas A&M Transportation Institute

Program Director
H. Gene Hawkins, Jr., Ph.D., P.E.
Associate Professor, Zachry Department of Civil Engineering
Research Engineer, Texas A&M Transportation Institute
Texas A&M University

Program Sponsored by:
Southwest Region University Transportation Center

August 9, 2013

STUDENT BIOGRAPHY

Adrian Contreras attends Texas A&M University in College Station, Texas. Adrian is from San Antonio, Texas and is a first-generation college student. He is currently working towards a Bachelor of Science in Civil Engineering with an expected graduation date of May 2014. Adrian is a member of the Texas A&M chapter of Chi Epsilon, where he currently serves as one of their officers.

Adrian is an active member of the Society of Hispanic Professional Engineers (SHPE), where he has served in various chair positions. He is also a member of the American Society of Civil Engineers (ASCE) and the Century Scholars Organization (CSO). Adrian also participates in the Aggie Pals program (becoming pen pals with young students to encourage college interest) and serves as a Regents' Scholars orientation leader (welcoming and assisting incoming Texas A&M freshmen). He hopes to attend graduate school and earn his professional engineer (P.E.) license in the future.

ACKNOWLEDGMENT

The research described in this paper was conducted as part of Project 0-6708, sponsored by the Texas Department of Transportation (TxDOT). The research activities were conducted in support of the Undergraduate Transportation Scholars Program. The findings and recommendations included in this paper are based on the student's summer activities. They should be considered preliminary and not as representative of the findings and recommendations of the parent project. This paper has not been reviewed or approved by the sponsor. The contents of this paper reflect the views of the author, who is responsible for the facts and the accuracy of these data presented herein. The contents do not necessarily reflect the official view or policies of TxDOT.

The author would like to express his appreciation to Melisa Finley for her guidance and support throughout the program.

SUMMARY

Temporary traffic control is most commonly used during lane closures in order to keep the flow of traffic moving. For example, two-lane, two-way roads require traffic to move in both directions, so it is necessary to stop vehicles on one end to allow vehicles on the other end to proceed. Taking that scenario and adding in the presence of access points along that lane closure adds an increased emphasis on safety. With the direction of travel changing on one open lane, drivers at the access point must take extra precautions to ensure that they are exiting in the correct direction. Flaggers and other forms of temporary traffic control can be used at these access points, but issues arise in terms of safety and efficiency. Texas A&M Transportation Institute (TTI) researchers have made progress in determining how to control traffic at these points. Through literature reviews and motorist surveys, researchers created two conceptual

designs for traffic control devices that could potentially be used at low-volume access points. These designs were then used to create two prototype devices to test in the field. Device 1 utilized a combination of existing signal indications, while device 2 implemented blank-out sign technology.

On separate days, each prototype device was set up at the same low-volume access point within a lane closure on a two-way, two-lane road. Subjects, accompanied by a TTI researcher, drove a TTI vehicle to the lane closure. In the first phase of the research process (observation), the subjects were instructed to enter the access point, turn around at a designated location, and exit the access point in a specific direction (i.e., right or left). During this phase, researchers observed the actions of the driver as they approached the prototype device and their response to the instructions given by the device. The second phase (survey) involved placing the driver in view of the device as the device cycled through each of its various states. TTI researchers asked the driver survey questions to gauge their overall understanding of the device. These two phases were repeated for 16 different subjects (eight for each device), ranging in age and gender. In addition to these methods, a TTI researcher positioned off the roadway observed non-study vehicles' reaction to both devices.

Field testing showed favorable results for the survey phase of each device. However, issues arose during the observation phase. Drivers appeared to be confused by device 1 with a number attempting to make incorrect turns upon first encountering the device. Most of the drivers also mentioned being confused or lack of understanding in their comments regarding device 1. Device 2 produced better results as 100 percent of drivers made the correct action during the observation phase. Drivers also had positive comments for device 2, and only one subject expressed initial confusion with the device. Non-study vehicle data were also generally supportive with 87 percent and 92 percent of these vehicles complying with device 1 and device 2, respectively. The analysis of collected data led to a recommendation that device 2 should undergo further testing and study.

TABLE OF CONTENTS

LIST OF FIGURES

LIST OF TABLES

INTRODUCTION

Work zones are implemented to allow for improvements to be made on an existing road or to repair any damage that may have occurred on a road. Lane closures on two-lane, two-way roads require temporary traffic control devices to be set up at both ends of the work zone to allow for vehicles to pass through the single open lane. Flaggers are the most common form of traffic control to be used in this situation. However, flagging requires a person to be very near the traveled way on high speed roads to control traffic. So, accidents that result in serious injuries to the flagger often occur. Portable traffic signals can also be used to control the main road traffic. Two signals (one at each end of the lane closure) are coordinated to allow for safe travel in both directions on the road. The use of portable traffic signals removes the need for flaggers, allowing them to conduct other work.

Low-volume access points occur where a driveway or a county road intersects with a main road. These are most common in rural areas, where long roads connect major cities to one another. Access points are factors that must be considered when setting up work zones, especially on two-lane roads. In this scenario, traffic must be controlled from both ends of the work zone and at the access points. While traditional temporary traffic control methods may be used at the access points, Texas A&M Transportation Institute (TTI) researchers were asked to identify and evaluate alternative methods for low-volume access point control as part of a Texas Department of Transportation (TxDOT) project. This paper documents field studies that were conducted as part of this research effort.

BACKGROUND INFORMATION

The following section details information that will assist in understanding the research conducted for this project.

Current Traffic Control at Low-Volume Access Points

Flaggers can be placed near an access point; however, there are safety and productivity concerns with using flaggers. The practicality of having a flagger stationed at a low-volume access point all day when very few vehicles are expected is questionable. The use of flaggers for work that requires a lane closure but no active work overnight (e.g., concrete curing) is also undesirable.

One potential solution would be to implement a portable traffic signal at the access point that would work in conjunction with the two portable traffic signals at each end of the lane closure. Currently, portable traffic signals used in Texas display steady circular red, yellow, and green indications. Thus, directional information (i.e., right or left turns allowed) cannot be conveyed to drivers at the access point. So, when the access point portable traffic signal displays the steady green circular indication, the other two portable traffic signals on the main road must display steady circular red indications. The access point traffic is then free to travel in either direction. One concern with this setup is the increase in traffic delay on the main road. Currently, vehicle actuation is not used with the portable traffic signals so even when there are no vehicles at the access point it would be serviced; yielding longer delays on the main road. Even if vehicle actuation was used, this setup encounters further coordination and delay issues if there are

multiple low-volume access points. Another potential solution would be to purchase portable traffic signals that provide directional information to use at the access points. However, TxDOT desired a lower cost solution that would work in conjunction with portable traffic signals on the main road.

Parent Project

As part of TxDOT Research Project 0-6708, Traffic Control for Access Points within a Lane Closure on a Two-Lane, Two-Way Road, TTI researchers were asked to identify and evaluate alternative methods to control traffic entering a lane closure on a two-lane, two-way road from low-volume access points.

Prior to the effort documented herein, TTI researchers completed a literature review of applicable traffic control devices, phone interviews with TxDOT personnel, and a motorist survey to gauge understanding of two conceptual device designs to temporarily control traffic at low-volume access points. Based on these efforts, TTI researchers worked with a manufacturer to build two prototype devices to test in the field.

Conceptual Designs and Prototype Devices

Device 1 (Figure 1) is composed of a circular red indication on top and two yellow arrow indications below. This design follows a sequence of phases: the stop phase, the proceed phase, the transition phase, and then a return to the stop phase. In the stop phase (Figure 1), the steady circular red indication is illuminated to inform drivers to remain stopped. In the proceed phase (Figure 2), the yellow arrow indications flash in the direction that drivers can travel (either left or right). The transition phase serves as a change interval between the other phases and consists of the yellow arrow indicator in the allowed direction of travel remaining steady. A NO TURN ON RED sign is also displayed to restrict turns during the stop phase.

Figure 1. Device 1 in the Stop Phase

Figure 2. Device 1 Allowing a Left Turn

Device 2 (Figure 3) is made up of a circular red indication and two internally illuminated movement prohibition signs that were altered such that the white arrows and red circles/slashes could be illuminated separately. In the stop phase (Figure 3), this device displays a steady circular red indication and both movement prohibition signs (white arrows and circles/slashes are illuminated). When a vehicle is allowed to proceed to the left (Figure 4), the circular red indication will flash and the red circle/slash will not display over the left arrow; allowing traffic to turn to the left only. The circle/slash on the sign with the right arrow will be displayed; prohibiting right turns. When right turns are allowed, the circular red indication will flash, the red circle/slash will not display over the right arrow, and the red circle/slash will display over the left arrow.

Figure 3. Device 2 in the Stop Phase

Figure 4. Device 2 Allowing a Left Turn

Both prototype devices were designed to work in synchronization with the portable traffic signals placed at each end of the work zone. For example, a north/south two-lane, two-way road with one access point will be considered. At the same time the portable traffic signal on the south end of the lane closure displays a steady circular green indication for northbound traffic to proceed, the prototype device in use would display the appropriate indication that would allow traffic at the access point to turn in the northbound direction only. When the portable traffic signal at the south end displays a steady circular red indication to stop northbound traffic, the prototype device in use would continue to allow northbound traffic to turn. This permitted traffic from the access point to turn before, during, or after the main road queue; thus, providing more opportunities to service access point vehicles and reduce the probability of access point vehicles not being able to join the end of the main road queue. The all-red duration must be adjusted appropriately. In order for the system described above to work properly, it was programmed using a hand-held control pad. The programming process required the following information: the expected or observed speed through the work zone, the distance between traffic control devices on the main road and at the access point, the number of access points, and the position of the prototype device. This allowed for appropriate timing for the various phases of the prototype devices to coincide with the phases of the portable traffic signals at each end of the lane closure.

Since the prototype devices are new traffic control devices, before field testing TxDOT submitted a request to the Federal Highway Administration (FHWA) to experiment the prototype devices. FHWA approved this request on June 27, 2013.

GOALS AND OBJECTIVES

The goal of the research effort documented herein was to determine if the two prototype devices were properly understood by drivers in an actual work zone setting. The following objectives assisted in reaching this goal:

- Document driver actions and comments.
- Conduct surveys focused on driver comprehension.
- Analyze collected data to gauge success of devices.
- Suggest recommendations for the use of the prototypes.

PROCEDURES

The following sections detail the field study location and methods that were practiced for this study.

Location

The field study site was near the city of Cleburne, Texas. This site (Figure 5) fit the required description of a lane closure on a two-lane, two-way road with a low-volume access point present. The access point was found at the intersection of County Road (CR) 418 into Farm-to-Market (FM) Road 916. Since both prototype devices inform drivers when to stop and when to proceed, researchers and TxDOT personnel decided the stop sign located at the intersection of the main road and access point should be covered while a prototype device was deployed. This removed any conflict that the driver may experience if they were to see both the device and stop sign. Based on TxDOT recommendations, the prototype devices were placed at the intersection across the main road in front of oncoming accessing point motorists to ensure that drivers could view the full device. The field testing process occurred over two days; one prototype device controlled the access point traffic each day.

Figure 5. Study Site with Access Point

Controlled Field Study

Subjects for this procedure were recruited through phone calls and the placement of flyers. These subjects were allowed to serve as drivers in this study if they had a valid driver's license, were over the age of 18, and met minimum levels of acceptable vision as set by TTI researchers. Potential drivers were also required to be able to read and speak English. A total of 16 subjects

(eight per device) were recruited for this study. The recruited subjects ranged in age from 18 to 65 and included both male and female drivers.

Subjects were checked in at a local hotel conference room, where their vision was tested before they were allowed to continue in the experiment. The vision procedures involved a Snellen chart for visual acuity testing and an Ishihara Color Test to check for colorblindness. In order for a subject to be a driver for the experiment, they were required to have at least a 20/40 vision and could not be colorblind.

Two state-owned 2009 Ford Explorers were used. Each vehicle contained a small video camera mounted on the dashboard to capture the forward road scene. In addition to capturing video of the road, the video camera also assisted in recording audio of the driver and researcher comments for later review and reduction.

Observation Phase

Each subject began with the observation phase. In this phase, the subject drove one of the state-owned vehicles to the work zone site. A TTI researcher rode with the subject in the front passenger seat. At the work zone, the subject was given instructions to enter the lane closure and then the access point. The subject was then instructed to turn around at a predetermined location and then exit the access point to the left or right when directed by the traffic control device (half of the subjects provided each direction). During the observation phase, the TTI researcher documented the actions and comments of the driver as they approached and reacted to the prototype devices. If a driver attempted to make an incorrect maneuver, the TTI researcher in the vehicle stopped them.

Survey Phase

After the observation phase, each subject was directed back to the access point and asked to park in a predetermined location where the subject could view the prototype device, while not impeding other traffic. The driver was then asked a series of questions while viewing the device cycle through its various phases. Survey questions included:

- Proceed Phase
  - Can you turn onto the main road?
  - Which direction can you turn?
  - Do you have to come to a complete stop before turning?
  - Do you need to yield to the vehicles traveling on the main road?
  - Which direction do you think the vehicles on the main road are going?
  - Do you have any other comments about the device you viewed?
- Stop Phase
  - Can you turn onto the main road?
  - Which direction(s) can't you turn?
  - Would you stop and then turn onto the main road or would you remain stopped until otherwise indicated?

Upon completion of the survey portion, the subject was instructed to return to the check-in site.

Non-Controlled Field Study

Drivers not involved in the controlled field study were also observed at the access point. Thus, this portion of the study focused on drivers that had no prior knowledge of the device or its operation and were encountering the device on their own. For each vehicle arrival, a TTI researcher located off the roadway noted the device phase and the driver's reaction. If a driver made an incorrect maneuver, workers on-site were notified and the vehicle was stopped.

DATA ANALYSIS

Data were separated into two categories based on which device was tested: device 1 and device 2. Observation data were organized according to a subject's response to the phases of a device that they saw. For example, a subject approaching device 1 may not have seen all the phases of that device. Each subject's comments and actions were reviewed to determine if they understood the phases seen. The order in which a subject saw the various phases was also noted. Due to potential interference, data from two subjects (one per device) were removed. These subjects approached the prototype device while another vehicle was already stopped on the country road at the intersection. Researchers agreed that these data should not be considered as the subjects could have been influenced by the actions of the driver in front of them, as opposed to what the device was telling them.

The survey responses for each question for each phase for each device were reviewed and determined to be correct or incorrect. Percentages were then calculated and used to compare subject understanding of the two devices. A comprehension level of 85 percent was used as the baseline for determining if a device was properly understood.

The non-controlled vehicle data were reduced to assess compliance with the prototype devices. The average number of vehicles traveling per hour through the access point was also computed.

RESULTS

The following sections detail the field study findings for both prototype devices.

Controlled Field Study Data

The data collected from the observation phase and survey phase of the study contribute to the controlled data.

Observation Data

Based on the subjects' responses to device 1, there was evidence of driver misunderstanding. Forty-three percent of the subjects had to be stopped from making the wrong turn by the TTI researcher. Two of these subjects were instructed to turn right when it was appropriate to do so, but they attempted to make a right turn when device 1 was displaying a flashing yellow left

arrow (i.e., only left turns allowed). The other subject was instructed to make a left turn when it was appropriate to do so, but attempted to make a left turn when device 1 was displaying a flashing yellow right arrow (i.e., only right turns allowed). All of the remaining subjects (57 percent) correctly reacted to device 1. Compared to device 1, device 2 appeared to be well understood by the subjects, as all of the subjects (100 percent) reacted correctly to device 2.

Survey Data

Table 1 shows the survey results for the proceed phases for both devices. As seen in this table, more than 85 percent of the subjects understood that for both devices they could turn onto the main road in the direction shown. All of the subjects for both devices (100 percent) also understood that they must yield to the main road traffic, and all but one subject (88 percent) understood which direction the main road traffic was going.

Table 1. Proceed Phase Data

Question	**Device 1 (n=8)**	**Device 2 (n=8)**
Can you turn onto the main road?		
Yes	100%	88%
No	0%	12%
Which direction can you turn?		
Correct Direction	100%	88%
Incorrect Direction	0%	12%
Do you have to come to a complete stop before turning?		
Yes	37%	100%
No	63%	0%
Do you need to yield to the vehicles traveling on the main road?		
Yes	100%	100%
No	0%	0%
Which direction do you think the vehicles on the main road are going?		
Correct Direction	100%	88%
Incorrect Direction	0%	12%

The two devices differed on whether or not a complete stop was needed before proceeding left or right. The flashing yellow arrow indications used on device 1 are intended to convey to motorists that they can cautiously enter the intersection only to make the movement indicated,

but must yield to the main road traffic; a complete stop is not required. So, 63 percent of the subjects were correct that a complete stop was not needed before turning. The other 37 percent, while technically not correct, were just more conservative in their response and therefore were not considered an incorrect action. Since device 2 displayed a flashing circular red indication when turns were allowed, motorists should come to a complete stop before turning. This was understood by all subjects (100 percent).

Table 2 shows the survey results for the stop phase for both devices. For both devices, all of the subjects (100 percent) understood they could not turn onto the main road. Subject comments regarding device 1 verified that the NO TURN ON RED sign indicated that right turns were not allowed when the steady circular red indication was illuminated. Subject comments regarding device 2 confirmed that the red circle/slashes clearly indicated that no turns were allowed. One subject (12 percent) for each device did believe that they could stop and then go (like at a stop sign) instead of remaining stopped until otherwise indicated. One subject commented that they would stop and go if no one else was around and if the red light remained on for too long. The other subject stated they would remain stopped during the day due to higher levels of main road traffic and the presence of workers, but at night, would most likely stop and go.

Table 2. Stop Phase Data

Question	**Device 1 (n=8)**	**Device 2 (n=8)**
Can you turn onto the main road?		
Yes	0%	0%
No	100%	100%
Which direction can't you turn?		
Right	0%	0%
Left	0%	0%
Left and Right	100%	100%
Would you stop and then turn onto the main road or would you remain stopped until otherwise indicated?		
Remain Stopped	88%	88%
Stop & Go	12%	0%
Unsure	0%	12%

The closing comments made by the subjects were also reviewed for indications of issues with the two devices. Seventy-five percent of the subjects indicated confusion with some aspect of device 1. These aspects included:

- The device does not look like a traffic signal – One subject commented that since the device was not like a standard signal, it was confusing and he/she thought the device was for the workers not motorists.

- The device displays – One subject mentioned that the device was confusing when the circular red indication was not illuminated (i.e., the proceed phase). Several subjects commented that the device did not indicate which direction they could go clearly. Although, one subject, while admitting that they were initially confused, said that they were able to understand the device after seeing all the phases and having time to think about what action to take.
- The height of the device – One subject commented that the device was too low, and that it should be the same height as the portable traffic signals.
- The length of the stop phase – In some cases, due to the initial programming, the stop phase was too short or longer than planned. As these issues arose, they were addressed in the field, but obviously impacted comprehension.
- The covered stop sign at the intersection – As indicated previously, researchers covered the stop sign at the intersection since the prototype devices were designed to convey the desired stop condition and did not want the stop sign to convey a conflicting message to motorists. However, the covered stop sign became a source of confusion, as motorists questioned the need to stop at all. The location of the covered stop sign and prototype device may have also contributed to the confusion, as the prototype device was located across the main road in front of oncoming access point motorists while the stop sign was located on the near side of the road.

In contrast, only 25 percent of the subjects who saw device 2 indicated some type of confusion with the device. But even these subjects, noted that with experience and education the device would be easily understood.

Non-Controlled Field Study Data

While device 1 was deployed, 39 vehicles not involved with the controlled field study arrived at the intersection; averaging 7 vehicles per hour (vph). Of these drivers, 13 percent made incorrect maneuvers and thus were considered non-compliant. Three drivers turned the opposite direction indicated by device 1, while two drivers turned when the device was in the stop phase. These vehicles were intercepted by workers and allowed to proceed when it was safe to do so. Other than the non-compliant vehicles, there were four drivers (10 percent) that asked workers what action they were expected to take.

The day device 2 was deployed only 13 non-controlled vehicles were observed; about 4 vph. Lower traffic volumes and a shorter data collection period contributed to the lower number of observed vehicles. Of the drivers observed, 23 percent did not comply with the device. However, some of the non-compliance (15 percent) was attributed to the timing of device 2 and not a misunderstanding of device. As discussed previously, device 2 should have been programmed to hold the proceed phase until after the main road queue had time to pass the access point; allowing access point vehicles to join the end of the queue. However, this did not occur initially, so the access point vehicles were stopped while the main road queue was traveling by. Instead, of waiting, two vehicles turned on red to join the end of the queue. After this timing issue was fixed, no further non-compliance of this type occurred. Overall, only 8 percent of the non-controlled vehicles were considered to be in non-compliance with device 2.

CONCLUSIONS AND RECOMMENDATIONS

Device 2 proved to be well understood in comparison to device 1. The results obtained from examining the observation data are important in comparing driver comprehension between the two devices. The actions that were observed in this phase reflect the first time that the subjects viewed the device without prior knowledge of it, which is exactly the situation that most drivers will go through if these prototype devices are implemented into the field. While some of the subjects struggled in understanding device 1, all subjects were able to comprehend device 2. While both devices saw favorable results in the survey phase, subjects did express confusion with various aspects of device 1. However, it was noted that with experience and education both devices could be understood. The data found from the non-controlled compliance study showed similar trends between the prototype devices. However, excluding the non-compliance with device 2 that resulted from the signal timing errors, the non-controlled data reinforced the perception that device 2 was more understood by drivers than device 1.

Various aspects of each device proved to be either detrimental or beneficial to the overall comprehension of the devices. As expected, the NO TURN ON RED sign used with device 1 informed motorists that a right turn was not allowed when the steady circular red indication was illuminated. However, there was evidence that the flashing yellow arrow indications were not well understood. Regarding device 2, the use of the circle/slashes over the directional arrows adequately informed motorists that they could not turn.

Overall, it is recommended that device 2 undergo further testing as it shows the most promise. Additional field studies at more work zones with a larger subject group are needed. Prior to conducting more studies, researchers should solidify the timing coordination between device 2 and the portable traffic signals on the main road. Another issue that should be addressed prior to conducting more studies is the presence of a stop sign at the access point. While researchers expected drivers to ignore the covered-up stop sign, this proved to raise more questions for the subjects.

It is not recommended to further study device 1 in its current state. Researchers should consider the addition of more signs or altering the main design. An example of a sign to possibly include is shown in Figure 6.

Figure 6. ONE WAY ACCESS Sign

Evaluation of Apparent Capacities through Freeway Lane Closures

Prepared for
Undergraduate Transportation Scholars Program

by

Kevin Mackan
Senior – Civil Engineering
Texas A&M University

Professional Mentor:
Gerald Ullman, Ph.D., P.E.
Senior Research Engineer
Texas A&M Transportation Institute

Program Director
H. Gene Hawkins, Jr., Ph.D., P.E.
Associate Professor, Zachry Department of Civil Engineering
Research Engineer, Texas A&M Transportation Institute
Texas A&M University

Program Sponsored by:
Southwest Region University Transportation Center

August 9, 2013

STUDENT BIOGRAPHY

Kevin Mackan is a senior at Texas A&M University in College Station, Texas. He will graduate in December 2012 with a Bachelor of Science in Civil Engineering.

Kevin is a national member of the American Society of Civil Engineers (ASCE), as well as a member of the Texas A&M University student chapter where he participates on the Steel Bridge Competition Team. He is also volunteers with organizations such as Big Event, and is an Eagle Scout.

After graduating, Kevin plans on entering the workforce for several years, before returning to pursue a Master's Degree in Civil Engineering.

ACKNOWLEDGMENT

The research described in this paper was conducted as part of Project 409107-010, sponsored by the Texas Department of Transportation (TxDOT). The research activities were conducted in support of the Undergraduate Transportation Scholars Program. The findings and recommendations included in this paper are based on the student's summer activities. They should be considered preliminary and not as representative of the findings and recommendations of the parent project. This paper has not been reviewed or approved by the sponsor. The contents of this paper reflect the views of the author, who is responsible for the facts and the accuracy of these data presented herein. The contents do not necessarily reflect the official view or policies of TxDOT.

The author would like to express his appreciation to Jerry Ullman for his guidance during the course of this research program.

SUMMARY

Lane closures through work zones are a cause of much delay and traffic congestion. They can form queues which hinder vehicles trying to reach their destination. There are many factors that go into the formation and length of queues that are generated by these lane closures. One such factor is the capacity of the lane closure itself. The capacity is a measure of the maximum flow rate at which vehicles can traverse a given stretch of road. In an effort to improve traveler awareness on the reconstruction of Interstate Highway 35, the Texas A&M Transportation Institute performs an analysis of each planned lane closure to predict wait times due to queues that may develop.

Two types of closures were analyzed in this research, single lane closures and full road closures. Apparent capacity was found to rely on multiple factors; the two that were examined by this study were the physical characteristics of the road leading up to the lane closure, and percentage of trucks present on the road. The results of this study found that apparent capacity trends are

influenced over time by both of these factors. For instance, the presence of a frontage road during a single lane closure allows, at least temporarily, for some drivers to bypass the lane closure and queue, raising the apparent capacity. Full road closures on the other hand cannot have these diversions because all vehicles must exit onto the frontage road, forming queues. A small correlation was found with percentage of trucks and apparent capacity. As percentage of trucks rose throughout the night, apparent capacity decreased.

TABLE OF CONTENTS

LIST OF FIGURES

LIST OF TABLES

INTRODUCTION

Lane closures are a necessary hindrance to traffic flow when work must be conducted on a roadway. When traffic volumes exceed capacity of a work zone lane closure, a queue develops upstream of the merging taper. These queues cause delays and traffic congestion which affects drivers, as well as delivery schedules of truck drivers. The Texas A&M Transportation Institute is monitoring and studying queues on a reconstruction project on Interstate Highway 35.

BACKGROUND

In order to fully understand the objectives and results of this research, some of the background information and terminology must be explained in further detail.

Parent Project

The foundation of this research project is the reconstruction of the I-35 corridor through central Texas. Figure 1 provides a map of the I-35 corridor with town locations along the roadway. The Texas A&M Transportation Institute is working with the Texas Department of Transportation to analyze lane closures and the resulting queuing conditions at locations along the reconstruction of Interstate Highway 35. This reconstruction affects a 90 mile stretch of the highway from Hillsboro, Texas to Salado, Texas. This route will be undergoing many lane closures over the span of this project, across the entire length of the reconstruction. These factors made it an ideal location to study the apparent capacities through work zone lane closures.

Part of the research TTI is performing on the I-35 corridor project is to try to predict the length of queues that will form at lane closures on the highway. This research will aid in these predictions by improving the accuracy of the prediction of these queues.

Figure 1. I-35 Corridor

Capacity

According to the *Highway Capacity Manual*, the capacity of a road is represented by the maximum sustainable hourly flow rate at which vehicles can be reasonably expected to pass through a given section of road. The stated capacity for a given road is a flow rate that can be achieved recurrently over peak periods of demand (*1*).In work zones, many factors can affect capacity. The percentage of trucks in the traffic stream, the number of lanes closed and remaining open to traffic, the type and proximity of work activities to travel lanes, and other factors can influence the capacity that a particular work zone lane closure can support.

Ideally, it would be possible to accurately estimate these capacities beforehand. Unfortunately, many of those factors listed above change day to day and even hour to hour, making accurate prediction difficult. TTI researchers desired to better understand the consistency (or conversely, the variability) of capacities occurring on I-35, but did not have the ability to actually go out and measure capacity at each lane closure. However, data on actual traffic volumes on the facility are being collected continuously at multiple locations along the facility. In addition, end-of-queue monitoring technology is being deployed to provide advance warning messages to approaching motorists of the presence and approximate location of stop-and-go, queued conditions. The end-of-queue technology monitors vehicle speeds at various points upstream of the lane closure. When average speeds detected are below a threshold value, 40 mph for the purposes of this study, it can be concluded that a queue has developed beyond the location of that sensor. By

comparing average speeds between sensors, then, one can then estimate the boundaries of the upstream end of the queue. If approach volume and approximate queue length are known at each point in time during the lane closure, it is possible to estimate the work zone capacity that would be required in order to generate the observed queues given the approach volumes that were measured.

Queuing Conditions

During nighttime lane closures on I-35 in central Texas, considerable variation in queuing has been observed relative to what would be predicted using existing work zone capacity estimates. This is likely the result of site-specific factors influencing capacity (grades, horizontal curves, entrance ramp traffic right before the merging taper, etc.), but may also be the result of diversion that sometimes occurs to exit ramps at or near the queue. The end result is that the amount of traffic going through and/or around a lane closure most likely differs from location to location, which affects the queues that occur. The combination of diversion around the closure and the capacity through the work zone itself can be viewed as the apparent capacity of the work zone. Conceptually, this apparent capacity could vary over the duration of a lane closure period.

DATA COLLECTION

Data for the I-35 reconstruction project has been collected in multiple forms for every lane closure over the lifespan of the project. The two types of data that were involved in this research project were volume data sets that were collected by radar sensors made by Wavetronix, and end of queue data sets that were collected by radar sensors made by iCone.

Site Selection

To select suitable locations for this research project, recent lane closures where a traffic queue developed and where queue end warning equipment had been deployed to monitor the presence and length of the queue over time were reviewed. A list of potential sites as well as the queue warning plans set out for these closures was reviewed to determine which locations would yield the most suitable data for this project. In order to gain a representative sample, two types of closures were examined for this project, single lane closures and full road closures. Single lane closures involve the closing of one of the lanes of traffic to set up a work zone. Full road closures are much more complex, involving shutting the entire roadway down and diverting all traffic onto the access roads for the duration of the work zone. Full road closures are reserved for activities such as demolition or construction of an overpass. In addition to these criteria, the number of nights of data collected was also a factor.

Based on the criteria above, three sites were chosen, all with two nights of data. Multiple nights of data were preferred since it would allow the research to examine any patterns from day to day. All of the sites chosen were on the northbound side of I-35, near West, Texas. The two single lane closure sites, ID 937 and 1099 were located several miles apart, just south of West, while the full road closure, ID 948 and 1018, which both covered the same span of road, was about ten miles away, to the north of the town of West. Table 1 shows the location, date, and type of each closure.

Table 1. Selected Closure Information

Type of Closure	Closure ID	Location	Dates
Single Lane Closure	937	Mile Marker 344-347	3/13/2013 & 3/14/2013
Single Lane Closure	1099	Mile Marker 347-353	5/22/2013 & 5/23/2013
Full Road Closure	948 & 1018	Mile Marker 355-356	4/10/2013 & 4/23/2013

Sensors

The data collected for this study came entirely from sensors located along Interstate Highway 35. As stated above, there were two types of sensors involved in the data collection for this research effort, volume sensors and end of queue sensors.

The volume sensors used on the I-35 corridor project are specialized radar sensors that detect the number of vehicles passing by on the road, as well as categorize them by size. There are seventeen of these sensors located at strategic points along the corridor in places of high traffic interaction, such as where a state highway crosses I-35.

The end of queue warning system sensors used on this project are also radar sensors that, rather than capture traffic volume like the Wavetronix sensors, detect speeds approaching work zones. The radar sensors are mounted in orange traffic barrels that are arranged in specific intervals leading up to a lane closure. Based on patterns of slowing speeds detected by the sensors, an upper and lower bound for the queue is able to be determined. Figure 2 shows the layout of the sensors for a typical lane closure on the I-35 reconstruction project.

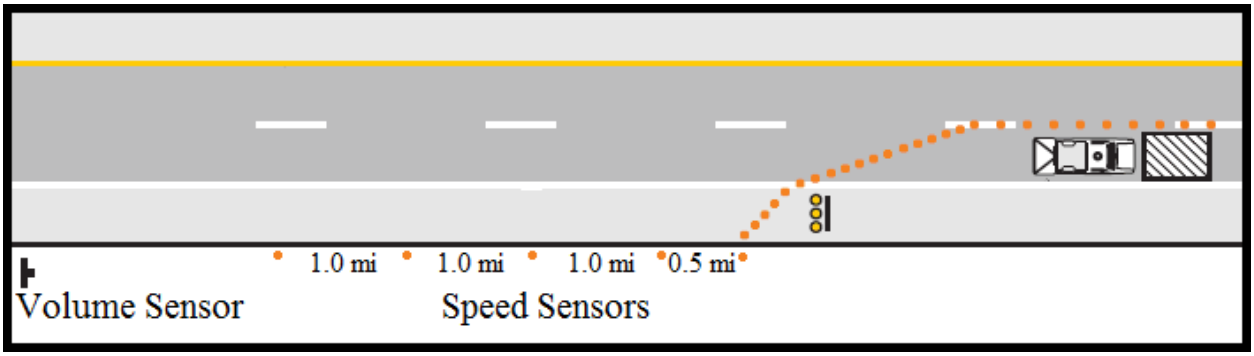

Figure 2. Sensor Layout

DATA REDUCTION AND ANALYSIS

In order to conduct this research, data had to be extracted and compiled from many sources and arranged to produce manageable data sets. First, the end of queue data was converted from speeds to queue boundaries. By examining the data and finding where speeds dropped below 40 mph, the upper and lower bounds of the queue can be estimated.

Once the queue bounds had been determined, they were merged with the data from the volume sensors to obtain volumes and queue lengths over the duration of each closure. The volumes are then compared to an estimated baseline work zone capacity, based on prior studies, and figures in the *Highway Capacity Manual* to be able to determine the new apparent capacity value. This

study used the baseline volume figures of 1500 vehicles per hour for single lane closures, and 1200 vehicles per hour for full road closures (*2*, *3*). With all figures now available, iterations must be performed based on Equation 1 in order to adjust apparent capacity until the predicted queue falls within the acceptable upper and lower bounds. Figure 3 displays an example iteration of the calculation of apparent capacity where the red bars represent the length of the calculated queue for each five minute interval. The top diagram shows a visual representation of an iteration where the queue prediction fell inside the bounds recorded by the sensors. The middle diagram shows an iteration that the predicted queue came up too short, meaning the apparent capacity needed to be lower. The final diagram represents an iteration that resulted in a queue beyond the upper bound, meaning the apparent capacity needed to be adjusted higher.

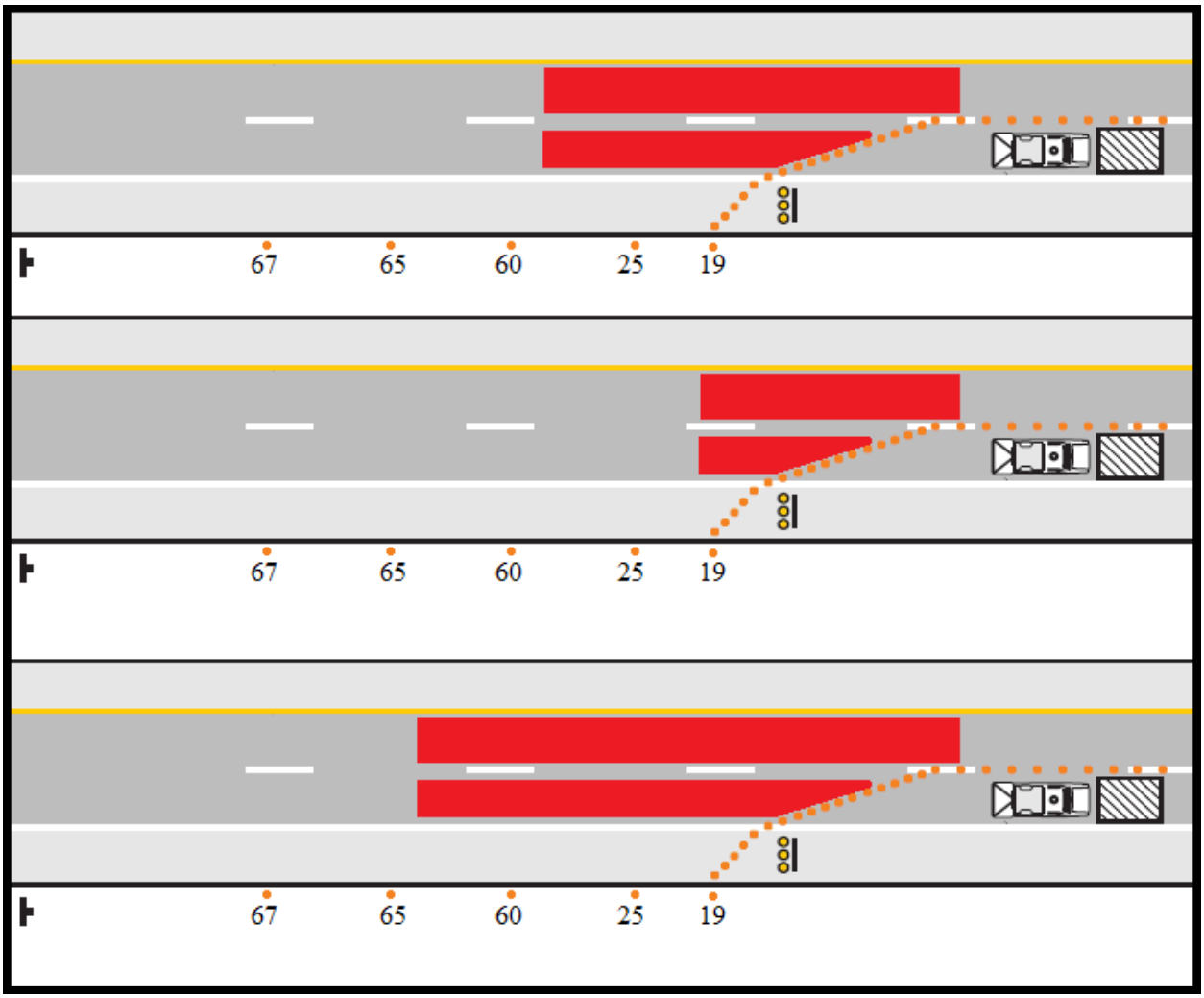

Figure 3. Example Evaluation of Queue Bounds

$$AV_i - EC_i + SV_{i-1} = Q_i \quad (1)$$

Where:

- AV = Approach Volume
- EC = Effective Capacity
- SV = Number of Vehicles Stored
- Q = Queue Length

RESULTS

This section outlines the results and analyses of the effects on capacities through the lane closures studied in this research project. The results have been broken down into two categories, those pertaining to the single lane closures, and those pertaining to the full road closure. For each of the lane closures, several factors were considered in the evaluation of apparent capacities, such as physical characteristics of the road around the lane closure as well as the percentage of trucks through the closure. These factors are discussed in further detail in this section.

Single Lane Closures

The two single lane closures proved to have the same general trends in apparent capacity throughout the duration of the closure. For each closure, the first night of data proved insignificant for various reasons. The second nights of data, however, provided more effective results.

Closure 937 occurred in mid-March 2013, near the beginning of the initial deployment of the end of queue warning system. The reason for this closure was so that a work crew could remove and reset a concrete barrier in between the northbound and southbound lanes of traffic. Each night, the closure began around 7:30 pm, and ran for several hours. As shown in Figure 4, the apparent capacity values are consistent until 10:00 pm, when the first night queue dissipates. If the queue had continued as it did the next night, the same downward trend in apparent capacity would be expected.

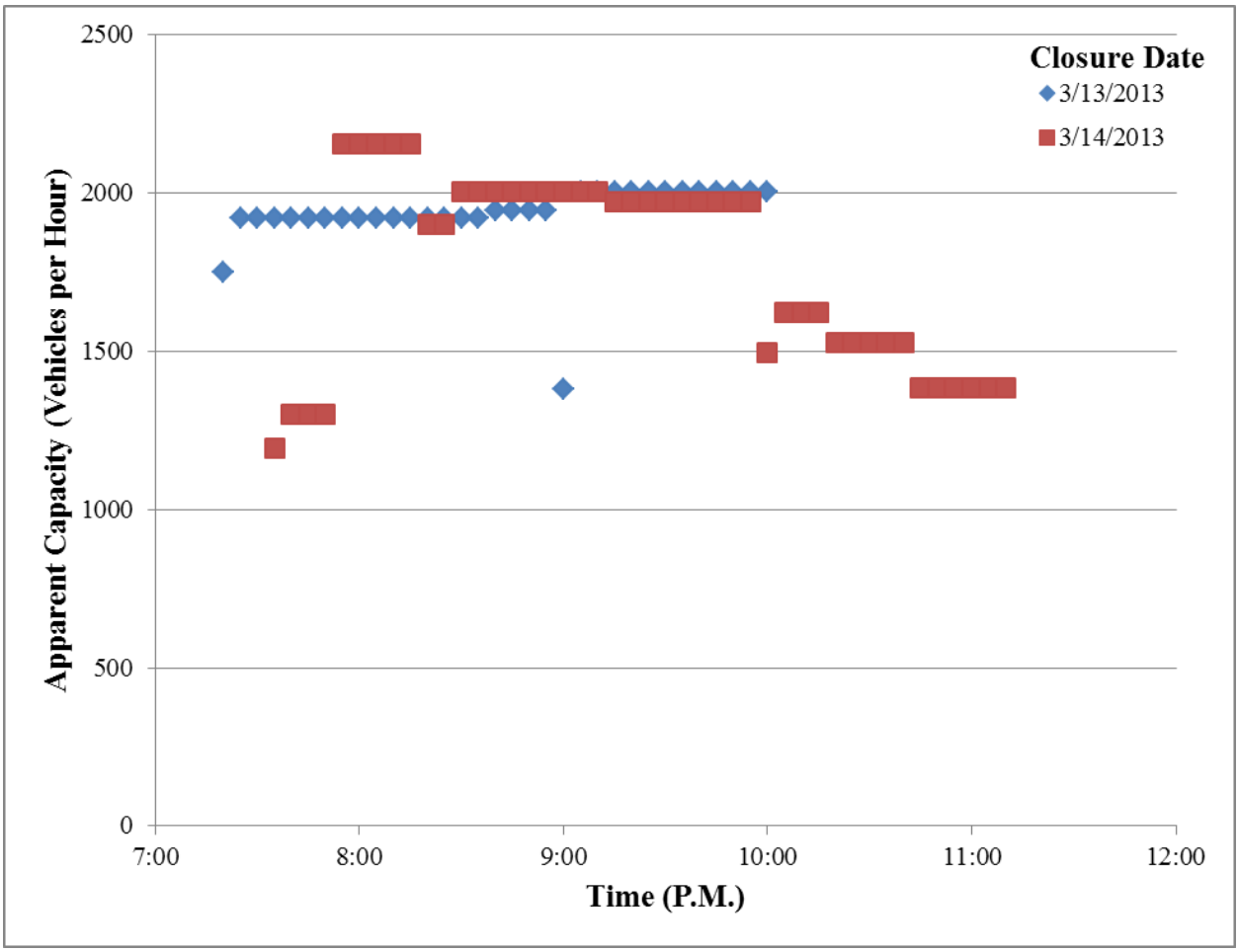

Figure 4. Apparent Capacity for Closure 937

When pairing the data above with the characteristics of the highway leading up to the lane closure, a potential explanation for the change in apparent capacity arises. Figure 5 displays a satellite image of closure 937. The blue dot labeled Lacy-Lakeview is the location of the volume sensor and the length of the closure runs from just before mile marker 344 to 347. Of note is that there are no major intersections between the volume sensor and the closure. Consequently, it is believed that most of the traffic measured at the upstream wavetronics sensor probably remained on the freeway up until reaching the traffic queue and lane closure. In other words, the demand volumes measured upstream are likely to be fairly accurate estimates of the approach volume at the lane closure and upstream end of the queue. However, most drivers are aware of the lane closure as they approach and are notified by the end of queue warning message displayed of portable changeable message signs (PCMS) deployed by TxDOT. With the knowledge of the approaching queue, it is likely that a significant portion of drivers exit the freeway to bypass the queue on the frontage road. This is the most probable cause of the rise in apparent capacity at the beginning of the closure.

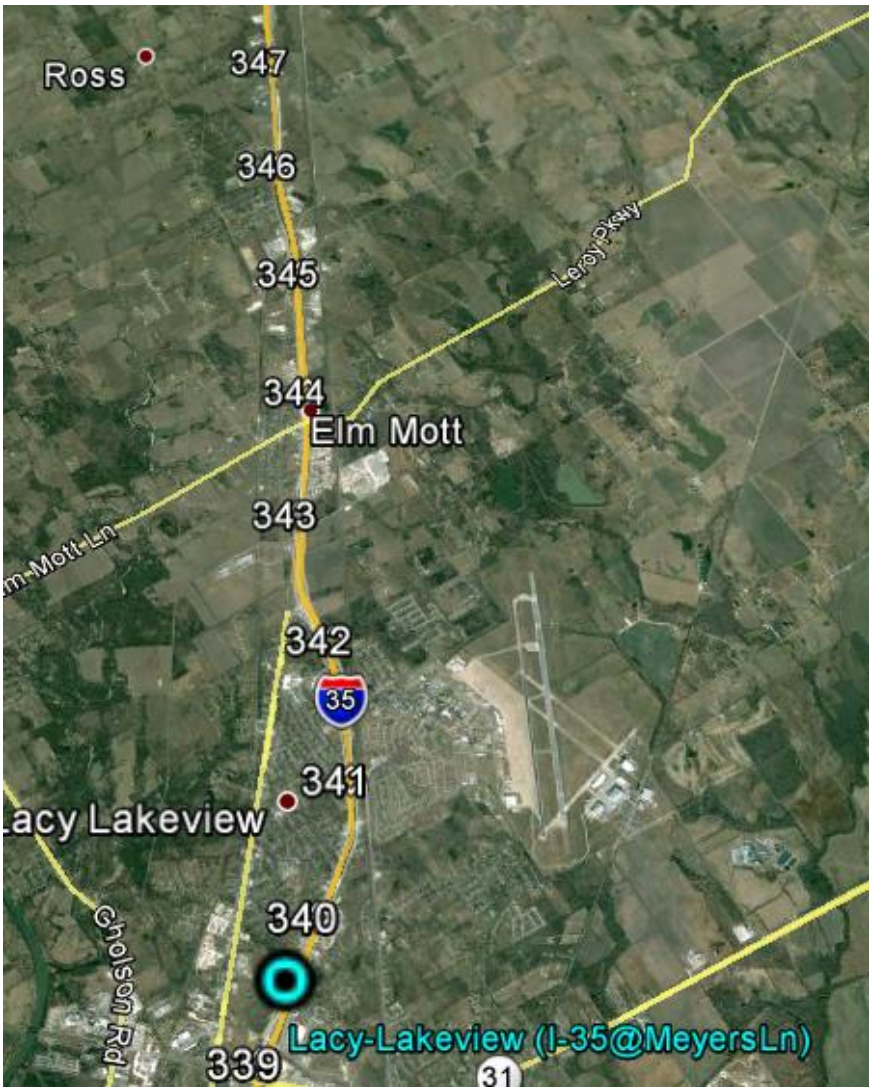

Figure 5. Map of Closure 937

Closure 1099 occurred in mid-May 2013, over the course of two days. The reason for this closure was to move the northbound traffic from the existing lanes to newly paved lanes. On the second night of data collected, the lane closure and queue began around 7:15 pm, and persisted for several hours until 11:00 pm. Unfortunately, the first night of data was incomplete. Sensor data from the end-of-queue system was not available until 10:00 pm, when the queue was already present. After some initial volatility in the apparent capacity computation process, it is evident that the apparent capacity values for the second night of the closure did become consistent with closure 937. Figure 6 shows the apparent capacities with respect to time. Although the first night of data was incomplete, a trend can still be identified. Because the queue was already present when the data began recording, the apparent capacity dropped to zero very early, due to the small number of iterations that had been performed. After more data became available, the apparent capacity began to converge near the same figure as the following night of data.

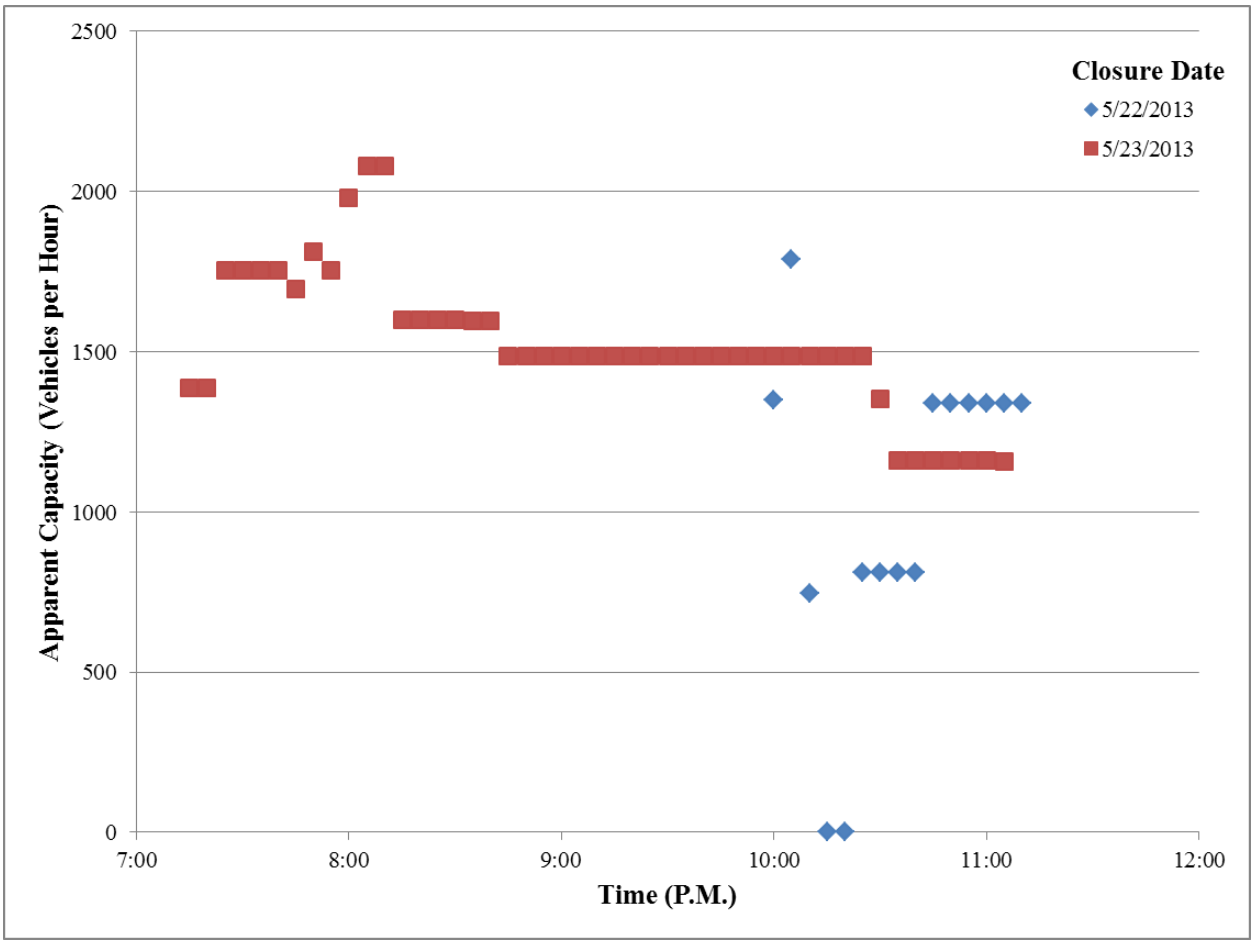

Figure 6. Apparent Capacity for Closure 1099

Figure 7 shows the area surrounding closure 1099, which runs from mile marker 347 to mile marker 353. The volume sensor for this closure is not pictured, but it is the same sensor that was used for closure 937, located between mile marker 339 and 340. Thus, much like for closure 937, there are no major intersections where large volumes of traffic may enter or exit the corridor. Since this closure was significantly longer than closure 937, it is possible that fewer drivers exited the freeway to attempt to bypass the queue, if they were notified via PCMS of the length of the closure, since that would involve driving on the frontage road for over six miles. This would help explain the slightly lower apparent capacity figures through closure 1099 when compared with closure 937.

Figure 7. Map of Closure 1099

The single lane closures demonstrate the same trend in capacity throughout the night. For both closures the capacity figure begins below the initial baseline estimate of 1500 vehicles per hour, before rising to around 2000 vehicles per hour, and then slowly tapering throughout the night eventually back down under 1500 vehicles per hour. The sharp rise at the beginning of the closure can most likely be contributed to drivers becoming aware of a queue forming, and exiting the freeway onto the access roads to avoid delays. If this is the case, the increase in apparent capacity would be due to a combination of traffic flow through the actual lane closures in addition to traffic diverted onto the frontage road, bypassing the lane closure. This would cause the capacity to appear higher than it actually is at that point. Eventually, the queue begins to build up, to sufficient length, causing enough vehicles to be stored in the queue that capacity is driven back down. Another possibility is that enough drivers may exit onto the frontage road that a queue may have formed there, decreasing the appeal of bypassing the lane closure.

One other potential contributing factor to the change in apparent capacity is the percentage of trucks traveling on I-35 at the time of closure. Figure 8 shows the apparent capacity compared with the percentage of trucks. Note that over the hours that the lane closures and queues were

monitored, the percentage of trucks in the traffic stream increased significantly from about 10 percent up to more than 30 percent. With the exception of a few outlying data points, a slight negative relationship is present. As the percentage of trucks rises, the apparent capacity decreases. The percentage of trucks most likely has a small effect on the apparent capacity for single lane closures, but it is difficult to determine to what extent, since there is not a strong correlation.

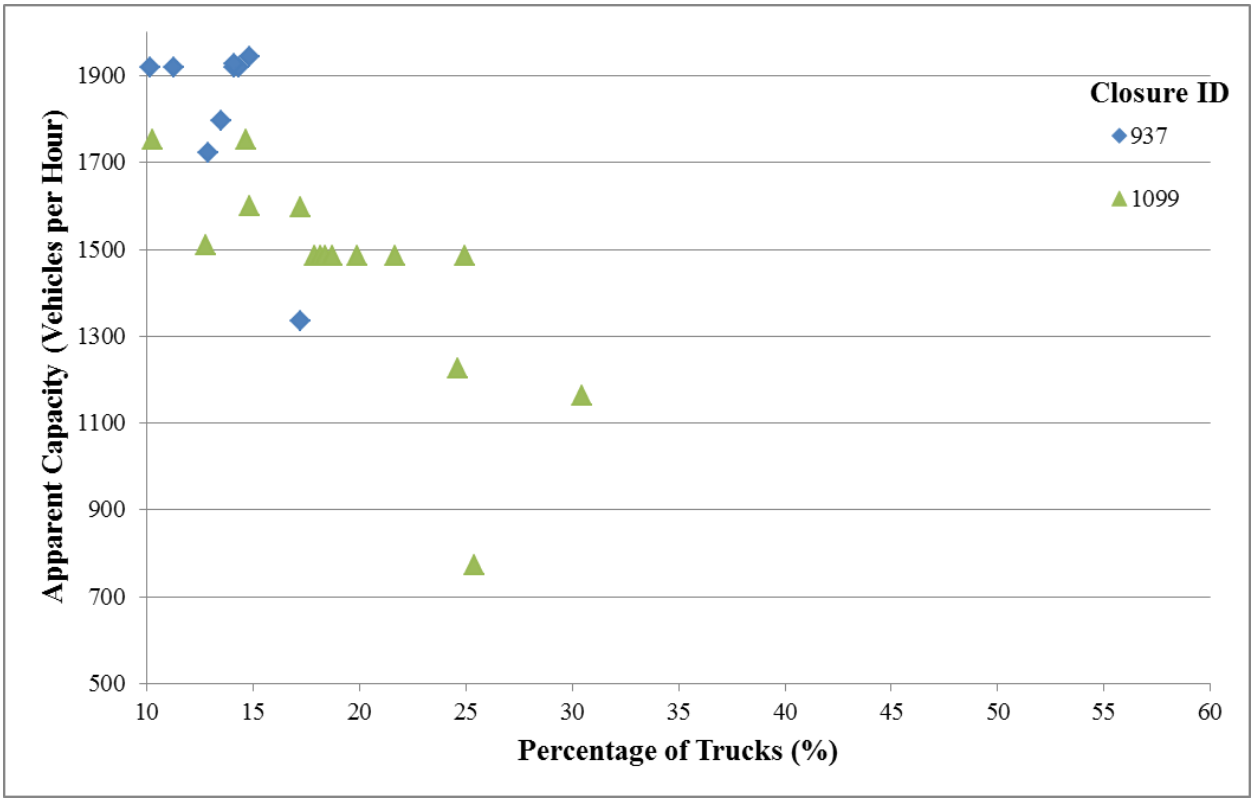

Figure 8. Single Lane Apparent Capacity vs. Truck Percentage

Full Road Closures

For the full road closure, the first day of data collection was again incomplete, leading to significantly different results between the two days of closures. Despite this fact, the second day, closure 1018, still provided trends consistent with those of the single lane closures.

Closure 948 occurred on April 10, 2013, and closure 1018 followed nearly two weeks later on April 23, 2013. According to the closure log, the reason for the full road closures was to demolish the County Line Road Bridge, which is an overpass that crosses I-35. Much like the previous analysis of single lane closures, the first day of data was incomplete. Figure 9 shows the second night of data shows a similar trend to the single lane closures, but without an increase of apparent capacity near the beginning of the closure.

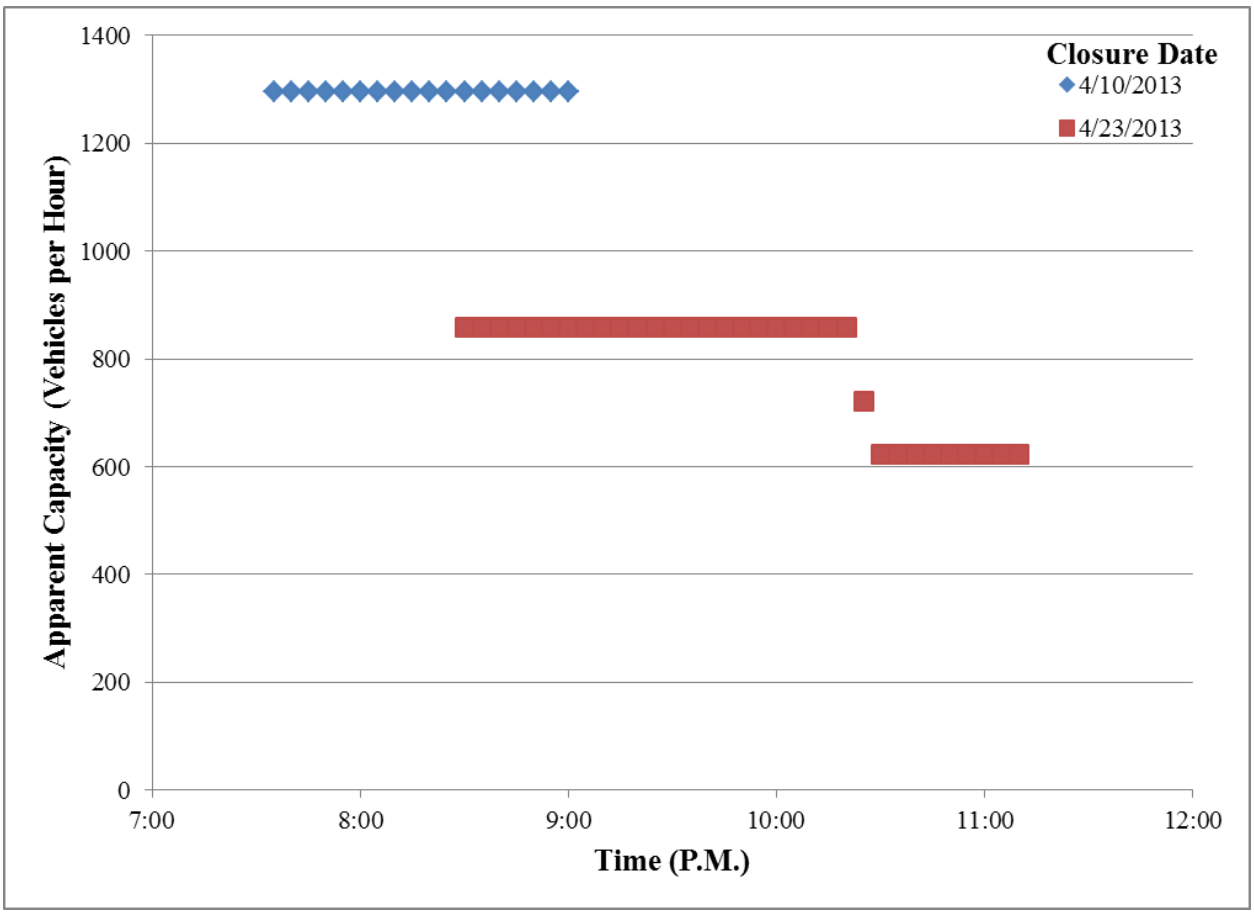

Figure 9. Apparent Capacity for Closures 948 and 1018

The physical characteristics of the road leading up to these closures are significantly different than those of the single lane closures. Closures 948 and 1018 run from mile marker 355 to mile marker 356 which, as shown in Figure 10, is about 2 miles north of the city of West, Texas. The volume sensor shown as a blue dot, labeled as West South, is three miles upstream from the location of the road closure. The entire town of West lies between the volume sensor and the beginning of the road closure, which introduces some unknown variability into the observation of apparent capacities. It is possible that a significant volume of vehicles may enter or exit between the sensor and lane closure, which may have led to the lower capacity number, but is impossible to know for certain.

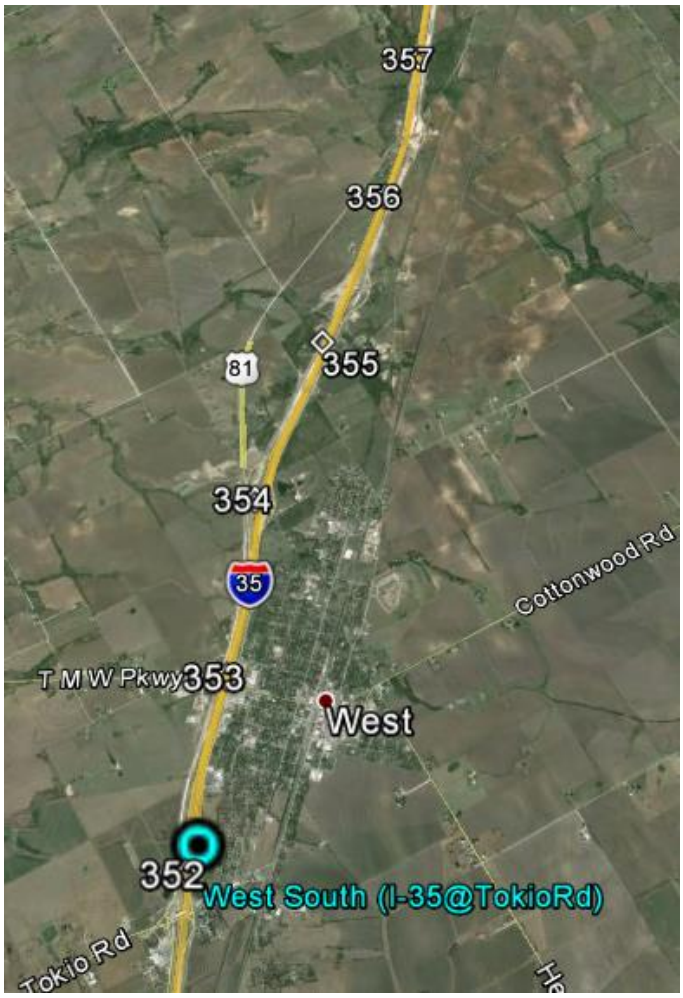

Figure 10. Map of Closures 948 and 1018

Due to the full road closure of closures 948 and 1018, the same diversions observed for the single lane closures cannot occur. Since all vehicles are forced off onto the frontage roads, there is no way for any vehicles to bypass the queue, other than to exit the I-35 corridor via a cross street that may lead to another nearby highway or street. This means the large volume of vehicles on I-35 must pass through a small intersection controlled only by a stop sign, or manually by a police officer directing traffic. This is why the apparent capacity is much lower than the presumed initial estimate of 1200 vehicles per hour. This is also why there is no early spike in apparent capacity.

As shown in Figure 11, on the night of closure 1018, the percentage of trucks ranges from 30 to 60 percent. Over this range, apparent capacity also drops significantly to around 650 vehicles per hour. This is a more significant drop, but in relation to the large rise in percentage of trucks, it suggests only a small amount of association.

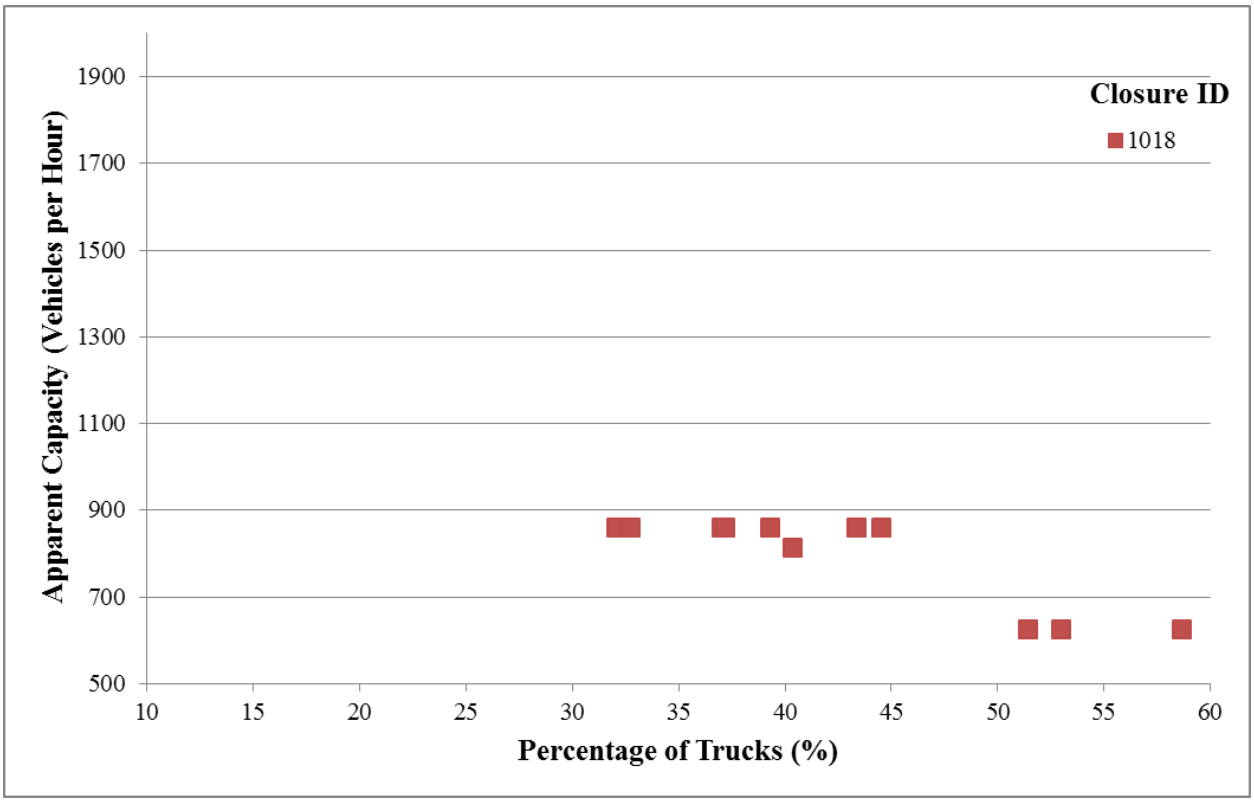

Figure 11. Full Road Closure Apparent Capacity vs. Truck Percentage

Composite

When analyzed as a whole, rather than individual closures on a nightly basis, trends emerge that display consistency for apparent capacity between lane closures. Figure 12 displays the three lane closures together with trend lines that show a steady decrease in apparent capacity through lane closures. The two single lane closures display the same initial rise in capacity, which then stabilizes, before trailing off as the queue dissipates. The full road closure shows the same results, but without the initial rise. It is also important to note that the initial rise in apparent capacity may also be due to the small data sample in the initial iterations of the computation of apparent capacity. The most important figure to analyze is the point at which the apparent capacity appears to stabilize or converge.

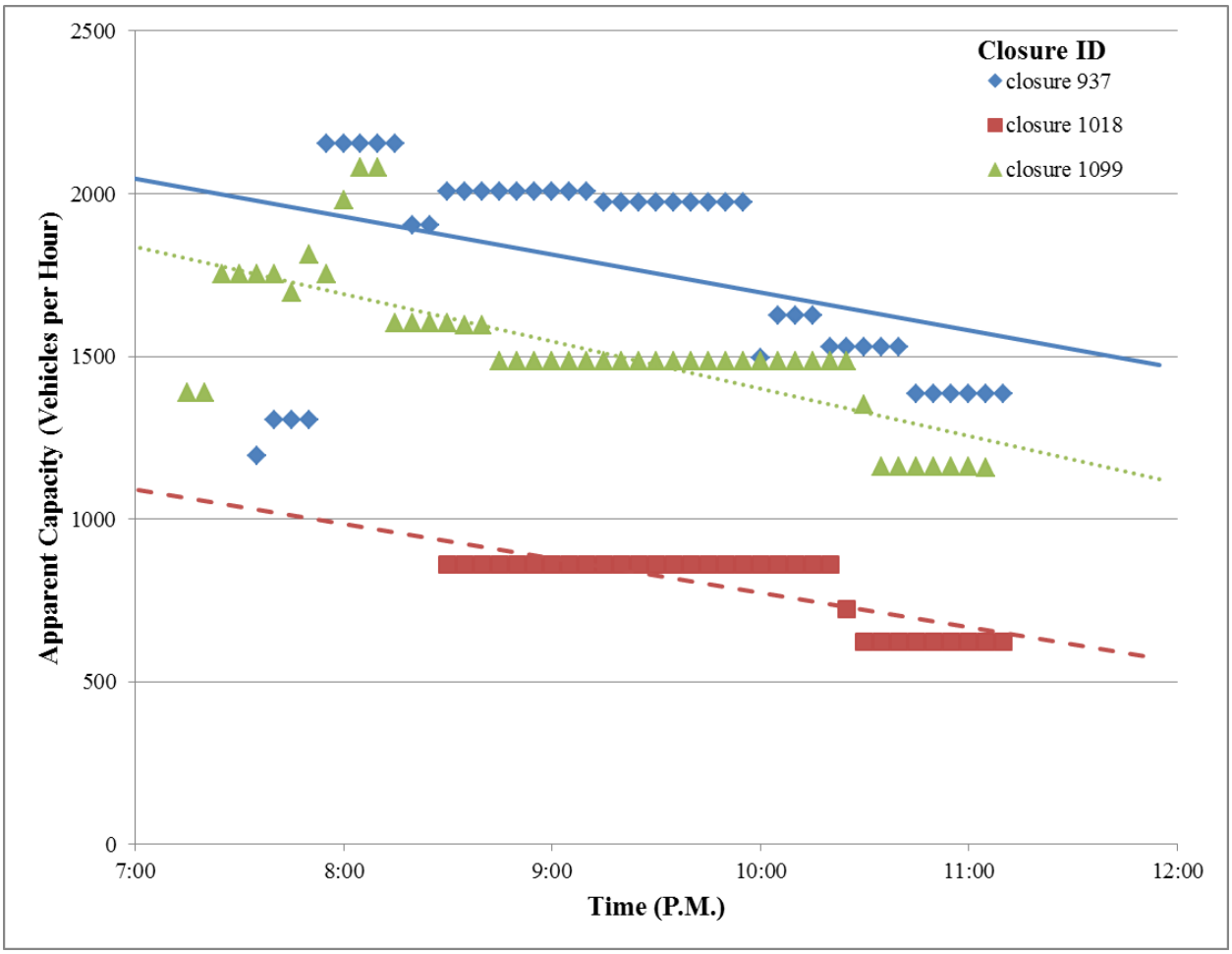

Figure 12. Capacities for All Second Day Closures

CONCLUSIONS

This research identified trends in the change of apparent capacity through work zone lane closures. Due to lack of complete data, the first nights of closures 948 and 1099 must be excluded in the findings of this research. Despite the exclusion of these figures, the remaining nights provide enough information to formulate conclusions.

Apparent capacity of single lane closures has been observed to rely more on the characteristics of the roadway leading up to the closure rather than the percentage of trucks on the road. Since vehicles have the opportunity to bypass the queue, the apparent capacity figures are inflated due to the discrepancy between volume of vehicles measured by the sensor, and actual volume of vehicles passing through the lane closure, rather than on the frontage road. While it is likely that the percentage of trucks has some effect on the apparent capacity, there is not enough data to support a claim to the extent of its effect.

The results for the full road closures proved similar to those of the single lane closures, but with several key differences. The physical characteristics of the roadway were shown to affect the apparent capacity, but for a different reason. As this is a full road closure, any drivers that

attempted to bypass the closure earlier on the frontage road will ultimately get caught in the queue as the rest of the I-35 traffic exiting due to the road closure. This even has the potential to cause more delay as they must merge back into the stream of traffic exiting I-35. As for the percentage of trucks, once again, while it is likely that it has some effect on the apparent capacity, the data indicates that it may affect full road closures less than single lane closures.

REFERENCES

1. TRB Committee on Highway Capacity and Quality of Service. *Highway Capacity Manual 2010*, Volumes 1 – 4. Transportation Research Board, Washington D.C. 2010.
2. Maze et al., *Capacity of Freeway Work Zone Lane Closures*, Mid-Continent Transportation Symposium 2000 Proceedings. Iowa Department of Transportation, 2000.
3. Krammes, R.A. and G.O. Lopez. *Updated Short-Term Freeway Work Zone Lane Closures Capacity Values.* Prepared by the Texas Transportation Institute for the Federal Highway Administration and for the Texas Department of Transportation, Austin, TX, Report No. FHWA/TX-92-/1108-5, 1992.

Operational Effects of Chevrons on Horizontal Curves Using Speed and Energy Differentials and Speed Profiles

Prepared for
Undergraduate Transportation Scholars Program

by

Mark Membreño
Senior Civil Engineer Student
Texas A&M University

Professional Mentor:
Bradford K. Brimley
Graduate Research Assistant
Texas A&M Transportation Institute

Program Director
H. Gene Hawkins, Jr., Ph.D., P.E.
Associate Professor, Zachry Department of Civil Engineering
Research Engineer, Texas A&M Transportation Institute
Texas A&M University

Program Sponsored by:
Southwest Region University Transportation Center

August 8, 2013

STUDENT BIOGRAPHY

Mark Membreño is currently a senior civil engineering student at Texas A&M University. He will be graduating in December 2014. He has been awarded the 2009-2010 National Hispanics Recognition Program Scholar. He is also currently a member of the Golden Key International Honour Society and Alpha Chi Honor Society and has received the Dean's List from Spring 2012 to Spring 2013.

His parents are from Nicaragua, and he visits once or twice a year. Since the summer of 2009, he has worked at a mission in the northern side of the country as a translator and construction worker to help the surrounding community. The projects ranged from constructing houses and school, conducting medical brigades, mentoring the local youth, and drilling water wells. He desires to return one day after working in the States to help in urban and rural development of the country as a consultant or in a similar capacity. Currently, he is committed to go to Officer Candidate School of the US Navy to become an officer in the Civil Engineer Corps right after graduation. After leaving the US Navy, he plans to pursue a Master's degree in Construction Management.

ACKNOWLEDGMENT

The research described in this paper was funded by Project 03-106 of the National Cooperative Highways Research Program. The research activities were conducted in support of the Undergraduate Transportation Scholars Program. The findings and recommendations included in this paper are based on the student's summer activities. The contents of this paper reflect the views of the author, who is responsible for the facts and the accuracy of the data presented herein. The contents do not necessarily reflect the official view or policies of SWUTC.

The author would like to express his love to his family, especially his parents and brother. Without them he would not be where he is today. There are no words to describe his undying gratitude towards them. Also, to his brothers of Sigma Lambda Beta International Fraternity, Inc., for all the great experiences and memories made with them at his time here and yet to be made. They are his family, and he thanks them for everything they have done for him.

SUMMARY

The current study focused on evaluating the effectiveness of chevrons on horizontal curves based on different measures of effectiveness (MOEs). Different TCD combinations (chevrons vs. no chevrons) were compared on different curves with similar geometric characteristics by test subjects' driving behavior. The MOEs measured are as follows:

- Speed and kinetic energy differentials
- Percent speed and energy reduction within curve
- Speed profiles

The study was conducted on a 16 mile section of FM 3090 near Navasota, Texas with 12 study participants over a period of two days. The subjects' ages are classified as young and old. The test subjects were provided with a Texas A&M Transportation Institute (TTI) test vehicle to navigate the course. The vehicle was equipped with instruments that included a GPS receiver. Both daytime and nighttime test runs were performed.

The tasks included the following:

- Reduce the gathered data with MATLAB
- Extract and analyzed the data
- Evaluate the effectives of the TCD combinations

Concerning the speed and energy differentials, the study revealed no consistent correlation between curves with chevrons and the differentials. In some instances the curves with chevrons provided higher differentials while in other situations the opposite was found. This variability in results was also shown in the percent reduction analysis. The inconsistency in the results may be because different curves were compared and in turn introduced uncontrolled variables that affected the results. It is suggested that the proximity of the previous curve and the operating speed of the driver approaching the curve were confounding factors. The night time drivers experienced higher differentials on average than their counterparts. Regarding the speed profile analysis, it can be seen that the curves with chevrons provided advance warning and better delineation. This resulted in less severe deceleration rates to the appropriate speed for curve navigation.

TABLE OF CONTENTS

LIST OF FIGURES

LIST OF TABLES

INTRODUCTION

The safety of drivers on horizontal curves has been a continuing focus of study. Horizontal curves tend to experience a larger number of crashes than tangents. In an effort to improve safety at these locations, traffic control devices (TCDs) can be installed to provide drivers advance warning or additional delineation while navigating the curve. Numerous studies have analyzed the benefit of various TCDs using multiple measures of effectiveness (MOEs).

Table 2C-5 of the 2009 MUTCD, shown in Figure 1, provides some guidelines on using TCDs for horizontal curves (*1*).

Table 2C-5. Horizontal Alignment Sign Selection

Type of Horizontal Alignment Sign	Difference Between Speed Limit and Advisory Speed				
	5 mph	10 mph	15 mph	20 mph	25 mph or more
Turn (W1-1), Curve (W1-2), Reverse Turn (W1-3), Reverse Curve (W1-4), Winding Road (W1-5), and Combination Horizontal Alignment/Intersection (W10-1) (see Section 2C.07 to determine which sign to use)	Recommended	Required	Required	Required	Required
Advisory Speed Plaque (W13-1P)	Recommended	Required	Required	Required	Required
Chevrons (W1-8) and/or One Direction Large Arrow (W1-6)	Optional	Recommended	Required	Required	Required
Exit Speed (W13-2) and Ramp Speed (W13-3) on exit ramp	Optional	Optional	Recommended	Required	Required

Note: Required means that the sign and/or plaque shall be used, recommended means that the sign and/or plaque should be used, and optional means that the sign and/or plaque may be used.

See Section 2C.06 for roadways with less than 1,000 ADT.

Sect. 2C.06 to 2C.07 December 2009

Figure 1. Table 2C-5 of the 2009 MUTCD 2nd Rev.

Specifically, chevrons are designed to provide advance warning to drivers of approaching curves and delineate the curve. It is hypothesized that drivers will experience a higher speed reduction at curves where chevrons are present as well as less severe deceleration because clearer advance warning is provided. This study seeks to evaluate the effectiveness of chevrons in their use in horizontal curves using the propose MOEs.

BACKGROUND

In an effort to address the high percentage of accidents occurring on horizontal curves, studies analyze TCDs through various MOEs to improve driver behavior and safety of the curve. One of the most common MOEs analyzed is operating speed on a curve. Researchers have sought to model speeds on curves based on geometric criteria as well as how effective TCDs are in reducing operating speeds to improve safety. One such model was developed by Bonneson et al. (*2*) which Miles and Pratt (*3*) evaluated that predicts operating speed in order to be able to place more appropriate advisory speeds for curves. The accurate advisory speeds would maintain driver's respect for the advisory speed, reduce the number of required signs, and reduce installation/maintenance costs.

Along with speed differentials, Pratt and Bonneson recommend evaluating curve severity through the concept of kinetic energy differentials (*4*). The idea is related to the side friction demand on the tire to prevent skidding on a curve. The severity of a curve is closely tied to a level of energy reduction when speed is reduced. In other words, a 10 mph reduction traveling at a 60 mph tangent speed may create more risk than a 10 mph reduction traveling at an initial speed of 40 mph, because more energy is dissipated during that deceleration.

While such models provide accurate predicted speeds for highway design, Misaghi (*5*) discovered that speed distributions are not uniform throughout the path of the curve. Furthermore, among the numerous models developed by researches, there seems to be no universally acceptable model utilized for operating speeds on curves (*6*). The inconsistency of models can be due to the local conditions at the time of the study. Also, the demographics of the population, climate of the region, and other regional characteristics of the location may have significant impact on the model.

Studies have also examined the acceleration and deceleration of vehicles in navigating curves to determine the level of safety. A study by Fambro et al. (*7*) focused on drivers' behavior specifically in braking with and without an Automatic Braking System (ABS) and dry/wet conditions on a closed course. The results indicated that there is no significant difference in braking distances between tangent and curve sections. Hu and Donnell (*8*) analyzed acceleration and deceleration profiles of drivers as they maneuver curves. They discovered that not all the acceleration and deceleration occurs solely on the tangents as previously assumed. While the majority of the time spent accelerating and decelerating does happen on the tangents, there is a significant portion that occurs within the curve itself. Furthermore, the deceleration profile is not constant (*7*).

The safety of horizontal curves is improved through installation of various types of TCDs. vast research has been conducted to analyze their effect on safety. Arien et al. (*9*) analyzed the effects of pavement marking width, transverse rumble strips (TRS), and herringbone patterns (HP) on the reduction of speed from tangent to curve sections. An increase in pavement marking width did not significantly reduce speed. However, TRS and HP both caused the driver to reduce speed and decelerate earlier, and TRS proved to be more effective than the HP. Chevrons are commonly used to delineate curves. Chevrons not only aid the driver in reducing speed and driving smoother within curves, they provide positive guidance which helps the driver navigate the curve more calmly than if chevrons were not present (*10*). Ré et al. (*11*) conducted a study of chevrons and chevrons with full retroreflective signposts and their effectiveness in speed reduction. Both situations significantly lowered the mean speed during curve navigation in comparison to the baseline. While the fully treated chevrons lowered the mean speed more than the ordinary chevrons, the difference is unsubstantial. Therefore, no changes were recommended for the MUTCD and that the chevrons with full retroreflective signposts should remain as optional. Charlton (*12*) studied the effect of warning signs with combinations of other TCDs. Warning signs by themselves did not yield any significant speed reduction for curve navigation. Chevrons provided the most effective speed reduction with warning signs than any other TCD with rumble strips as another significant method. Gates et al. (*13)* evaluated the effect of fluorescent yellow chevrons in speed reduction. The fluorescent yellow chevrons provided an extra 1 mph speed reduction in comparison to its counterpart in both mean and 85^{th} percentile

speed. Various other TCDs such as delineators are utilized to reduce speed for drivers within curves. Chrysler et al. (*14*) found delineators did reduce speed but there was no difference between single and double delineators. Furthermore, drivers could not distinguish between delineator colors and their meaning in curves.

In addition to the presence of a device improving safety, some researchers have investigated the effect of spacing for delineation-type devices. Carlson et al. (*15*) and Chrysler et al. (*14*) analyzed the impact of chevron and delineator placement and spacing on driver behavior. Both studies found that uniform spacing within the curve and increased number of signs provides benefits in the reduction of speed and consistency of steering within curves. Also, placing them on the tangent section before the entrance of the curve further improves the safety of the curve. Carlson et al. (*15*) proposed two methods to determine chevron and delineator spacing: advisory speed method and GPS method. These methods provide clear and more consistent criteria for spacing than the current MUTCD.

RESEARCH APPROACH

The experiment gathered data from test runs of the participants on an open-road course with a vehicle provided by TTI. The study took place over two days at both day and night times.

Course

The course consists of a 16 mile section of highway on FM 3090. This section of road contains many curves with varying geometric features. Only 11 "study" curves were selected due to their severity, current state of TCD configuration, and geometric features. Points of interest (POI) were identified for study and included all the points of curvature, points of tangency, midpoints, and points along the tangent before and after the PC and PT at set distances. Figure 2 displays the 16 mile stretch of FM 3090. Table 1 lists the study curves and their basic characteristics. The curves were matched in pairs based on geometric characteristics, one with Chevrons and the other without. Table 2 lists the paired curves used for analysis. Curve 2 is paired with both Curve 1 and 7 because of similar characteristics. However Curve 1 and 7 are not similar enough to warrant these curves be paired.

Driver Selection

Twelve drivers participated in the study with both young and old drivers. The ages for the young drivers ranged from 19 – 24 while the ages for the old drivers ranged from 58 – 82. Table 3 lists the drivers' characteristics and the time of day they participated in.

Equipment

The vehicle was equipped with a GPS receiver that records the position of the vehicle in a frequency of 10 Hz. Data from the GPS receiver provided speed and longitudinal acceleration throughout the highway section.

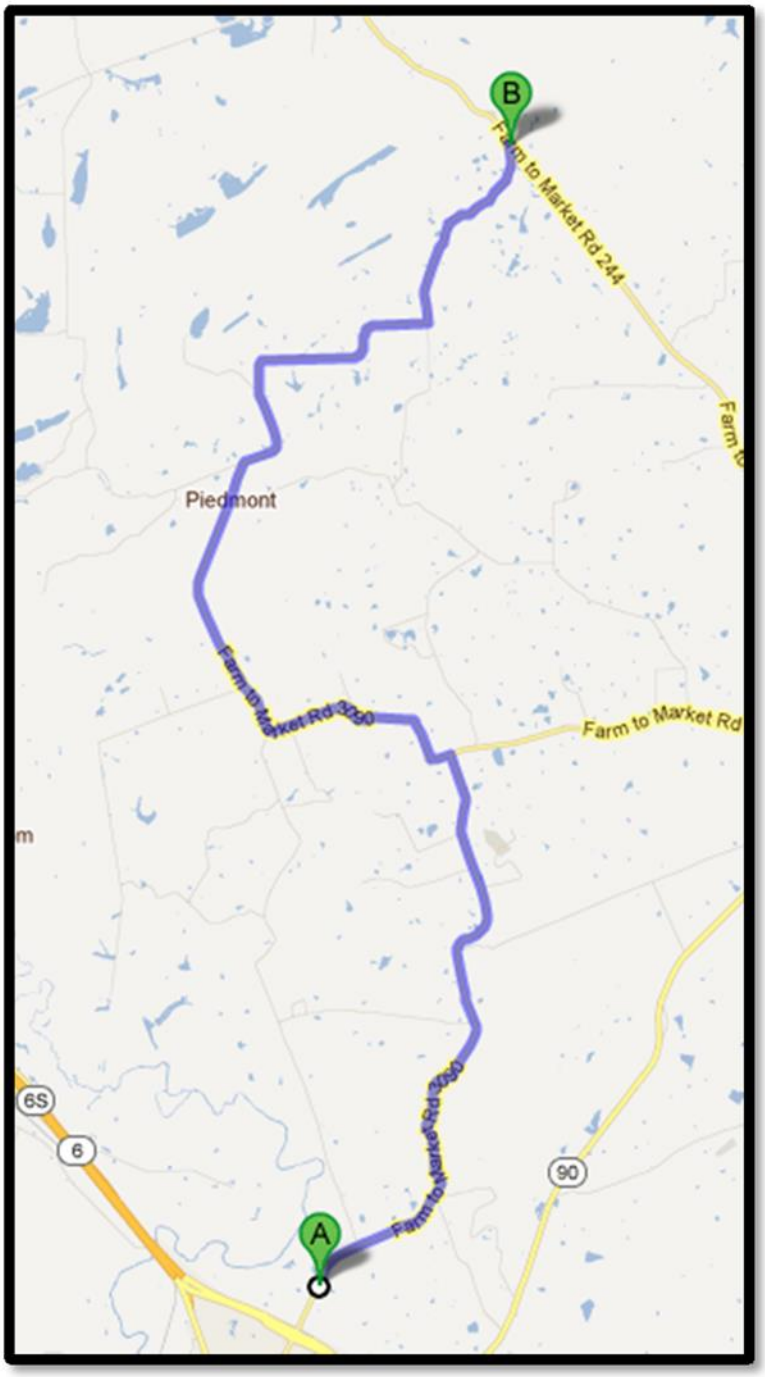

Figure 2. FM 3090

Table 1. Horizontal Curve Characteristics

Curve	Radius (ft)	Deflection (degrees)	Length (ft)	Superelevation (degrees)*	Warning Sign*	Posted Adv. Speed (mph)*	Use of Chevrons*
1	444	89.9	802	3.6/9.9	Curve	35	Yes
2	467	83.7	765	4.6/4.7	Reverse Curve	35	No
3	400	65.4	575	5.7/5.2	Curve	30	Yes
4	391	90.0	584	10.3/8.1	Turn	30	No
5	366	40.8	302	NA/5.5	Curve	35	Yes
6	337	48.8	389	4.8/4.9	Curve	35	No
7	496	72.1	741	8.8/5.0	Curve	40	Yes
8**	284	86.4	558	7.4/6.5	Turn	30	Yes
9**	380	47.8	412	6.1	Winding Road	35	No
10	371	89.2	694	9.7/6.2	Turn	30	No
11	54	82.8	111	-0.9/0.1	Turn	15	Yes/No
Max.	1,247	90.0	1,030	13.5/9.9			
Mean	562	51.5	481	5.8/5.6			
Min.	54	12.9	111	-0.9/0.1			

* Superelevation, warning sign, posted advisory speed, and chevrons may have two entries: one for each direction, outbound and inbound.
** Only the inbound direction is used for analysis for Curve 8 and 9

Table 2. Paired Curves

Pair	Chevrons	No Chevrons
1	1	2*
2	3	4
3	5	6
4	7	2*
5	8-In	9-In / 10
6	11-Out	11-In

* Curve 2 is paired twice

Table 3. Test Subject Profiles

Participant	1	2	3	4	5	6	7	8	9	10	11	12
Date	12/11/2012						12/12/2012					
Gender	M	F	F	F	F	M	M	F	M	F	M	M
Age	74	73	24	19	67	58	24	70	82	66	63	24
Day/Night	Day	Day	Day	Night	Night	Night	Day	Day	Day	Night	Night	Night

DATA ANALYSIS

The following MOEs were used in the study:

- Speed differentials of test subjects
- Energy differentials
- Percentage of speed and energy reduction in curve

Speed Differentials

From the GPS data, the maximum speed from of the tangent section up to 1000 feet from the PC (if applicable to certain curves with the allowable lengths), the speed at the PC, and the minimum speed within the curve were analyzed. The mean and standard deviation for the speed results were calculated for each pair of curves and their respective outbound/inbound directions. The differentials between these three speeds were calculated.

Energy Differentials

The speeds used to calculate the energy differentials are the same as the speed differentials. In this way, the speed and energy differentials can be compared. In the study, specific energy was used in order to remove the mass from the analysis with the following formula. The energy differentials were constructed using the same speed data for each study curve.

$$e = \frac{1}{2}v^2$$

Where e = specific energy (mph^2)
v = velocity (mph)

Percent of Speed and Energy Reduction within Curve

From the speed and energy differentials, the percent of speed reduction and energy dissipation occurring within the curve was calculated. The ideal situation is to have as much reduction occur before the PC. Therefore we compared the differentials between the maximum and minimum speeds with the differentials between the PC and the minimum speeds. The mean and standard deviation for each pair of curves were calculated for the analysis.

$$\%\ Reduction = \frac{PC - Min\ Diff}{Max - Min\ Diff} * 100\%$$

Where % Reduction = percent of speed or energy reduced within curve
PC – Min Diff = differential between the PC and minimum curve speed
Max – Min Diff = differential between the maximum and minimum speed

Speed Profiles

From the GPS data, speed profiles were constructed to display the behavior of drivers as they approach and navigate curves. The speed profiles are high resolution due to the GPS tracker's 10 Hz frequency. The speed profiles display a distance of to 1000 feet before the PC to the PT.

RESULTS AND DISCUSSION

The following section discusses the results for the MOEs: speed and energy differentials, percent speed and energy reductions, and speed profiles. Calculating the difference of the averages of all curves between day and night time drivers, night time drivers experience higher reduction on the maximum and minimum differentials with 0.2 mph and 43.2 mph^2. The same is true with the PC and minimum differentials with 0.1 mph and 24.0 mph^2. In the tables that summarizes the results, the curve pairs are within the heavier weighted borders for easier distinction. Curve 2 is listed twice in the tables since it is paired with both Curve 1 and 7.

Speed and Energy Differentials

The following are the results of the speed and energy differentials. A comparison between day and night shows that the night time participants on average experience a higher differential than day time drivers.

Speed

The speed differentials of paired curves were analyzed to evaluate the effectiveness of chevron presence for horizontal curve navigation. The mean and standard deviation are compared. Table 4 summarizes the results of the study and data reduction of the speed differential MOE.

There was variability in the results across the table. No significant pattern showed through the paired curves. For example, sometimes the curve with chevrons yielded lower speed reductions while other instances only a certain direction yielded a significant reduction. Furthermore, it seems that the proximity of the previous curve to the outbound or inbound direction is a greater factor to speed reduction than the presence of chevrons on the curves. For example, Curve 2 has no chevrons but experiences a much less speed reduction in the inbound direction from its close proximity to Curve 11. Figure 3 and Figure 4 illustrate the variability of the results for the speed differentials for both the maximum tangent and minimum speed as well as the differential between the PC and minimum speed. The white bars denote the averaged results of the day time participants while the solid bars show the night time participants.

Table 4. Speed Differential Results

			Max – Min (mph)				PC – Min (mph)			
Curve	**Chevrons**	**Direction**	**Day Avg.**	**Day Std.**	**Night Avg.**	**Night Std.**	**Day Avg.**	**Day Std.**	**Night Avg.**	**Night Std.**
1	Yes	Out	14.4	3.7	12.8	1.6	6.5	3.2	4.3	1.7
	Yes	In	16.3	4.8	18.6	2.4	7.2	4.1	8.7	3
2	No	Out	22.6	4.6	20.4	3.4	5.3	1.4	9.2	3.6
	No	In	10.8	2.9	12.2	2.3	6.9	2.2	9.5	1.9
3	Yes	Out	10.8	4.4	14.6	4.3	4.5	2.9	5.6	2.2
	Yes	In	16.7	2.4	14.5	3.9	5.6	2.9	6	1.8
4	No	Out	18.6	4.7	18.3	3.7	7.4	3.1	4.7	3.3
	No	In	15.1	2.6	16.6	3.4	5	1.7	5.1	2.6
5	Yes	Out	11.3	2.7	14.9	2	7	3	6.3	2.1
	Yes	In	16.9	4.9	15.4	3.8	4.7	2	4.4	1
6	No	Out	20.9	3.8	19.3	5.6	5.7	1.3	6.3	2.3
	No	In	17	4.1	15.5	4.2	9.3	4.7	10.6	3.9
7	Yes	Out	12.4	4.2	14.9	3.3	7.9	4.1	7.3	2.6
	Yes	7.785	2.7	7.7	1.1	2.6	4	2.2	3.7	1.9
2	No	Out	22.6	4.6	20.4	3.4	5.3	1.4	9.2	3.6
	No	In	10.8	2.9	12.2	2.3	6.9	2.2	9.5	1.9
8	Yes	In	17.6	3.5	18.9	4.2	7.4	2.3	6.7	1.5
9	No	In	15.6	4.1	16.2	2.5	6.8	2.2	6.9	2.5
10	No	Out	15.1	2.4	14.2	2.8	8.4	4.3	7	1.8
	No	In	18.6	4.7	16.8	3.8	7.3	4	6.6	3.7
11	Yes	Out	37.7	3.8	37.3	5.7	9.2	1.9	9.9	2.5
	No	In	35.2	4.2	37.1	3.3	8.9	3.4	12.6	6

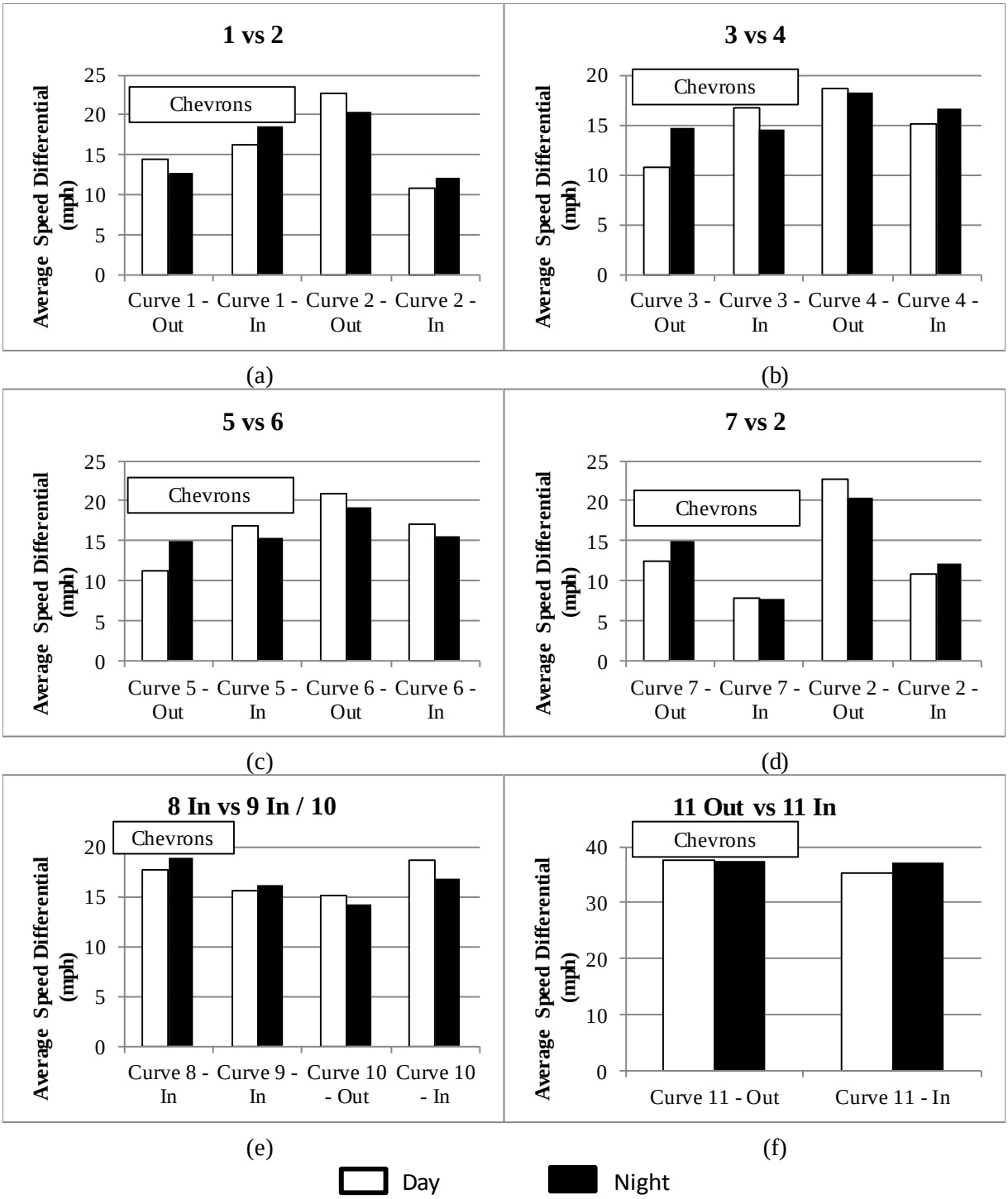

Figure 3. Maximum and Minimum Speed Differentials

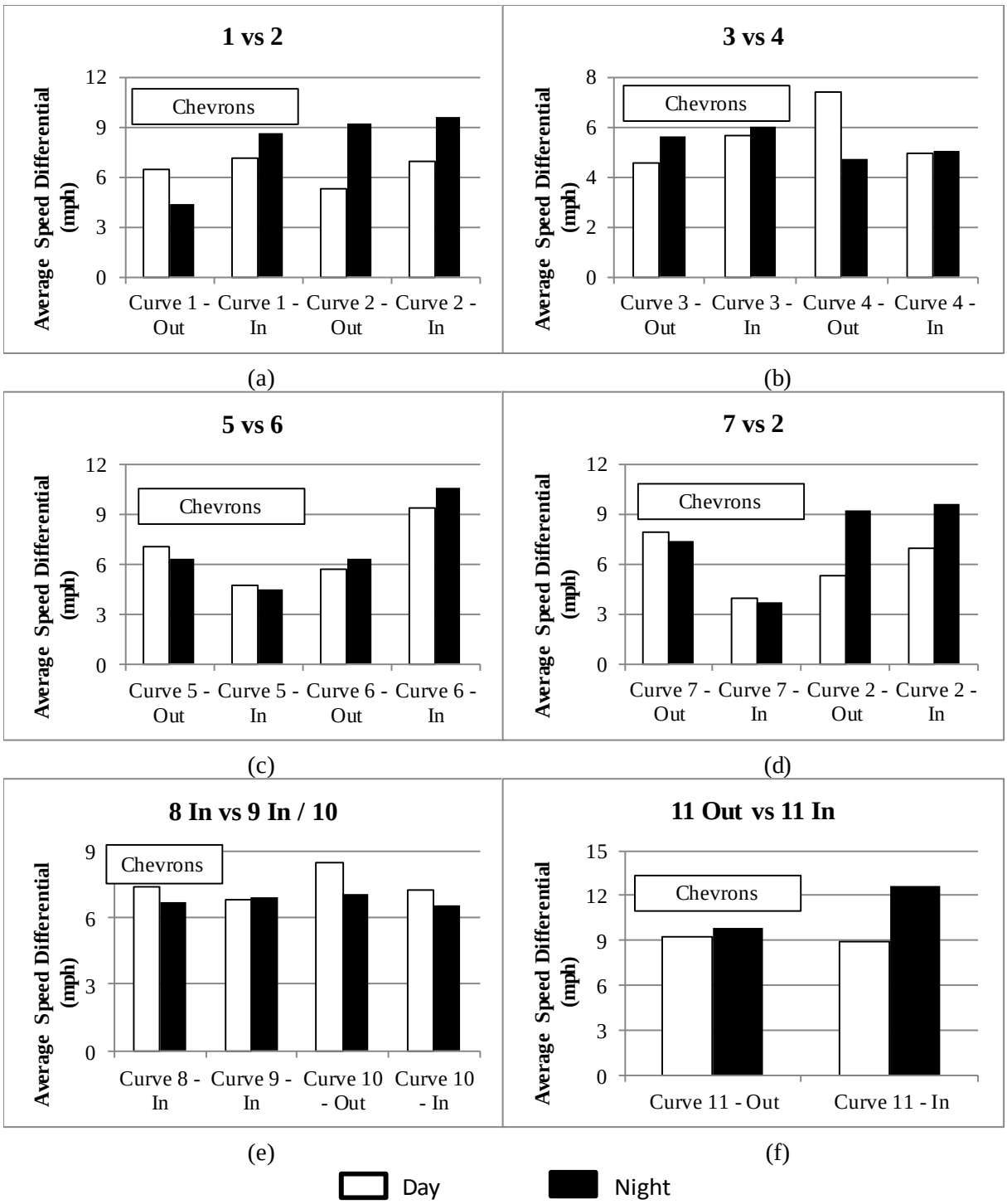

Figure 4. PC and Minimum Speed Differentials

Energy

The kinetic energy differentials were analyzed as a supplement to the traditional speed differential approach. The mean and standard deviations are derived from the twelve participants. Table 5 summarizes the results of the energy differential MOE.

Table 5. Energy Differential Results

			Max – Min (mph^2)				PC – Min (mph^2)			
Curve	**Chevrons**	**Direction**	**Day Avg.**	**Day Std.**	**Night Avg.**	**Night Std.**	**Day Avg.**	**Day Std.**	**Night Avg.**	**Night Std.**
1	Yes	Out	565.8	141.5	530.8	70.4	227.9	111.1	163.2	66.7
	Yes	In	696.1	250	795.5	116.8	271.6	159.2	335	144.3
2	No	Out	1021.4	217.2	1005.9	197.7	192.5	57.4	409.2	191.8
	No	In	407.7	121.3	516.1	109.2	247.8	86.6	392.7	93.3
3	Yes	Out	413.4	179.9	592.4	201.1	158	101.8	202.5	86.8
	Yes	In	629.2	123.7	575.6	167.4	185.9	103.8	210.9	68.2
4	No	Out	769.5	217.9	800	191.3	264.1	117.8	176.5	130.1
	No	In	592.9	127.7	691.3	153.2	169.4	60.8	180.6	92.2
5	Yes	Out	468	117.7	621.7	107.1	278.2	123.8	236.5	80
	Yes	In	691.8	240.3	629.5	179.5	165.3	76.8	157	42.3
6	No	Out	918.3	173.5	915.9	284.1	207	52	259.5	101.8
	No	In	705.2	195	667.9	227.1	355.2	193.6	432	178.2
7	Yes	Out	527.5	193.9	645.7	175.9	317.5	168.5	289.2	108.5
	Yes	In	287.3	100	284.6	45.9	138	75.5	127.4	64.6
2	No	Out	1021.4	217.2	1005.9	197.7	192.5	57.4	409.2	191.8
	No	In	407.7	121.3	516.1	109.2	247.8	86.6	392.7	93.3
8	Yes	In	689.7	173	755.6	200.6	252	89.7	224.2	55.3
9	No	In	671.2	217.8	741.1	153	262.4	91.5	282.7	108.8
10	No	Out	595.1	118.5	590.3	140.3	309.4	175.7	266.2	74.9
	No	In	797.5	236	787.1	213.9	275.6	161.5	273.9	158.1
11	Yes	Out	1223.7	115.9	1287.8	273.2	166.4	18.9	204.2	56.8
	No	In	1076.3	153.1	1178	145	156.8	61.5	258.5	163.4

The study did not show the expected results. It was assumed that for the curves with chevrons, there would be less energy dissipated within the curve than their counterparts. Again, there was variability throughout all of the curve pairs. For the differential between the maximum tangent and minimum speed, Curve 3 had the differentials for both directions lower than its counterpart. However for Curve 7, only the inbound direction was lower than both directions of Curve 2. Again, it seems that the proximity of the previous curve is a significant factor in the energy differentials as with Curve 2 inbound. Figures 5 and 6 illustrate the variability of the results for the energy differentials for both the maximum tangent and minimum speed as well as the differential between the PC and minimum speed. The white bars denote the averaged results of the day time participants while the solid bars show the night time participants.

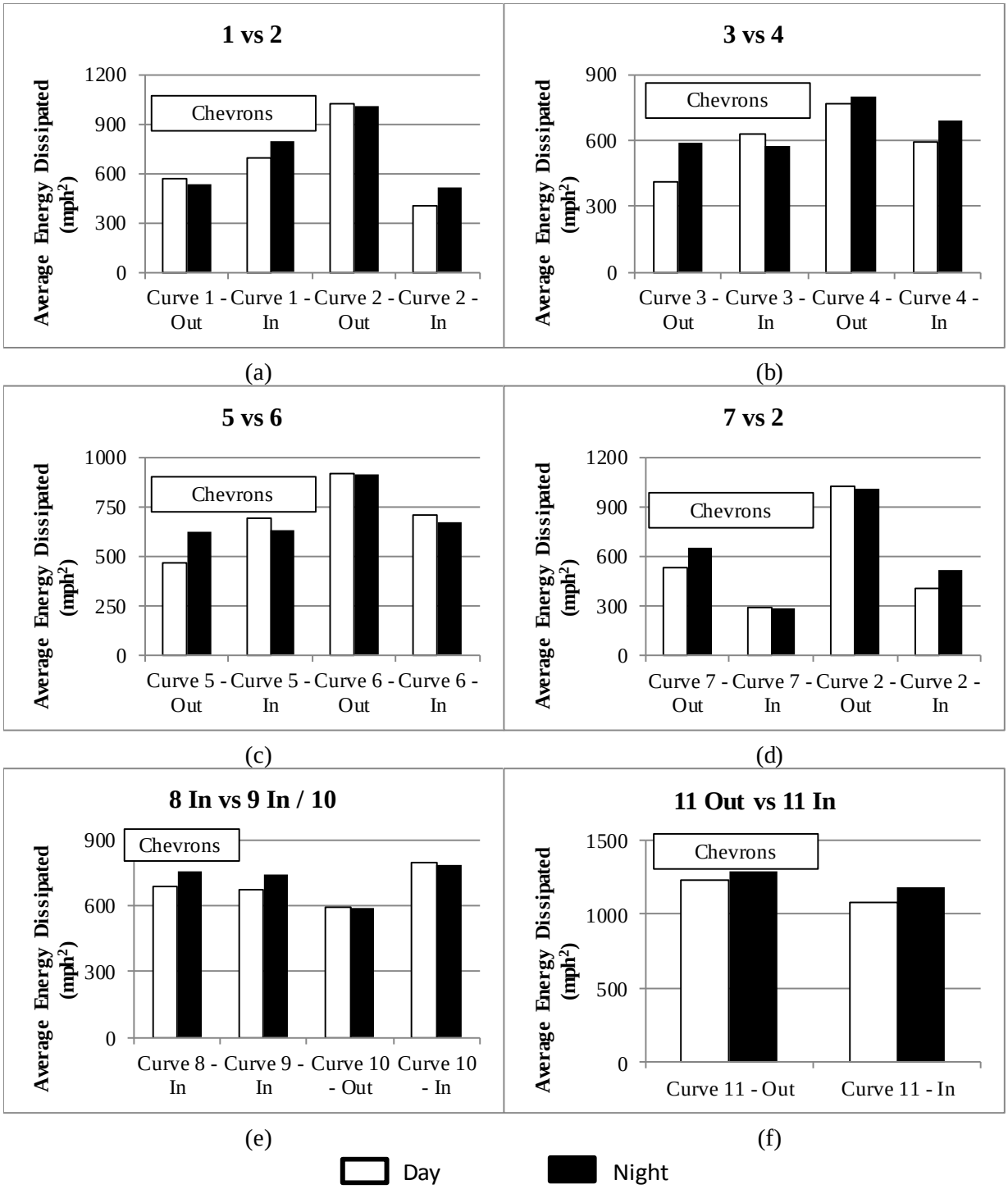

Figure 5. Maximum and Minimum Energy Differentials

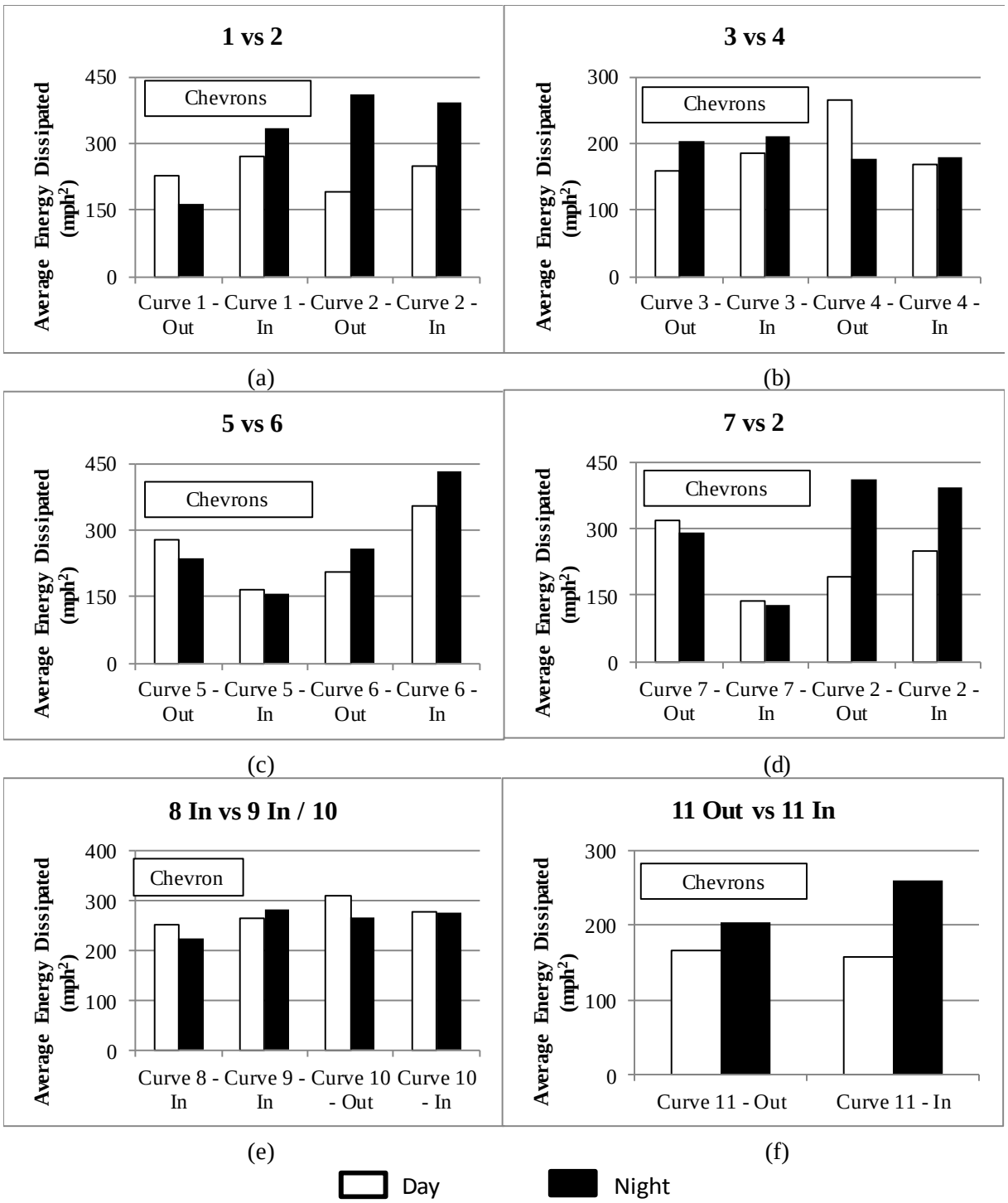

Figure 6. PC and Minimum Energy Differential

Percent of Speed and Energy Reduction within Curve

The percentages of speed and energy reduction within the curves were calculated to compare the effectiveness of chevrons in having drivers reduce speed before entering the curve. The night time drivers on average experienced a higher percentage of reduction within the curve than day

time drivers. For both speed and energy percent reduction, the night time participants averaged 1.6 and 1.7 percent greater reduction respectively. The mean and standard deviation were calculated across the 12 participants for the comparison. Table 6 summarizes the results of the percentage data analysis.

Table 6. Percent of Speed and Energy Reduction within Curve

			Speed (%)				Energy (%)			
Curve	**Chevrons**	**Direction**	**Day Avg.**	**Day Std.**	**Night Avg.**	**Night Std.**	**Day Avg.**	**Day Std.**	**Night Avg.**	**Night Std.**
1	Yes	Out	43.4	14	33.5	11.4	39.2	13.4	30.1	10.6
	Yes	In	41.9	18.1	48.3	19.9	37.7	17.4	43.7	20.1
2	No	Out	23.8	7.2	46.1	17.5	19.4	6.7	41.5	17.8
	No	In	63.2	8.1	79.9	15.9	60	8.2	77.8	17.1
3	Yes	Out	39.7	16.9	37.6	4.9	36.6	16	33.4	3.9
	Yes	In	32.7	15	42.1	11.1	28.1	13.6	37.8	11.1
4	No	Out	39.2	13.7	27.4	20.2	34.2	12.9	24	19.1
	No	In	32.8	9.4	33.1	21.3	28.7	8.7	29.5	20.5
5	Yes	Out	61.7	18.2	43.1	15	58.8	18.7	39	14.8
	Yes	In	28.2	11.4	30.7	10.4	24.3	10.9	27	10.2
6	No	Out	27.4	5	36.3	18.4	22.8	4.9	32.3	18.3
	No	In	52.9	15.8	67.4	16.6	48.2	15.3	63.8	16.9
7	Yes	Out	60.5	15.6	53.2	25.4	57.4	15.9	49.7	26.2
	Yes	In	48.9	15.6	46.8	23	46.5	15.2	44.7	23
2	No	Out	23.8	7.2	46.1	17.5	19.4	6.7	41.5	17.8
	No	In	63.2	8.1	79.9	15.9	60	8.2	77.8	17.1
8	Yes	In	41.5	7.9	37.7	14.9	36.1	7.4	32.6	15.1
9	No	In	43.8	7.4	43	14.7	18.8	12.5	16	26.4
10	No	Out	54.6	22.5	49.4	7.4	50.7	23.3	45.2	7.2
	No	In	37.1	15.9	38.2	17.5	32.4	14.4	34.4	16.9
11	Yes	Out	24.4	2.9	26.7	6.6	13.6	1.2	16.3	5.6
	No	In	24.7	7.9	33.4	12.8	14.1	4.8	21.2	10.9

The results do not show any strong correlation between the presence of chevrons and the amount of speed and energy reduction within the curve. Some situations even showed the opposite of what was expected as in Curves 3 and 4. Curve 3 has chevrons within the curve but had more speed and energy reduced within the curve than Curve 4. In some curve pairs, the directions yielded significantly different results as in Curves 5 and 6. For the pair, chevrons did not seem to be a significant factor since both Curve 5 and 6 had a direction with low percentage of speed and energy reduction. For both of those directions with low percentages, the directions of the turn are right hand curves. However, this correlation is not consistent throughout the pairs as seen in

Curves 1 and 2. In this pair, the lower percentages of reduction are associated with left hand curves. Figures 7 and 8 illustrate the percentages of speed and energy reduction throughout the paired curves. The white bars denote the averaged results of the day time participants while the solid bars show the night time participants.

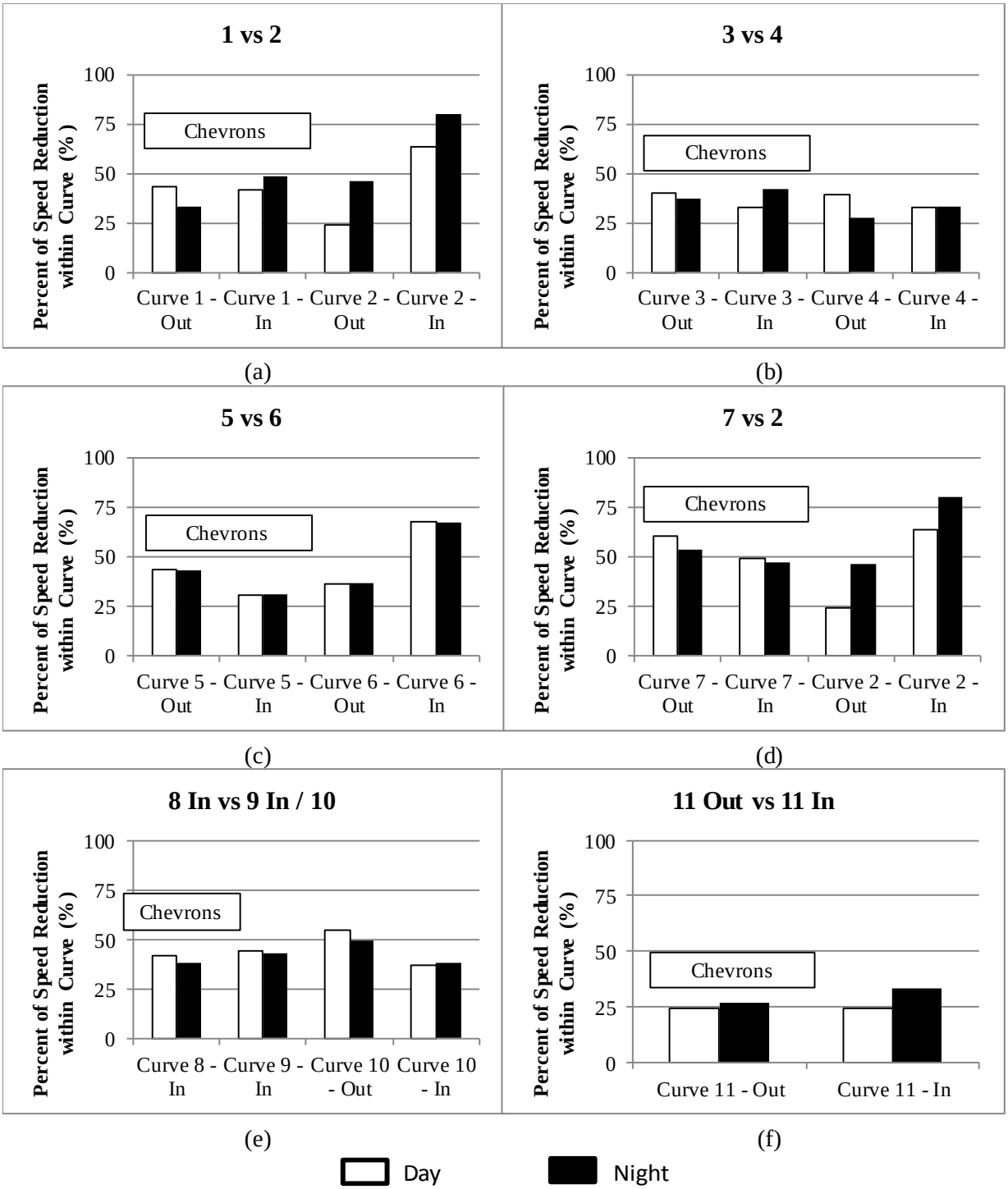

Figure 7. Percent of Speed Reduction within Curve

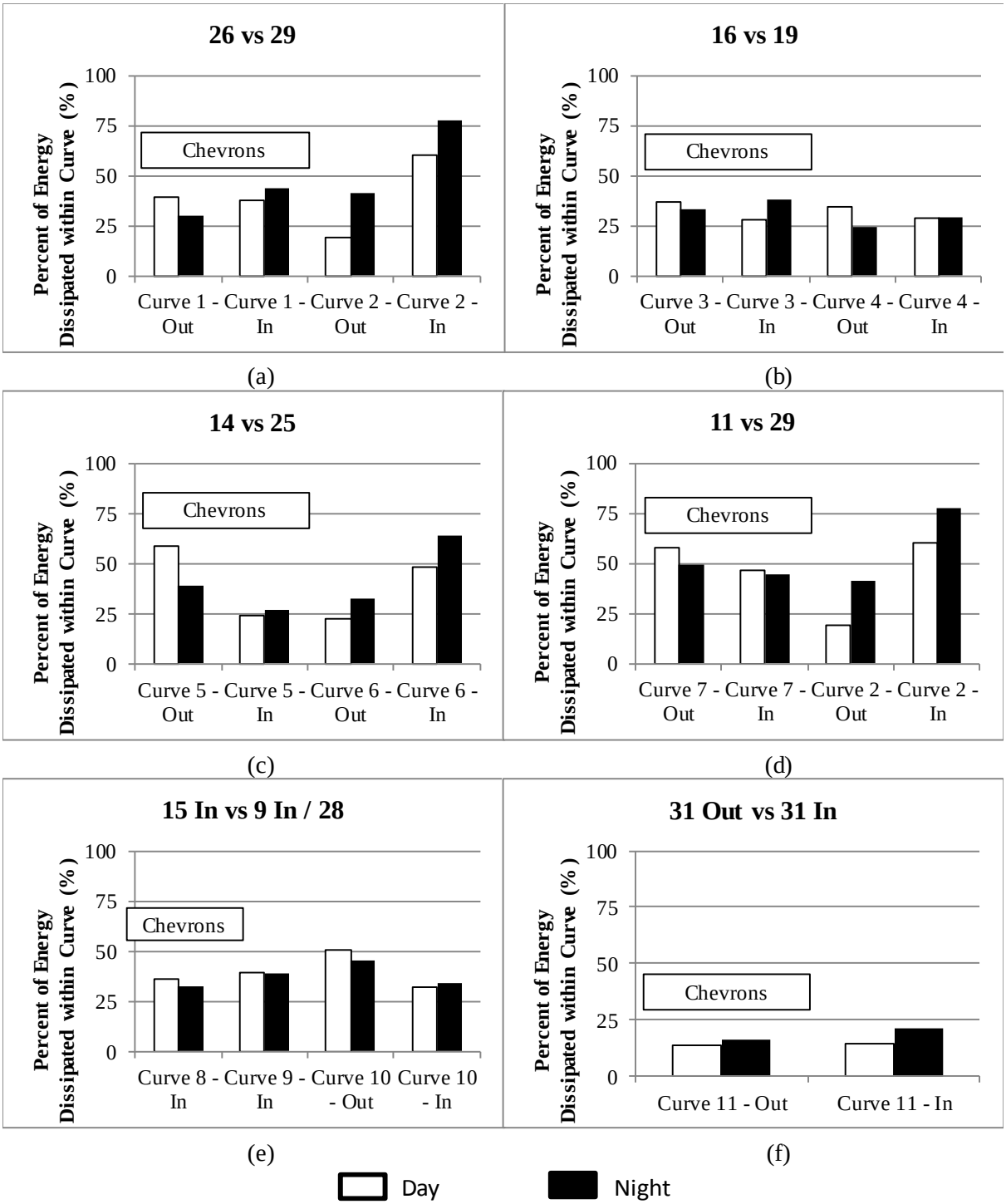

Figure 8. Percent of Energy Dissipation within Curve

Speed Profiles

The speed profiles were constructed with the speed data from up to 1000 feet before the PC until the PT. The speed profiles are high resolution since it is constructed from the GPS data which recorded speed data at 10 Hz (ten times per second). The test subjects' driving behavior can be

viewed as they approach and navigate the curve. Only 3 of the curve pairs for the first six participants of the study are shown below. The set of speed profiles on the left shows the curve with chevrons in comparison to its counterpart on the right. The thick red dot denotes the location of the PC of the subjects' trips. The x axis is in milliseconds in order to maintain the high resolution since the points between participants do not line up perfectly. The y axis is in mph.

Curves 3 Versus 4

Curve 3 contains chevron on the curve. From the speed profile comparison with Curve 4, the average trend throughout is that Curve 3 illustrates a less severe deceleration rate as the driver approaches the curve. This trend can be seen in both outbound and inbound directions. The operating speeds for both curves as the drivers approach the tangent are slightly different. There does not seem to be much significant difference of the driving behavior between the day and night time participants. Participant 6 on Curve 3 experiences a sharper deceleration rate but is not consistent with Participants 4 and 5. The drivers on Curve 3 approach the curve slower than Curve 4 at 1000 feet before the PC. Figures 9 and 10 illustrate the speed profiles for the curve pair. The speed profile for participant 3 for the inbound direction of Curve 3 is ignored because the participant had to stop during curve navigation because of the close proximity of a car in front.

Curves 5 Versus 6

Curve 5 contains chevrons within the curve and is portrayed as the graphs on the left. Again, the average trend throughout is that Curve 6 displays a steeper deceleration rate than its counterpart with chevrons. The comparison in the inbound direction shows that Curve 5 show sharper deceleration than the outbound direction. The operating speeds for Curve 6 are higher than Curve 5 as the subjects approach 1000 feet before the PC. This may be a factor in the difference of deceleration rates since the participants navigating Curve 6 are approaching the curve at higher speeds and have to decelerate more to reach the appropriate speed. For Curve 6 without chevrons, there does not seem to be a significant difference between day and night time participants. Curve 5's night time participants have steeper deceleration rates in the outbound direction while the day time participants have the steeper deceleration rates in the inbound direction. Figures 11 and 12 illustrate the speed profiles for the outbound and inbound directions for both curves.

Curves 11 Outbound Versus 11 Inbound

For Curve 11 the comparison occurs between directions. The outbound direction contains chevrons within the curve while the inbound direction does not. The outbound direction is displayed on the left graph. This pair was the best data for comparison since it dealt with the same curve, even though in different directions. Again, the general behavior for the participants is a less severe braking for the outbound directions with chevrons. Both directions have similar operating speeds at 1000 feet before the PC. The driving behavior is similar for both day and night time participants. Figure 13 displays the speed profiles between the outbound and inbound directions for Curve 11.

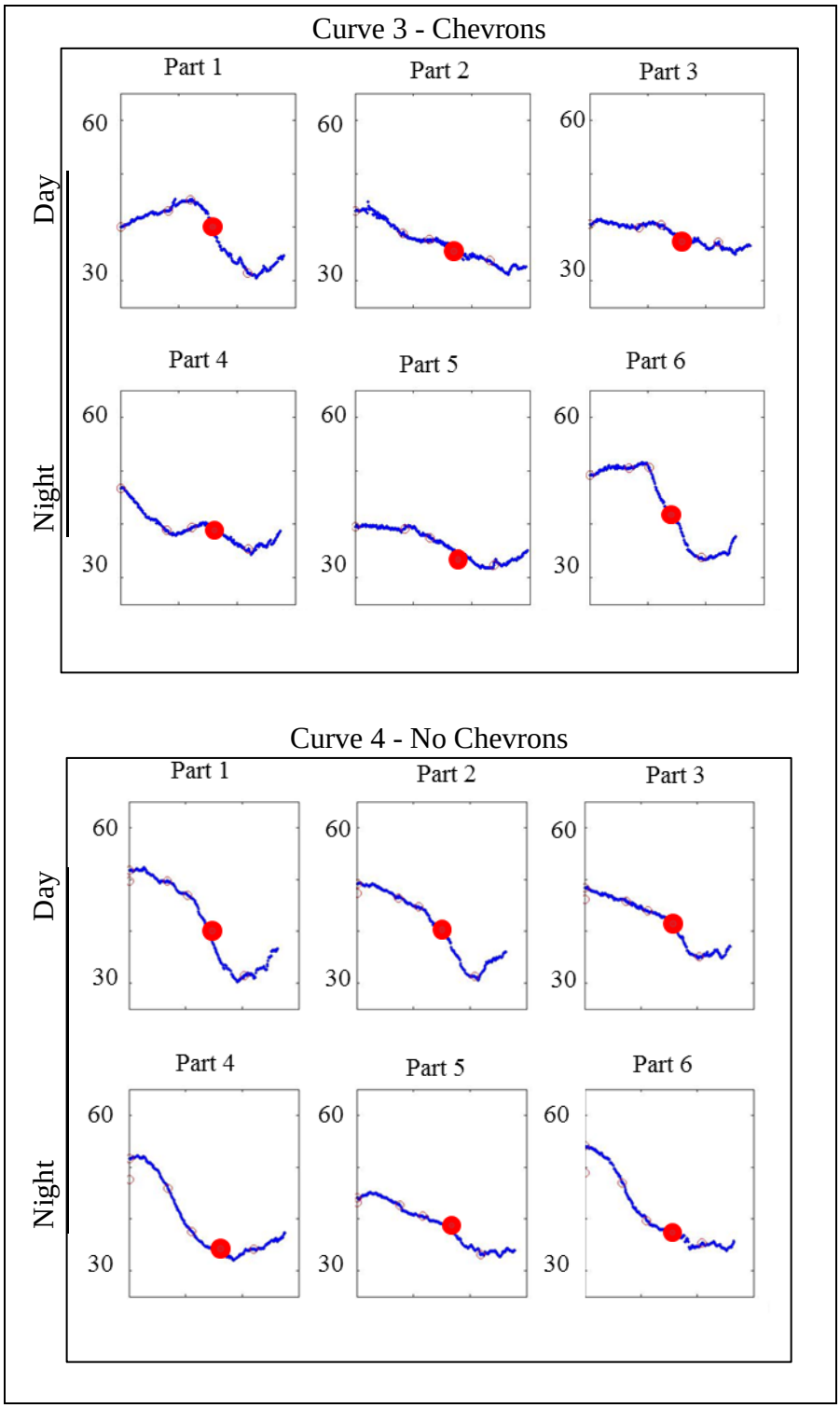

Figure 9. Curve 3 vs. 4 Outbound

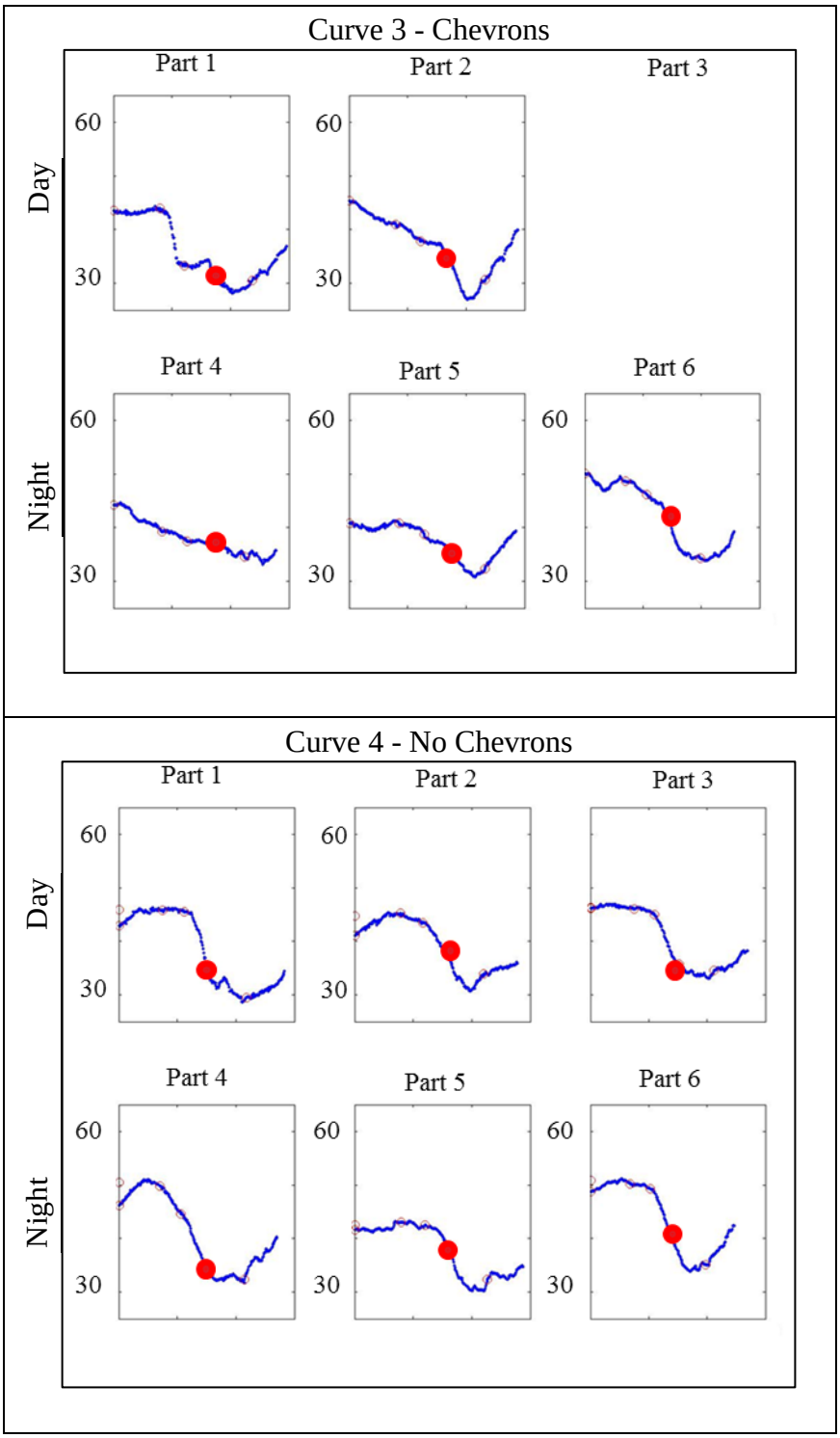

Figure 10. Curve 3 vs. 4 Inbound

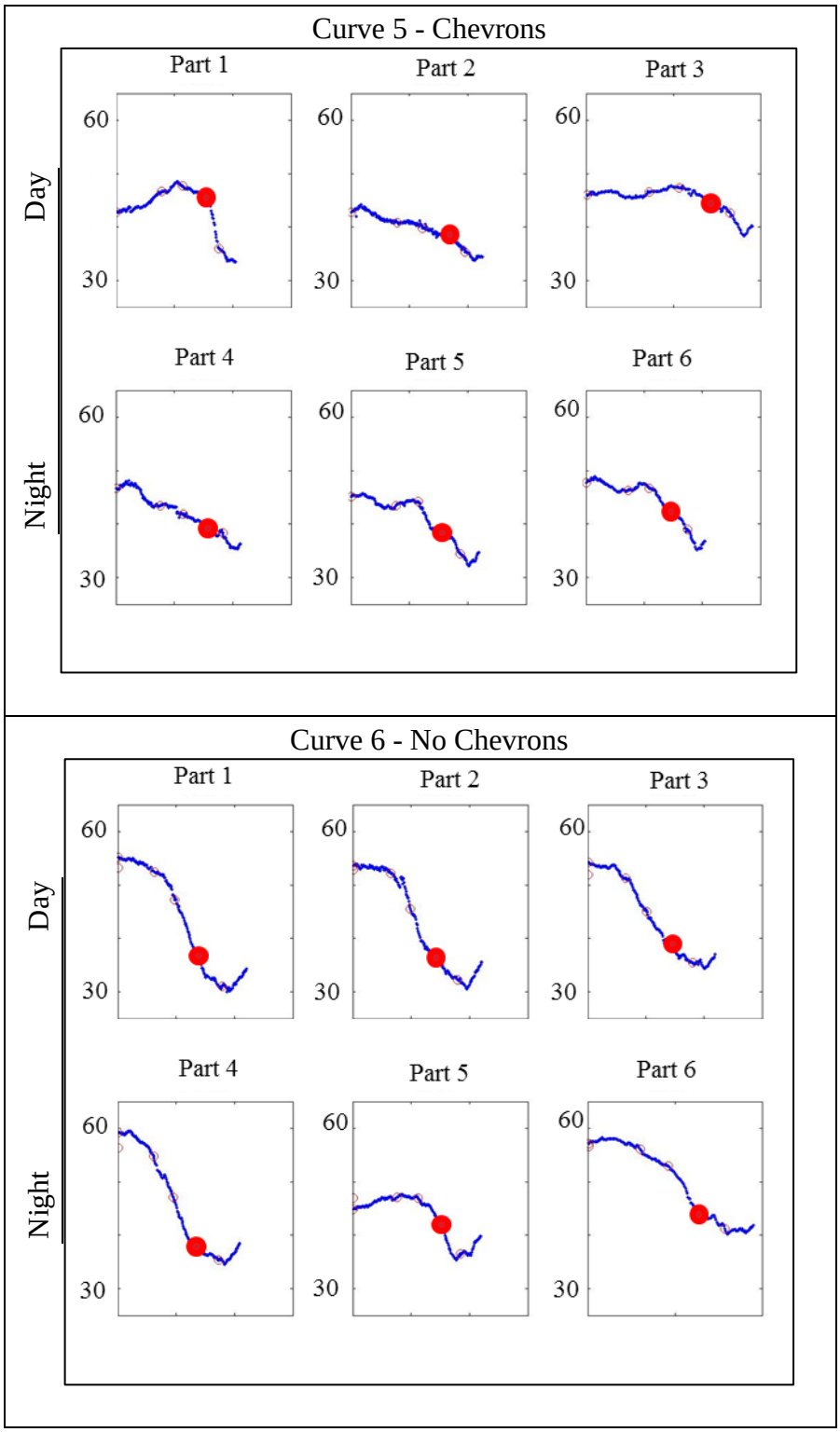

Figure 11. Curve 5 vs. 6 Outbound

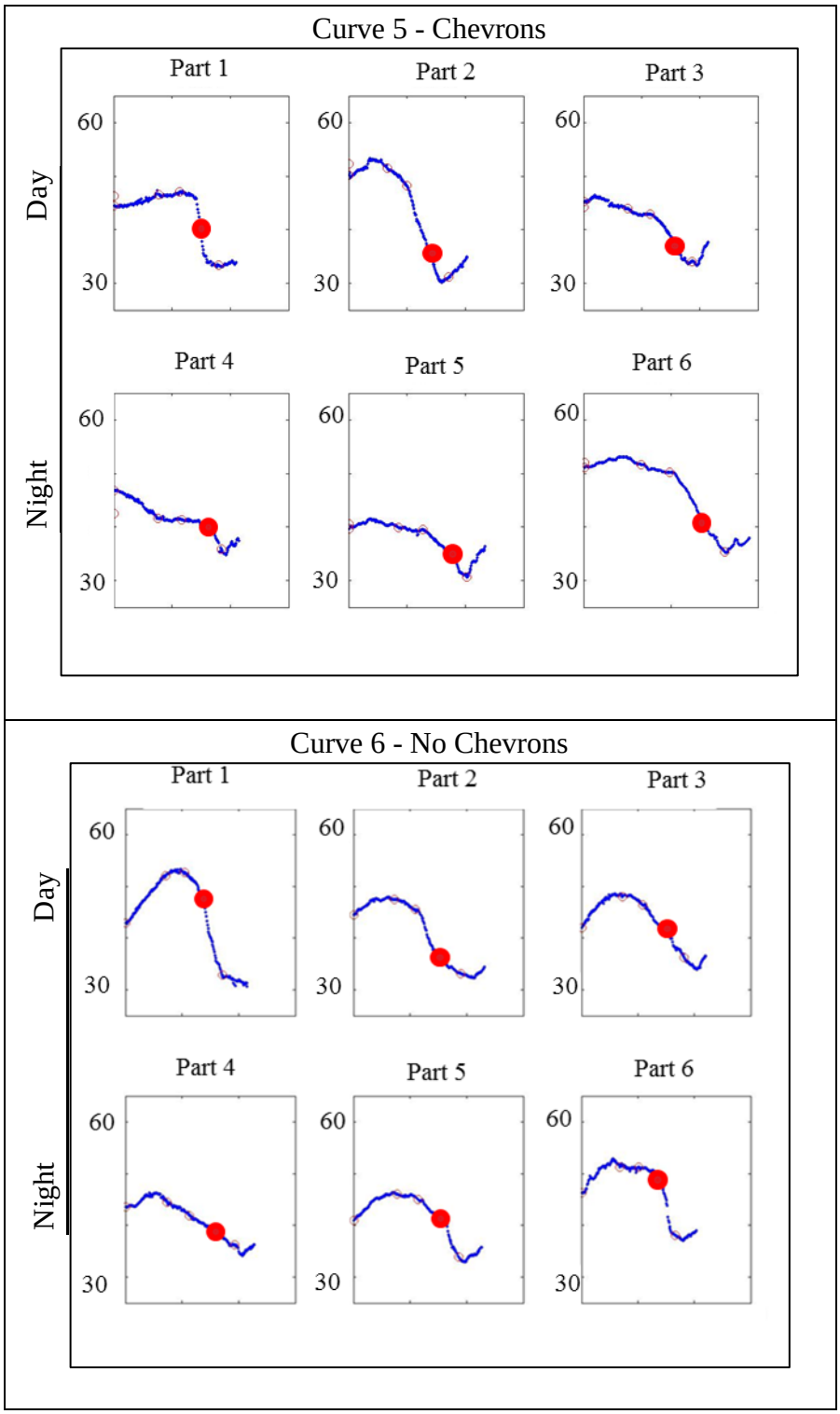

Figure 12. Curve 5 vs. 6 Inbound

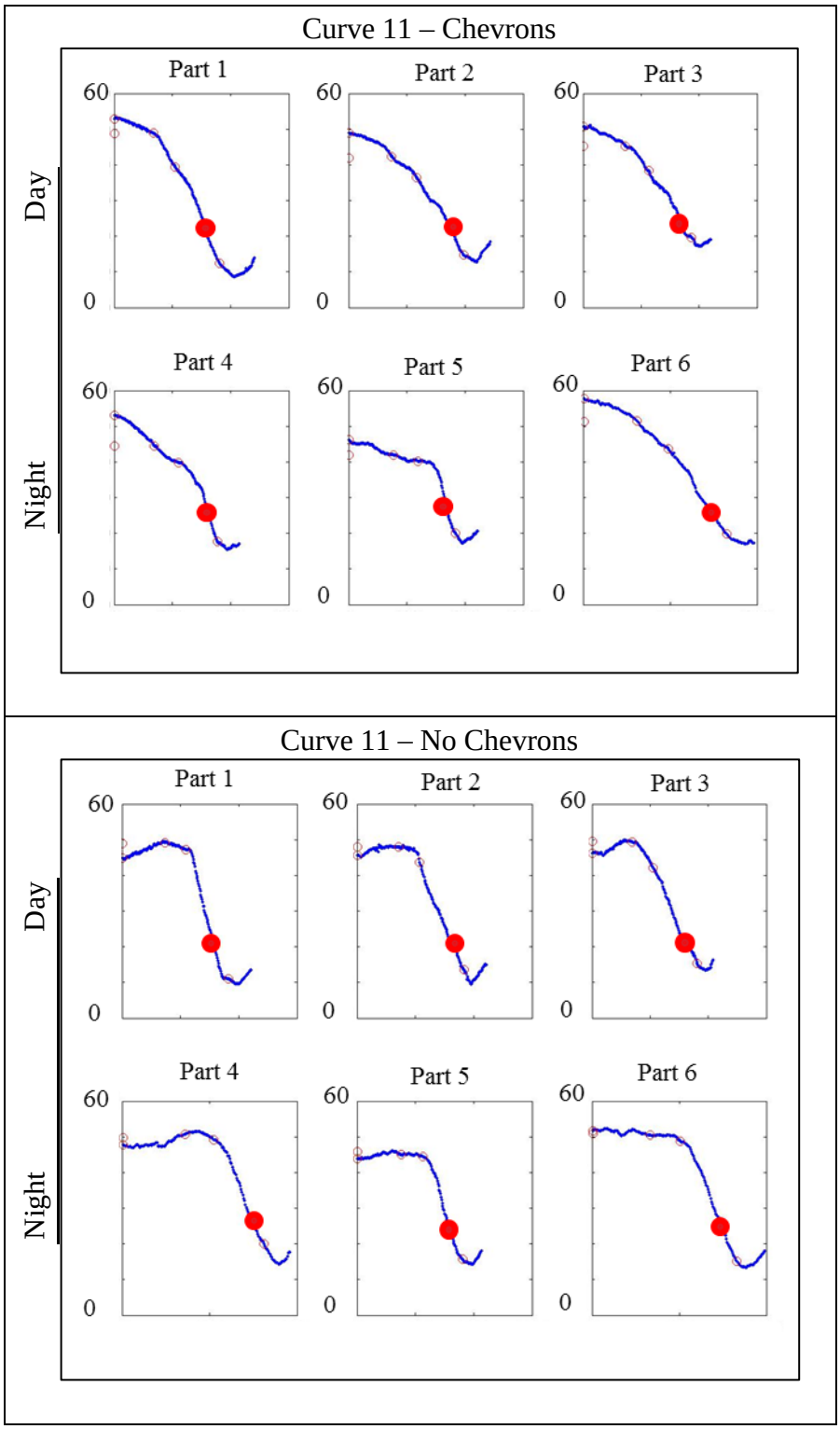

Figure 13. Curve 11 Outbound vs. 11 Inbound

Observations about Speed Profiles

The curves with chevrons seem to provide improved advance warning to the test participants as they approached the curve. This allowed the participants to start decelerating earlier and at a less severe rate than the curves that did not contain chevrons. However, sometimes the operating speeds as the participants approached the curve can be a factor to the deceleration rates. For example, in for Curve 5 (chevrons) and 6 (no chevrons), Curve 6 had higher operating speeds throughout the participants. These higher operating speeds require the drivers to have a higher reduction of speed to reach the appropriate speed for curve navigation. The need for a higher speed reduction could factor into the steeper deceleration rate. There seems to be no substantial difference in the driving behavior between the day and night time test runs.

CONCLUSIONS AND RECOMMENDATIONS

The data from the GPS tracker contained hundreds of thousands of data points from the 10 Hz frequency. MATLAB was used to reduce the data for analysis and the construction of the speed profiles. After the data was reduced, an evaluation of the results was made based on the MOEs: speed and energy differentials, percent reduction of speed and energy within the curve, and speed profiles.

The study did not show any strong correlation between the presence of chevrons and any of the MOEs. The night time drivers experienced higher differentials on average. There was too much variability between all of the curve pairs. In some situations, the opposite of what was expected occurred. For example, in the percent reduction evaluation for Curve 5 (chevrons) and 6 (no chevrons), Curve 5 is expected to have a lower percentage of reduction since the chevrons would provide advance warning. However, Curve 6 experienced a lower percent reduction of both speed and energy within the curve. Even though geometrically similar curves were paired together for the analysis, it seems that this method was the cause of the absence of a significant relationship and variability in the results. Even with Curve 11 where the outbound (chevrons) and inbound (no chevrons) directions were compared, there was still no significance in the presence of chevrons with the speed and energy differentials or the percent reduction. In the evaluation of the speed profiles, the curves with chevrons experienced less severe deceleration rates. The less severe rates are attributed that the chevrons provide advance warning to the approaching curve and aids in delineation. The difference in day and night time drivers did not show any significant difference in driving behavior overall but it seems that night time drivers did have slightly higher deceleration rates when approaching the curve. This could be due to the limited visibility during night.

The limitations to comparing different curves are mainly the proximity to the previous curve and different operating speeds approaching the curve. The operating speeds as the driver approaches the curve affect the speed and energy differential results. If the drivers approach a curve at a slower speed, they do not have to slow down as much to reach the appropriate speed to navigate the curve. The proximity of the previous curve in turn affects the operating speeds as drivers approach the PC. The participants do not have enough time to accelerate to a high speed before entering the curve. Therefore, the participants drive with lower operating speeds and do not have to slow down as much as they would have if they had a longer tangent section before the PC.

For further studies in the effectiveness of TCDs in horizontal curves to reduce variability and to reveal significant relationships, an increase of the amount of participants is desired for a higher quality of statistical analysis. Rather than comparing similar curves, a controlled experiment using the same curve with different configurations of TCDs would address that limitation. For example, conduct a study where a portion of the test participants drive the course with some curves without any TCDs. Then place chevrons or delineators on those same curves for the remaining participants. This method would remove problems experienced in this study as in the variable of the proximity of the previous curve affecting the results.

REFERENCES

1. *Manual on Uniform Traffic Control Devices for Streets and Highways*. Federal Highway Administration, U.S. Department of Transportation, Washington, DC, 2009.
2. Bonneson, J. A., M. Pratt, J. Miles, and P. Carlson. *Development of Guidelines for Establishing Effective Curve Advisory Speeds*, 2007.
3. Miles, P., J. David, and M. P. Pratt. Evaluation of New Speed Prediction Model for Rural Horizontal Curves. In *Transportation Research Board 91st Annual Meeting*, 2012.
4. Pratt, M. P., and J. A. Bonneson. Assessing Curve Severity and Design Consistency using Energy-and Friction-Based Measures. *Transportation Research Record: Journal of the Transportation Research Board*, Vol. 2075, No. 1, 2008, pp. 8-15.
5. Misaghi, P. *Modelling Operating Speed and Speed Differential for Design Consistency Evaluation.* , 2004.
6. Castro, M., J. A. Sánchez, C. M. Vaquero, L. Iglesias, and R. Rodríguez-Solano. Automated GIS-Based System for Speed Estimation and Highway Safety Evaluation. *Journal of Computing in Civil Engineering*, Vol. 22, No. 5, 2008, pp. 325-331.
7. Fambro, D. B., R. J. Koppa, D. L. Picha, and K. Fitzpatrick. Driver Braking Performance in Stopping Sight Distance Situations. *Transportation Research Record: Journal of the Transportation Research Board*, Vol. 1701, No. 1, 2000, pp. 9-16.
8. Hu, W., and E. T. Donnell. Models of Acceleration and Deceleration Rates on a Complex Two-Lane Rural Highway: Results from a Nighttime Driving Experiment. *Transportation Research Part F: Traffic Psychology and Behaviour*, Vol. 13, No. 6, 2010, pp. 397-408.
9. Arien, C., K. Brijs, W. Ceulemans, E. Jongen, S. Daniels, T. Brijs, and G. Wets. The Effect of Pavement Markings on Driving Behavior in Curves: A Driving Simulator Study. *Transportation Research*, Vol. 13, 2012, pp. 14.
10. Wu, Y., X. Zhao, J. Rong, and J. Ma. Effects of Chevron Alignment Signs on Driver Visual Perception, Manipulating Behavior, and Psychological Reactions. In *Transportation Research Board 92nd Annual Meeting*, 2013.
11. Ré, J. M., H. G. Hawkins, and S. T. Chrysler. Assessing Benefits of Chevrons with Full Retroreflective Signposts on Rural Horizontal Curves. *Transportation Research Record: Journal of the Transportation Research Board*, Vol. 2149, No. 1, 2010, pp. 30-36.
12. Charlton, S. G. The Role of Attention in Horizontal Curves: A Comparison of Advance Warning, Delineation, and Road Marking Treatments. *Accident Analysis & Prevention*, Vol. 39, No. 5, 2007, pp. 873-885.

13. Gates, T. J., P. J. Carlson, and H. G. Hawkins. Field Evaluations of Warning and Regulatory Signs with Enhanced Conspicuity Properties. *Transportation Research Record: Journal of the Transportation Research Board*, Vol. 1862, No. 1, 2004, pp. 64-76.
14. Chrysler, S. T., P. J. Carlson, and A. A. Williams. Simplifying Delineator Applications for Horizontal Curves. *Transportation Research Record: Journal of the Transportation Research Board*, Vol. 1918, No. 1, 2005, pp. 68-75.
15. Carlson, P. J., E. R. Rose, S. T. Chrysler, and A. L. Bischoff. Simplifying Delineator and Chevron Applications for Horizontal Curves. *Texas Transportation Institute, College Station*, 2004.

Preliminary Development of a Trip Generation Manual for Texas

Prepared for
Undergraduate Transportation Scholars Program

by

Parker C. Moore
Senior, Civil Engineering
Georgia Southern University

Professional Mentor:
Benjamin R. Sperry, Ph.D.
Assistant Research Scientist
Texas A&M Transportation Institute

Program Director
H. Gene Hawkins, Jr., Ph.D., P.E.
Associate Professor, Zachry Department of Civil Engineering
Research Engineer, Texas A&M Transportation Institute
Texas A&M University

Program Sponsored by:
Southwest Region University Transportation Center

August 9, 2013

STUDENT BIOGRAPHY

Parker Moore is a senior at Georgia Southern University in Statesboro, Georgia. He is scheduled to graduate in May 2015 with a Bachelor of Science degree in Civil Engineering, with emphases in Transportation and Environmental, along with a minor in business. He has made the Dean's list at Georgia Southern for the past two semesters.

For the past two summers, Parker has worked at Story, Clarke & Associates, Inc., a land surveying and planning company in Warner Robins, Georgia. Outside of class, Parker is a member of Sigma Nu Fraternity, American Society of Civil Engineers (ASCE), and the National Society of Leadership and Success. Some of Parker's hobbies include golf, fishing, and spending time with friends.

Parker plans to attend graduate school to earn a master's degree in Civil Engineering and become a licensed Professional Engineer.

ACKNOWLEDGMENTS

The research described in this paper was conducted as part of Project 0-6760, "Improved Trip Generation Data for Texas Using Workplace and Special Generator Surveys," sponsored by the Texas Department of Transportation (TxDOT). The research activities were conducted in support of the Undergraduate Transportation Scholars Program. The findings and recommendations included in this paper are based on the student's summer activities. They should be considered preliminary and not as representative of the findings and recommendations of the parent project. This paper has not been reviewed or approved by the sponsor. The contents of this paper reflect the views of the author, who is responsible for the facts and the accuracy of these data presented herein. The contents do not necessarily reflect the official view or policies of TxDOT.

The author would like to thank Ben Sperry for his guidance while working on this project, as well as Brian Bochner and Ed Hard for their assistance.

SUMMARY

Trip generation is an important component of a typical traffic impact analysis (TIA). Accurate estimates of trip generation are important to ensure that the infrastructure surrounding a proposed development is adequate for the expected traffic demand. The purpose of the research presented herein was to perform preliminary analysis of trip generation rates from workplace and special generator surveys conducted by the Texas Department of Transportation (TxDOT). Part of the information collected in these surveys is counts of vehicles that enter and leave an establishment. These counts are used to develop the trip generation rates analyzed in this paper.

The analysis conducted as part of this research was divided into two parts: (1) calculation of trip generation rates using Texas data and (2) comparison of these rates to the rates published in the Institute of Transportation Engineers (ITE) *Trip Generation Manual*. The trip generation rates were calculated using a weighted average rate equation along with a weighted standard deviation. For comparison with ITE rates, a *t*-test was used to evaluate the statistical difference between the two rates and a percent difference was used to evaluate the practical difference. The results from the comparison revealed that Texas trip generation rates are generally lower than ITE rates. Therefore, this research and the preliminary analysis show that continuing development of a Texas–specific trip generation manual is justified.

TABLE OF CONTENTS

LIST OF FIGURES

LIST OF TABLES

INTRODUCTION

When land developments are proposed, many state and local agencies (i.e., state DOTs, municipalities, or counties) require that a traffic impact study be performed. A traffic impact study is a specialized study of the impact that traffic produced by a certain type and size of development will have on the surrounding transportation system (*1*). The purpose of a traffic impact study is to determine what impact site-generated traffic will have on the existing and proposed roadway network and what impact the existing and projected traffic on the roadway system will have on the proposed development (*1*). In the site planning process, trip generation data are used to develop an estimate of the total demand for travel to or from a specified geographical area. In order to ensure that all potential variables are taken into consideration during the development process, the trip rate data produced by this analysis are used. Through this, land development companies can foresee how new or improved land use(s) will be affected by existing or future roads (*2*). Using data from the Institute of Transportation Engineers (ITE) *Trip Generation Manual*, local or state agencies use this information for estimating trip generation for development sites (*3*).

The purpose of this project was to develop trip generation rates for as many land use types as possible, using data from Texas workplace surveys that have been conducted over the course of about the past decade. The methods for developing these trip rates will be the same as used in the ITE *Trip Generation Manual*. Once the rates have been developed for the different land uses, the data will then be compared with the rates from the same land use types in the *Trip Generation Manual*.

BACKGROUND INFORMATION

This research project is a component of a parent project sponsored by the Texas Department of Transportation (TxDOT), entitled; Improved Trip Generation Data for Texas Using Workplace and Special Generator Surveys (Project No. 0-6760). The goal of this project is to analyze the Texas workplace and special generator surveys in order to determine whether a generic attraction model can be developed for different land use types. Researchers with the Texas A&M Transportation Institute (TTI) and the University of Texas Center for Transportation Research (UT/CTR) have already begun this research project. The research that was conducted herein was part of task 4 of project 0-6760, Conduct Analysis to Develop Trip Generation Rates for Land Development. A critical element of a traffic impact study is estimating the amount of traffic a proposed development will produce. This estimate is obtained through a trip generation analysis (*4*). Certain data obtained as part of the TxDOT workplace/special generator surveys can be used to develop trip generation rates for land development purposes.

Trip Generation Rates for Land Development

Trip generation data is maintained by ITE and published in the *Trip Generation Manual*, currently in its 9th edition (*5*). This manual contains a database of site-level trip generation data for 172 unique Land Use Codes (LUC) with data from more than 5,500 studies. Similar studies on trip generation analysis have already been conducted by some other states, such as Vermont (*4*) and South Dakota (*6*), which has led to the creation of state-specific trip generation guidance

for these states. The studies performed by other states showed that their local rates are different than the rates published by ITE. These states also concluded that local rates were different across small and medium regions when compared to the rates from the larger regions. For example, Vermont concluded that ITE rates were greater than for regions outside of Chittenden County, the county containing the state's largest city (*4*).

Independent Variables for Trip Generation

Another important aspect of developing trip generation data is the process of selecting the proper independent variable to relate the estimated trip generation with characteristics of the site (*3*). The dependent variable for trip generation is always vehicle trips, but the independent variable will vary depending on the type of land use. For site planning purposes, the recommended independent variables that are typically used are as follows:

- Size of building(s) at the site (square footage);
- Size of the site (acres); and
- Number of servicing positions at the site (e.g., fuel pumps).

Along with the independent variables listed above, additional independent variables could be needed depending on the results the data may reflect. Other independent variables with corresponding land use could include:

- Number of beds (hospitals);
- Number of students (schools, colleges, universities);
- Number of seats and/or movie screens (cinemas);
- Average flights per day (airports); and
- Number of drive-in lanes (banks).

Texas Workplace/Special Generator Survey Program

Over the past two decades, the TxDOT has collected workplace and special generator surveys from areas all over the state. The purpose of these surveys is to develop trip attraction rates for workplace and special generators to be used in urban travel demand models. The data collected from these surveys include trip origin, destination, modes of travel, demographics, and any other data that may be relevant. Surveys are conducted of employees and visitors to establishments. The three types of establishments surveyed as part of this program are as follows:

- Free-Standing Workplaces- establishments which occupy the entire portion of one or more buildings at a site such that all site traffic can be attributed to the workplace;
- Non-Free-Standing Workplaces- establishments which share a portion of a building at a site such that site traffic cannot be attributed solely to that workplace; and
- Special Generators- very large developments such as hospitals, universities, or airports which are given special consideration in urban travel demand models.

The geographic areas in which the surveys are conducted are certain Metropolitan Planning Organization (MPO) regions within the state. TxDOT has collected workplace and special

generator survey data at approximately 20 small, medium, and large MPO in Texas over the past 20 years. Approximately 200 establishments of each workplace type within an MPO region are typically surveyed, plus any special generators.

Traffic Count Data from Texas Workplace/Special Generator Surveys

Traffic counts are also collected as part of the TxDOT workplace/special generator survey program. The purpose of these counts is to determine the daily total traffic at an establishment. The count data are used to expand survey results to reflect total activity at the establishments. At free-standing workplaces, vehicle counts are typically obtained while person counts are typically obtained at non-free-standing workplaces. Counts of commercial vehicles and service vehicles are obtained at both types of workplaces.

For the purposes of this research, only vehicle count data was used. Currently, TxDOT's workplace survey projects only require 24-hour total counts for survey analysis. However, for the purposes of developing trip generation rates for land development, hourly or 15-minute count data must be used because the focus of typical TIAs is on peak hours rather than daily travel. Although not required by the survey specifications, some traffic data vendors supply hourly or 15-minute count data in addition to the required 24 hour counts. These hourly or 15-minute count data were used in this project to develop trip generation rates.

GOALS AND OBJECTIVES

While this particular task is part of a parent project in process, the purpose of this research was to develop trip generation rates using Texas data for as many land use types as possible following the same procedures as the ITE *Trip Generation Handbook* (*3*). The trip generation rates developed through this project were compared to those of the same LUC in the ITE *Trip Generation Manual* (*5*). The objectives of this project were as follows:

1. Using the master site list from Task 3 of the parent project, conduct a review of available traffic count data from the workplace and special generator surveys.
2. Group workplace surveys by LUC in order to determine the number of surveys for each and to determine any other relevant data necessary.
3. Develop trip generation rates per each independent variable and compare to ITE rates provided in the *Trip Generation Manual* (*5*).

RESEARCH METHODS

This section discusses the methods on how the aforementioned goals and objectives were achieved. In order to ensure the process was consistent with ITE recommended procedures, three tasks were undertaken: data review, database preparation, and data analysis.

Data Review

The purpose of the data review process was to identify which establishments were suitable for analysis as part of Task 4.The master site list, which was developed from Task 3 of the parent

project, was reviewed. This master site list contains all of the data from the surveyed establishments as part of the TxDOT work place and special generator survey program from 2009 to 2012. The master site list also included survey data from establishments from the Victoria (2011) and Bryan/College Station (2013) MPO regions that were acquired. The surveyed establishments included basic, service, retail, and education employment types as well as large special generators. The master site list contained a total of 2,729 establishments across eight MPO regions.

Using the master list of sites for the eight MPO regions, additional review was conducted to determine if the establishments could be used for this analysis. The criteria for the establishments included:

- vehicle vs. person counts
- availability of 15-minute or hourly count data
- complete data from MPO regions

Also part of the review of suitable establishments was to determine if traffic count sheets were available in either electronic or paper format. The result of this review was a list containing a total of 938 establishments with suitable vehicle counts from Bryan/College Station, El Paso, Killeen-Temple, Sherman-Denison, and Waco regions. Figure 1 shows the geographical location of these five regions.

Database Preparation

Database preparation involved three major steps: assignment of the LUC, locating independent variable data, and extracting peak hour traffic volumes. To ensure that establishments were classified correctly, the LUC descriptions provided in the *Trip Generation Manual* were consulted as a guide along with aerial photos, street-level images, and websites of the establishments. Assistance from TTI experts was also solicited in the classification process.

Independent variables are used to relate trip generation to site characteristics. Different methods were used in obtaining independent variable data for different LUCs. The number of employees was already in the database as part of the original survey data. For square footage and acres, property searches on county Central Appraisal District (CAD) websites were used. For independent variable data not found in the CAD data, measurement tools in aerial images were used to approximate square footages. Special independent variable data, such as fuel pumps, drive through lanes, and number of rooms, were found using street-level imagery and travel websites.

Once establishments were classified and independent variable data was obtained, the individual count sheets were located and saved to a specific LUC folder. These folders included the count sheets along with a peak hour volume extractor spreadsheet. These peak hour extractor worksheets were programmed to find five peak hours of traffic volume once the traffic counts were entered into it. The peak hours of analysis included:

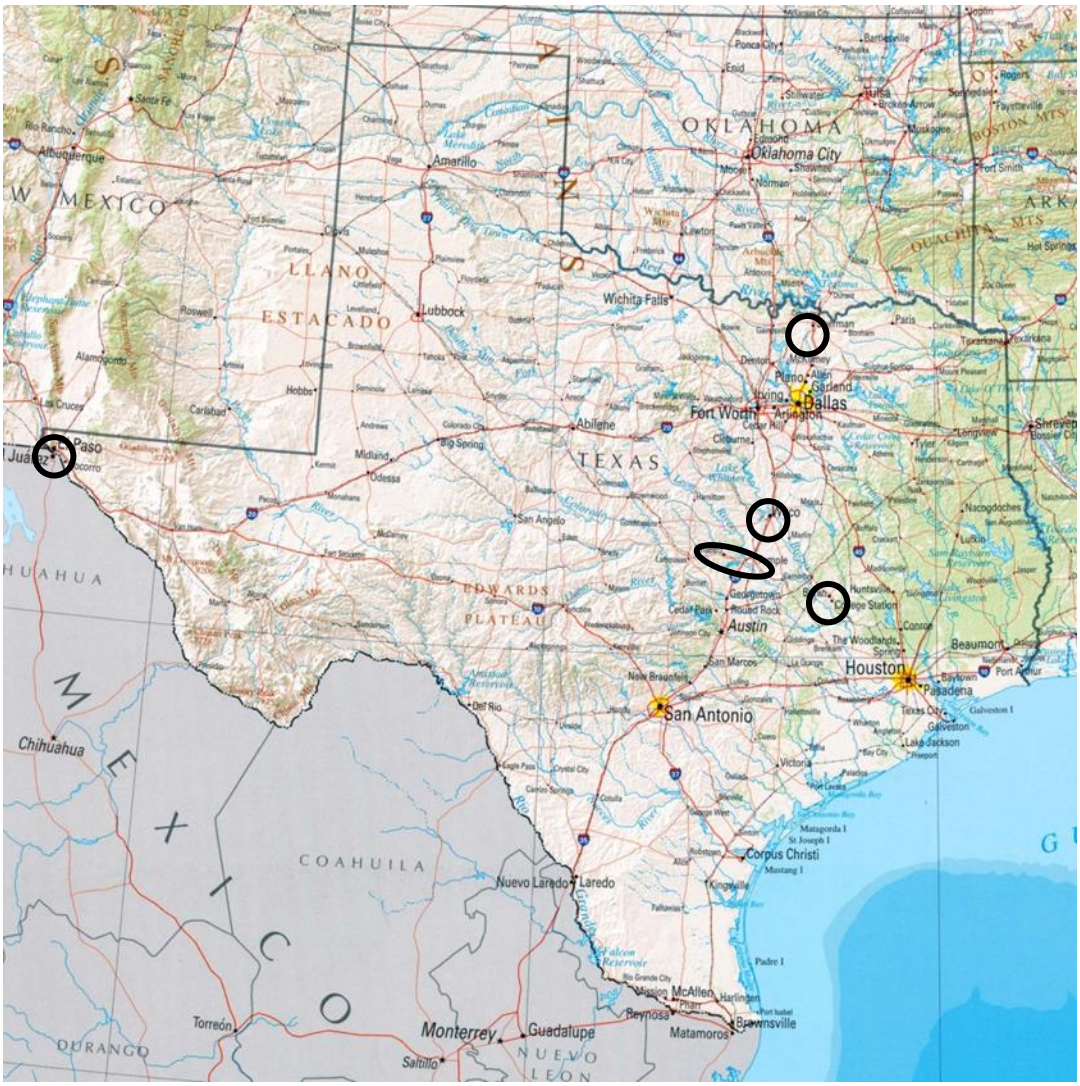

Figure 1. Map of MPO Areas
(source: www.mappery.com with author annotations)

- Daily: 24 hour total vehicle count
- A.M. Peak Hour of Adjacent Street Traffic: highest hourly period of vehicle counts between 7 – 9 A.M.
- P.M. Peak Hour of Adjacent Street Traffic: highest hourly period of vehicle counts between 4 – 6 P.M.
- A.M. Peak Hour of the Generator: highest hourly period of vehicle counts from midnight to noon
- P.M. Peak Hour of Generator: highest hourly period of vehicle counts from noon to midnight

Along with the peak hours, the spreadsheet was also set up to calculate the percent entering and percent commercial vehicles for each time period. After all LUC worksheets were complete, the master site list was merged with the results from the peak hour calculations using the unique site identification as a key. The result of these two databases merging was a single analysis database

which included 390 establishments, 34 LUCs, peak hour traffic volume for five time periods, and independent variable data. Table 1 shows a list of these LUCs and the corresponding number of establishments for each.

Data Analysis

The purpose of analyzing the data was to develop trip generation rates for as many LUC and independent variable combinations as possible across the five different time periods. The rates generated were also compared to ITE rates where possible.

Calculation of Trip Generation Rates

The analysis procedures were followed in accordance with the procedures outlined in the *Trip Generation Handbook* (*3*). A weighted average rate and weighted standard deviation were calculated for each LUC. The trip generation rate calculated is a weighted average and was calculated using Equation 1 (*4*).

$$T = \frac{\sum_{i=1}^{n} T_i}{\sum_{i=1}^{n} X_i} \quad \text{(Equation 1)}$$

where

T = Overall trip generation rate
T_i = Trips generated at site i
X_i = Value of independent variable at site i
n = Number of sites

The standard deviation was calculated using Equation 2 (*4*).

$$s = \sqrt{\frac{1}{1-V_2} \sum_{i=1}^{n} w_i (T_i - T)^2} \quad \text{(Equation 2)}$$

where

s = Sample standard deviation
T, T_i, and n are as above
$w_i = \frac{X_i}{\sum_{i=1}^{n} X_i}$
$V_2 = \sum_{i=1}^{n} w_i^2$

Comparison of Texas Rates with ITE Trip Generation Rates

The second part of data analysis was the comparison of Texas trip generation rates to ITE rates. The purpose of this was to determine if Texas rates were statistically and/or practically different from the existing ITE rates. A total of 256 comparisons were made. To determine the statistical difference, a weighted *t*-test was calculated using Equation 3 (*4*).

Table 1. Total Establishments in Database by Land Use

ITE LUC	Land Use Description	Number in Database
110	General Light Industrial	30
140	Manufacturing	17
150	Warehousing	9
151	Mini-Warehousing (Self-Storage)	6
170	Utilities	14
254	Assisted Living	4
310	Hotel	6
540	Junior/Community College	7
565	Day Care Center	17
610	Hospital	6
620	Nursing Home	4
630	Clinic	3
640	Animal Hospital/Vet Clinic	7
720	Medical-Dental Office Building	16
812	Building Materials and Lumber Store	9
814	Variety Store	9
816	Hardware/Paint Store	5
820	Shopping Center	7
841	Automobile Sales	21
842	Recreational Vehicle Sales	5
843	Automobile Parts Sale	7
852	Convenience Market (Open 15-16 Hours)	3
853	Convenience Market w/ Gas Pumps	26
881	Pharmacy/Drugstore w/ Drive Through	4
890	Furniture Store	7
912	Drive-In Bank	16
932	High-Turnover Sit Down Restaurant	32
933	Fast-Food w/out Drive Through	4
934	Fast-Food w/ Drive Through	26
935	Fast Food w/ Drive Through/No Indoor Seating	5
943	Automobile Parts and Service Center	37
944	Gasoline/Service Station	7
945	Gas Station w/ Convenience Market	11
946	Gas Station w/ Convenience Market/Car Wash	3
	Total Establishments in Database	**390**

$$t = \frac{T - \mu}{s/\sqrt{f}} \quad \text{(Equation 3)}$$

where

T, s, and V_2 are as above

μ = Trip generation rate from ITE *Trip Generation Manual*

f = sample size, defined as $f = \frac{1}{V_2}$

To determine if Texas rates were practically different from ITE rates, Equation 4 was used.

$$d\,(\%) = \frac{T - \mu}{\mu} * (100\%) \quad \text{(Equation 4)}$$

where

d (%) = percent difference

μ and T are as above

ITE lists four criteria for examining the difference between ITE and local rates (*3)*.

- The trip generation rate for each of the locally surveyed sites falls within one standard deviation of the *Trip Generation* rate;
- Of the sites surveyed locally, at least one has a higher rate than the *Trip Generation* weighted average rate or equation and one has a lower rate; **or** all of the survey sites generated trips with totals within 15 percent of the *Trip Generation* average rate or equation (calculated using Equation 4);
- The locally collected data generally fall within the scatter of points shown in the current *Trip Generation* data plot;
- Common sense derived from the local trip generation study indicates that the *Trip Generation* data are valid for local application.

Since this project was a preliminary development of trip generation rates for Texas, only a practical difference criterion of 15 percent was used for examining the difference in generated rates. That is to say, any rate outside of ± 15 percent of the ITE rate was considered practically different.

RESULTS

This section contains the results from the analysis of the data. LUCs were grouped into seven different types of land use classifications that were analyzed from the workplace and special generator surveys. The tables and figures included in this section show the statistical and practical differences between Texas and ITE rates. The appendix section contains the detailed tables, which include sample size, trip generation rates, standard deviation, P-value, and percent difference, for each independent variable across each time period that was analyzed.

Comparison of Texas Rates with ITE Trip Generation Rates

The following section discusses the findings from the comparison of Texas trip generation rates to ITE trip generation rates. Table 2 shows the total number of compared rates, along with the statistical and practical differences, across the different land uses. Figures 2 and 3 also show the comparison rates. Figure 2 shows the statistical difference and Figure 3 shows the practical difference. A total of 400 rates were calculated from the Texas data, of which 256 were able to be compared with ITE.

Table 2. Summary of Comparisons between Texas and ITE Trip Generation Rates

LUC Grouping	Number of Comparisons	Number Statistically Different*	Statistically Lower*	Number Practically Different**	Practically Lower**
Industrial (LUC 100s)	59	24	22	48	36
Assisted Living (254)	2	0	0	0	0
Lodging (300s)	10	5	5	10	5
Institutional (500s)	25	4	4	11	9
Medical/Office (600s/720)	35	8	3	28	9
Retail (800s)	76	31	27	60	39
Service (900s)	49	18	17	29	22
Total	**256**	**90**	**78**	**186**	**120**
*Number of comparisons with a statistically significant difference between Texas and ITE rates ($p \leq 0.1$)					
**Number of comparisons with a practical difference between Texas and ITE rates ($d \leq -15\%$ or $\geq 15\%$)					

Industrial Land Uses

For industrial land uses (LUC 100s), 59 comparisons between Texas and ITE trip generation rates were calculated, of which 24 (41 percent) revealed a statistically significant difference and 48 (81 percent) were practically different. Of the 24 statistically significant differences between the Texas and ITE trip generation rates, 22 (92 percent) were found to be lower than ITE rates. Of the 48 practical significant differences between the Texas and ITE trip generation rates, 36 (75 percent) were found to be lower than ITE rates.

LUC 110 (General Light Industrial), LUC 140 (Manufacturing), and LUC 150 (Warehousing) were industrial land uses that showed the greatest amount of difference for all three independent variables across the different time periods. All of the industrial LUCs had an acceptable sample size.

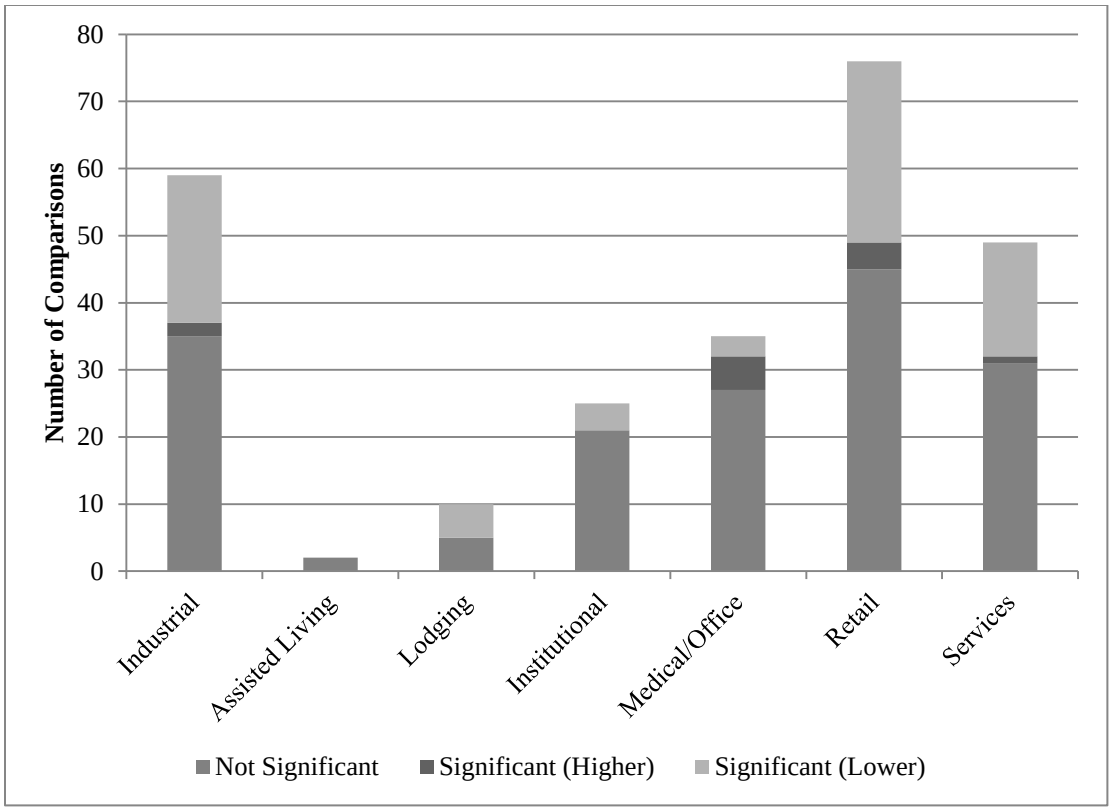

Figure 2. Statistical Difference between Texas and ITE Rates

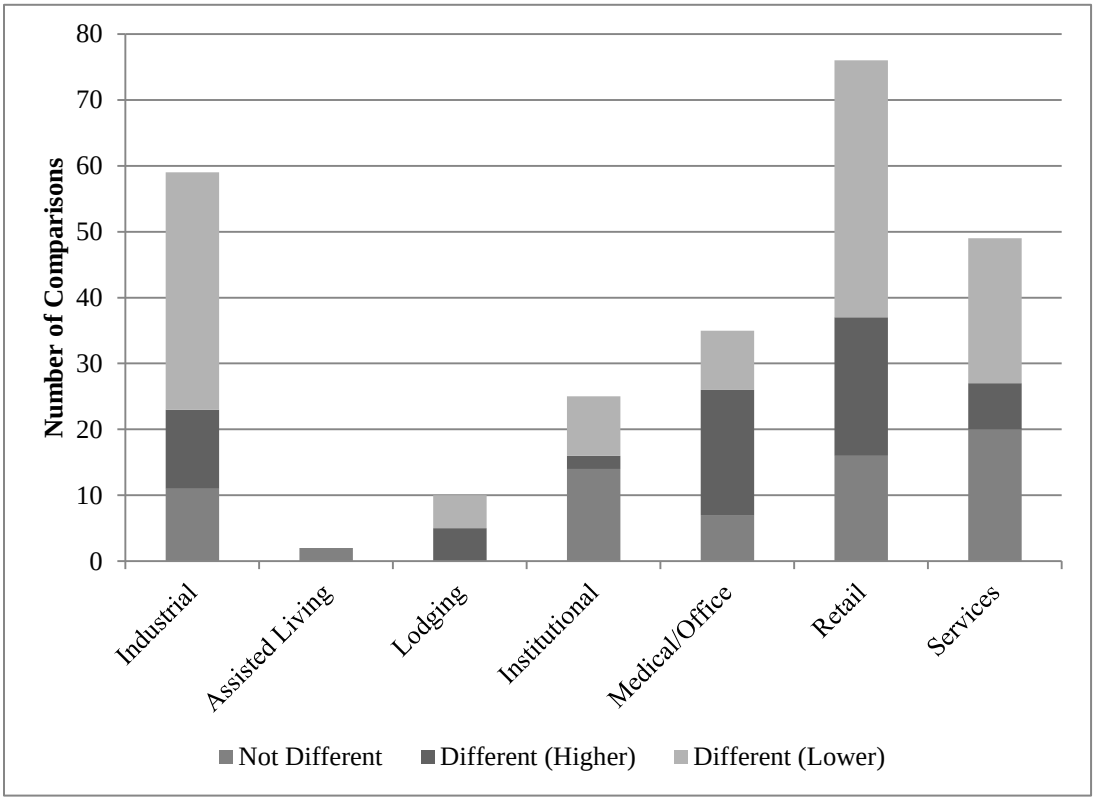

Figure 3. Practical Difference between Texas and ITE Rates

Assisted Living, Lodging, and Institutional Land Uses

For assisted living, lodging, and institutional land uses (LUC 254, 300s, and 500s), a total of 37 comparisons between Texas and ITE trip generation rates were calculated. Assisted living showed no statistical or practical difference when compared to ITE rates. Lodging had a total of 10 comparisons, of which 5 (50 percent) revealed a statistical significance and lower rates while 10 (100 percent) were practically different with 5 (50 percent) having lower rates. Institutional had 25 comparisons, of which 4 (16 percent) showed statistical and lower difference, 11 (44 percent) showed practical difference, and 9 (82 percent) revealed a lower practical rate.

It was found that some land use types were practically different from ITE rates. The results showed that difference from ITE rates varied for each of the independent variables. An overall view of these land use results showed that LUC 310 (Hotel) and LUC 565 (Day Care Center) were the two most practically different land uses. LUC 540 (Junior/Community College) showed no practical difference when analyzed per the number of students and LUC 254 (Assisted Living) had a small sample size.

Medical and Office Land Uses

For medical and office land uses (LUC 600s and 700s), 35 comparisons between Texas and ITE trip generation rates were calculated, of which 8 (23 percent) revealed a statistically significant difference and 28 (80 percent) were practically different. Of the 8 statistically significant differences between the Texas and ITE trip generation rates, 3 (38 percent) were found to be lower than ITE rates. Of the 28 practical significant differences between the Texas and ITE trip generation rates, 9 (32 percent) were found to be lower than ITE rates.

For medical and office land uses (LUC 600s and 700s), it was found Texas rates were practically different from ITE rates. No special independent variable data was analyzed for these land uses. LUC 610 (Hospital) and LUC 720 (Medical-Dental Office Building) showed the most practical difference for this land use. Both LUC 610 and 720 rates were practically different than the ITE rates for three of the five time periods analyzed on a per employee and 1,000 square feet basis. LUC 620 (Nursing Home) and LUC 630 (Clinic) had a small sample size.

Retail Land Uses

For retail land uses (LUC 700s), 76 comparisons between Texas and ITE trip generation rates were calculated, of which 31 (41 percent) revealed a statistically significant difference and 60 (79 percent) were practically different. Of the 31 statistically significant differences between the Texas and ITE trip generation rates, 27 (87 percent) were found to be lower than ITE rates. Of the 60 practical significant differences between the Texas and ITE trip generation rates, 39 (65 percent) were found to be lower than ITE rates.

For retail land uses (LUC 800s), the results showed that Texas rates were very different from ITE rates. When analyzed on a per 1,000 square feet basis, the retail land uses all showed practical difference from ITE rates. For LUC 812 (Building Materials and Lumber Store), LUC 816 (Hardware/Paint Store), LUC 841 (Automobile Sales), the Texas trip generation rates were

practically different than the ITE rates for three of the five time periods analyzed on a per employee basis. LUC 853 (Convenience Market w/ Gas Pumps) and LUC 881 (Pharmacy/Drugstore w/ Drive Through) had a small sample size.

Services Land Uses

For services land uses (LUC 900s), 49 comparisons between Texas and ITE trip generation rates were calculated, of which 18 (37 percent) revealed a statistically significant difference and 29 (59 percent) were practically different. Of the 18 statistically significant differences between the Texas and ITE trip generation rates, 17 (94 percent) were found to be lower than ITE rates. Of the 29 practical differences between the Texas and ITE trip generation rates, 22 (76 percent) were found to be lower than ITE rates.

For services land uses (LUC 900s), it was found that some land uses were practically different from ITE rates. LUC 912 (Drive-in Bank) showed to be practically different for every independent variable across and of the five time periods. For LUC 932 (High Turnover Sit Down Restaurant), LUC 933 (Fast-Food w/out Drive Through), and LUC 945 (Gas Station w/ Convenience Market), the Texas trip generation rates were practically different than the ITE rates for three of the five time periods analyzed on a per employee basis. LUC 933 and LUC 946 (Gas Station w/ Convenience Market/Car Wash) had a small sample size, but did show relevance to ITE rates when compared by special independent variable data (gas pumps).

Rates Higher than ITE Rates

The results also revealed that Texas did in fact have some land uses that were higher than ITE rates. When compared on the basis of per employee, LUC 110 (General Light Industrial), LUC 150 (Warehousing), LUC 310 (Hotel), LUC 610 (Hospital), and LUC 720 (Medical-Dental Office Building) had higher rates. On the basis of per 1,000 square feet, LUC 610 (Hospital, LUC 841 (Automobile Sales), LUC 881 (Pharmacy/Drugstore w/ Drive Through), and LUC 890 (Furniture Store) had higher rates than those of ITE. Lastly, on the basis of special independent variable, the only variable that generated higher rates was the number of gas pumps for LUC 945 (Gas Station w/ Convenience Market) and LUC 946 (Gas Station w/ Convenience Market/Car Wash).

CONCLUSIONS

Summary of Findings

This research revealed trip generation rates for Texas are different from ITE rates. This preliminary development of trip generation rates, across small and medium size MPO regions, showed that Texas generally has lower trip generation rates than ITE. From an overall perspective, Texas trip generation rates were not statistically different (35 percent). On the other hand, Texas rates were practically different (73 percent), meaning that the application of these rates would in fact have a noticeable difference between the two rates. Of these practically different rates, 65 percent of the Texas trip generation rates were found to be lower than ITE rates. The prominent differences observed were for industrial, medical-office, and retail land

uses. Therefore, in the foreseeable future, traffic impact analysis studies should use local rates rather than ITE rates. ITE recommends the use of local trip generation rates if available (*3*). The use of these local trip generation rates could save time and money by providing the right amount of infrastructure around a site.

Recommendations

Based on this preliminary research, it is recommended that TxDOT proceed with the creation of a Texas specific trip generation manual through subsequent tasks of project 0-6760. It is also recommended that workplace and special generator surveys from other small and medium MPOs be added to the existing database in order to develop more accurate trip generation rates for these regions. Also, the addition of survey data from large size MPOs would help to develop trip generation rates for the region and bring area type balance to the Texas trip generation manual.

REFERENCES

1. Stover, V. G. and F. J. Koepke. Institute of Transportation Engineers. *Transportation and Land Development*. 2nd Edition. 2002
2. *Development and Application of Trip Generation Rates – Final Report January 1985* http://ntl.bts.gov/DOCS/382DNA.html. Accessed June 3, 2013.
3. Institute of Transportation Engineers. *Trip Generation Handbook*, 2nd Edition. 2012
4. Byrne, B. M. Carr, and J. Sumner. Preparation of the Vermont Trip Generation Manual. *ITE Journal*, June 2012, pp. 42-47.
5. Institute of Transportation Engineers. *Trip Generation Manual*, 9th Edition. 2012
6. South Dakota Department of Transportation. *Verify Certain ITE Trip Generation rate Applications in South Dakota*. Publication SD2005-02-F. FHWA, U.S. Department of Transportation, 2005.
7. Institute of Transportation Engineers. *Trip Generation User's Guide,* 9th Edition. 2012

APPENDIX

This section contains the detailed tables from the data analysis. Tables 3-17 include the sample size, trip generation rates, standard deviation, P-value, and percent difference, for each independent variable across each time period that was analyzed.

Table 3. Trip Generation Rates per Employee (Weekday Daily)

ITE LUC	Sample Size	Average Rate	Standard Deviation	P-Value*	% Diff.*
110	30	3.86	2.87	0.280	27.8%
140	17	2.45	0.92	0.498	15.0%
150	9	4.89	2.19	0.386	25.7%
151	6	14.72	7.20	No ITE Rate	No ITE Rate
170	14	4.11	2.10	No ITE Rate	No ITE Rate
254	4	4.24	2.74	0.846	7.9%
310	6	20.81	28.44	0.671	45.1%
540	7	13.88	10.91	0.737	-10.7%
565	17	18.85	11.02	0.055	-29.5%
610	6	5.08	2.72	0.764	12.9%
620	4	3.27	1.60	0.992	0.3%
630	3	10.66	2.17	0.191	33.1%
640	7	10.40	9.91	No ITE Rate	No ITE Rate
720	16	10.55	6.55	0.474	18.4%
812	9	14.40	21.83	0.083	-55.2%
814	9	95.59	39.30	No ITE Rate	No ITE Rate
816	5	36.53	18.92	0.136	-31.3%
820	7	13.59	14.60	No ITE Rate	No ITE Rate
841	21	10.22	4.87	<0.001	-51.7%
842	5	7.89	5.67	No ITE Rate	No ITE Rate
843	7	33.74	17.03	No ITE Rate	No ITE Rate
852	3	61.16	33.48	No ITE Rate	No ITE Rate
853	26	215.11	63.44	No ITE Rate	No ITE Rate
881	4	69.18	52.33	No ITE Rate	No ITE Rate
890	7	6.98	3.53	0.056	-42.7%
912	16	28.31	14.10	0.571	-8.5%
932	32	20.95	17.69	No ITE Rate	No ITE Rate
933	4	66.89	48.43	No ITE Rate	No ITE Rate
934	26	45.50	22.15	No ITE Rate	No ITE Rate
935	5	34.38	13.03	No ITE Rate	No ITE Rate
943	37	11.10	6.30	No ITE Rate	No ITE Rate
944	7	365.00	148.33	No ITE Rate	No ITE Rate
945	11	240.84	58.99	No ITE Rate	No ITE Rate
946	3	280.85	147.70	No ITE Rate	No ITE Rate

*Comparison of average rate to corresponding ITE trip generation rate. P-Value obtained from weighted T-test.

Table 4. Trip Generation Rates per Employee (Weekday A.M. Peak Hour of Adjacent Street Traffic)

ITE LUC	Sample Size	Average Rate	Standard Deviation	P-Value*	% Diff.*
110	30	0.50	0.44	0.604	13.6%
140	17	0.23	0.18	0.066	-42.5%
150	9	0.64	0.44	0.555	25.5%
151	6	1.79	1.05	No ITE Rate	No ITE Rate
170	14	0.68	0.30	0.507	-10.5%
254	4	0.40	0.19	No ITE Rate	No ITE Rate
310	6	1.43	1.22	0.232	107.2%
540	7	1.41	1.00	0.597	-14.0%
565	17	5.39	3.50	0.655	11.1%
610	6	0.53	0.17	0.050	71.0%
620	4	0.34	0.10	No ITE Rate	No ITE Rate
630	3	1.12	0.14	No ITE Rate	No ITE Rate
640	7	1.52	1.42	No ITE Rate	No ITE Rate
720	16	1.14	0.99	0.071	115.1%
812	9	1.50	1.75	0.200	-38.0%
814	9	3.04	2.12	No ITE Rate	No ITE Rate
816	5	4.32	2.33	0.005	282.3%
820	6	0.42	0.54	No ITE Rate	No ITE Rate
841	21	0.86	0.52	No ITE Rate	No ITE Rate
842	5	0.73	0.51	No ITE Rate	No ITE Rate
843	7	1.92	1.56	No ITE Rate	No ITE Rate
852	3	3.74	3.97	No ITE Rate	No ITE Rate
853	26	16.14	5.84	No ITE Rate	No ITE Rate
881	4	2.51	2.57	No ITE Rate	No ITE Rate
890	7	0.56	0.30	0.674	16.7%
912	16	2.12	1.00	0.114	-19.4%
932	9	2.00	4.35	No ITE Rate	No ITE Rate
933	0	0	0.00	No ITE Rate	No ITE Rate
934	9	3.17	1.59	No ITE Rate	No ITE Rate
935	3	2.33	1.31	No ITE Rate	No ITE Rate
943	37	1.15	0.79	No ITE Rate	No ITE Rate
944	7	22.42	8.38	No ITE Rate	No ITE Rate
945	11	15.64	4.77	No ITE Rate	No ITE Rate
946	3	20.93	5.17	No ITE Rate	No ITE Rate
*Comparison of average rate to corresponding ITE trip generation rate. P-Value obtained from weighted T-test.					

Table 5. Trip Generation Rates per Employee (Weekday P.M. Peak Hour of Adjacent Street Traffic)

ITE LUC	Sample Size	Average Rate	Standard Deviation	P-Value*	% Diff.*
110	30	0.46	0.34	0.661	9.5%
140	17	0.23	0.16	0.095	-36.1%
150	9	0.63	0.40	0.839	6.8%
151	6	2.15	1.36	No ITE Rate	No ITE Rate
170	14	0.70	0.27	0.587	-7.9%
254	4	0.49	0.27	No ITE Rate	No ITE Rate
310	6	1.60	2.12	0.457	100.0%
540	7	1.32	1.11	0.884	-5.0%
565	17	2.34	2.08	0.001	-50.5%
610	6	0.41	0.17	0.308	41.4%
620	4	0.30	0.11	<0.001	-68.8%
630	3	0.99	0.45	No ITE Rate	No ITE Rate
640	7	1.05	1.12	No ITE Rate	No ITE Rate
720	16	0.87	0.57	0.325	-17.9%
812	9	1.35	2.00	0.084	-51.3%
814	9	10.48	5.54	No ITE Rate	No ITE Rate
816	5	3.69	2.37	0.230	-26.9%
820	7	1.36	1.40	No ITE Rate	No ITE Rate
841	21	1.04	0.80	No ITE Rate	No ITE Rate
842	5	0.91	0.80	No ITE Rate	No ITE Rate
843	7	3.21	1.75	No ITE Rate	No ITE Rate
852	3	7.14	8.36	No ITE Rate	No ITE Rate
853	26	17.07	5.65	No ITE Rate	No ITE Rate
881	4	7.30	4.67	No ITE Rate	No ITE Rate
890	7	1.05	0.94	0.932	-4.5%
912	16	2.85	1.77	<0.001	-47.4%
932	32	1.97	1.55	No ITE Rate	No ITE Rate
933	4	4.36	5.27	No ITE Rate	No ITE Rate
934	26	3.16	1.74	No ITE Rate	No ITE Rate
935	5	2.96	1.79	No ITE Rate	No ITE Rate
943	37	1.32	0.99	No ITE Rate	No ITE Rate
944	7	27.00	9.42	No ITE Rate	No ITE Rate
945	11	21.22	6.42	No ITE Rate	No ITE Rate
946	3	20.74	17.12	No ITE Rate	No ITE Rate
*Comparison of average rate to corresponding ITE trip generation rate. P-Value obtained from weighted T-test.					

Table 6. Trip Generation Rates per Employee (Weekday A.M. Peak Hour of Generator)

ITE LUC	Sample Size	Average Rate	Standard Deviation	P-Value*	% Diff.*
110	30	0.76	0.52	0.043	58.3%
140	17	0.39	0.26	1.000	0.0%
150	9	0.74	0.47	0.420	34.5%
151	6	3.15	1.80	No ITE Rate	No ITE Rate
170	14	0.74	0.49	No ITE Rate	No ITE Rate
254	4	0.51	0.32	No ITE Rate	No ITE Rate
310	6	2.25	4.00	0.471	184.8%
540	7	1.66	1.25	0.868	-5.1%
565	17	5.46	3.45	0.750	7.5%
610	6	0.55	0.20	0.126	61.8%
620	4	0.42	0.21	0.210	61.5%
630	3	1.27	0.38	0.052	56.8%
640	7	1.83	1.49	No ITE Rate	No ITE Rate
720	16	1.71	1.40	0.057	113.8%
812	9	2.08	2.71	0.095	-47.2%
814	9	8.32	2.64	No ITE Rate	No ITE Rate
816	5	5.37	1.64	0.959	0.8%
820	7	1.28	1.42	No ITE Rate	No ITE Rate
841	21	1.20	0.66	0.017	79.1%
842	5	1.35	0.91	No ITE Rate	No ITE Rate
843	7	3.46	1.36	No ITE Rate	No ITE Rate
852	3	4.56	4.69	No ITE Rate	No ITE Rate
853	26	17.03	5.17	No ITE Rate	No ITE Rate
881	4	6.30	4.59	No ITE Rate	No ITE Rate
890	7	1.04	0.52	0.877	-4.6%
912	16	3.35	1.63	0.098	35.1%
932	9	2.93	4.29	No ITE Rate	No ITE Rate
933	4	8.39	4.45	No ITE Rate	No ITE Rate
934	26	4.34	2.57	No ITE Rate	No ITE Rate
935	5	4.30	1.84	No ITE Rate	No ITE Rate
943	37	1.68	1.07	No ITE Rate	No ITE Rate
944	7	25.66	9.06	No ITE Rate	No ITE Rate
945	11	17.00	4.41	No ITE Rate	No ITE Rate
946	3	21.27	6.15	No ITE Rate	No ITE Rate
*Comparison of average rate to corresponding ITE trip generation rate. P-Value obtained from weighted T-test.					

Table 7. Trip Generation Rates per Employee (Weekday P.M. Peak Hour of Generator)

ITE LUC	Sample Size	Average Rate	Standard Deviation	P-Value*	% Diff.*
110	30	0.71	0.48	0.120	39.2%
140	17	0.48	0.16	0.332	20.0%
150	9	0.68	0.39	0.609	17.2%
151	6	3.08	1.32	No ITE Rate	No ITE Rate
170	14	0.75	0.50	No ITE Rate	No ITE Rate
254	4	0.60	0.31	0.763	9.1%
310	6	2.48	4.08	0.444	175.6%
540	7	1.68	1.33	0.742	12.8%
565	17	4.08	2.26	0.182	-20.3%
610	6	0.44	0.22	0.842	7.3%
620	4	0.43	0.21	0.760	-8.5%
630	3	1.16	0.40	0.234	34.9%
640	7	1.85	1.68	No ITE Rate	No ITE Rate
720	16	1.47	1.00	0.143	51.5%
812	9	2.04	2.93	0.137	-46.7%
814	9	12.65	5.28	No ITE Rate	No ITE Rate
816	5	4.53	1.91	0.323	-16.6%
820	7	1.54	1.63	No ITE Rate	No ITE Rate
841	21	1.41	0.91	0.141	46.9%
842	5	1.22	1.01	No ITE Rate	No ITE Rate
843	7	4.33	2.45	No ITE Rate	No ITE Rate
852	3	7.19	8.31	No ITE Rate	No ITE Rate
853	26	19.66	5.46	No ITE Rate	No ITE Rate
881	4	7.82	4.70	No ITE Rate	No ITE Rate
890	7	1.22	0.92	0.930	-3.9%
912	16	3.76	1.87	0.114	-20.2%
932	32	3.68	3.18	No ITE Rate	No ITE Rate
933	4	11.45	3.13	No ITE Rate	No ITE Rate
934	26	5.70	2.94	No ITE Rate	No ITE Rate
935	5	5.48	1.67	No ITE Rate	No ITE Rate
943	37	1.75	1.07	No ITE Rate	No ITE Rate
944	7	36.32	13.47	No ITE Rate	No ITE Rate
945	11	22.02	5.93	No ITE Rate	No ITE Rate
946	3	25.27	14.01	No ITE Rate	No ITE Rate
*Comparison of average rate to corresponding ITE trip generation rate. P-Value obtained from weighted T-test.					

Table 8. Trip Generation Rates per 1,000 Sq. Feet Gross Floor Area (Weekday Daily)

ITE LUC	Sample Size	Average Rate	Standard Deviation	P-Value*	% Diff.*
110	30	3.58	5.17	0.046	-48.6%
140	17	4.64	4.06	0.534	21.5%
150	9	2.44	4.75	0.687	-31.5%
151	6	0.69	0.53	0.001	-72.4%
170	14	13.24	14.20	No ITE Rate	No ITE Rate
254	4	4.20	2.96	No ITE Rate	No ITE Rate
310	6	9.72	3.96	No ITE Rate	No ITE Rate
540	7	17.08	20.43	0.259	-37.9%
565	17	63.36	65.66	0.555	-14.4%
610	6	42.21	69.38	0.529	219.3%
620	4	5.45	5.65	0.592	-28.3%
630	3	38.17	31.22	0.760	21.3%
640	7	21.22	16.30	No ITE Rate	No ITE Rate
720	16	26.45	16.29	0.079	-26.8%
812	9	8.73	11.90	<0.001	-80.7%
814	9	61.30	29.82	0.792	-4.3%
816	5	9.14	4.68	<0.001	-82.2%
820	7	24.01	86.02	0.629	-43.8%
841	21	29.93	23.59	0.790	-7.3%
842	5	7.26	30.40	No ITE Rate	No ITE Rate
843	7	50.58	26.52	0.306	-18.3%
852	3	126.52	78.79	No ITE Rate	No ITE Rate
853	26	491.81	251.82	<0.001	-41.8%
881	4	139.35	51.44	0.235	44.2%
890	7	3.70	4.55	0.618	-26.9%
912	16	65.80	50.92	<0.001	-55.6%
932	32	90.55	94.01	0.120	-28.8%
933	4	297.80	271.65	No ITE Rate	No ITE Rate
934	26	427.90	270.31	0.256	-13.8%
935	5	459.20	300.74	No ITE Rate	No ITE Rate
943	37	18.23	16.53	No ITE Rate	No ITE Rate
944	7	1386.20	2217.15	No ITE Rate	No ITE Rate
945	11	613.58	397.26	No ITE Rate	No ITE Rate
946	3	522.92	234.89	No ITE Rate	No ITE Rate

*Comparison of average rate to corresponding ITE trip generation rate. P-Value obtained from weighted T-test.

Table 9. Trip Generation Rates per 1,000 Sq. Feet Gross Floor Area (Weekday A.M. Peak Hour of Adjacent Street Traffic)

ITE LUC	Sample Size	Average Rate	Standard Deviation	P-Value*	% Diff.*
110	30	0.47	0.77	0.072	-48.9%
140	17	0.43	0.56	0.109	-41.1%
150	9	0.32	0.51	0.946	6.7%
151	6	0.09	0.04	0.043	-35.7%
170	14	2.18	2.34	0.129	172.5%
254	4	0.39	0.16	No ITE Rate	No ITE Rate
310	6	0.67	0.35	No ITE Rate	No ITE Rate
540	7	1.73	1.47	0.080	-42.1%
565	17	18.11	23.84	0.372	48.7%
610	6	4.35	5.35	0.351	357.9%
620	4	0.56	0.39	0.970	1.8%
630	3	4.01	3.51	No ITE Rate	No ITE Rate
640	7	3.09	2.29	0.367	-24.3%
720	16	2.85	2.22	0.522	19.2%
812	9	0.91	1.33	0.017	-65.0%
814	9	1.95	1.36	0.004	-48.8%
816	5	1.08	0.40	1.000	0.0%
820	6	0.70	1.88	0.781	-27.1%
841	21	2.52	2.64	0.548	31.3%
842	5	0.67	2.49	No ITE Rate	No ITE Rate
843	7	2.88	2.26	0.467	30.3%
852	3	7.73	3.71	0.011	-75.1%
853	26	36.91	17.83	0.288	-9.8%
881	4	5.05	2.13	0.272	46.4%
890	7	0.30	0.45	0.626	76.5%
912	16	4.92	3.54	<0.001	-59.3%
932	9	15.74	25.34	0.642	45.6%
933	0	0.00	0.00	0.000	0.0%
934	9	35.83	25.64	0.346	-21.1%
935	3	37.47	18.10	No ITE Rate	No ITE Rate
943	37	1.88	1.98	No ITE Rate	No ITE Rate
944	7	85.13	128.47	No ITE Rate	No ITE Rate
945	11	39.84	26.23	0.001	-51.5%
946	3	38.96	13.87	No ITE Rate	No ITE Rate
*Comparison of average rate to corresponding ITE trip generation rate. P-Value obtained from weighted T-test.					

Table 10. Trip Generation Rates per 1,000 Sq. Feet Gross Floor Area (Weekday P.M. Peak Hour of Adjacent Street Traffic)

ITE LUC	Sample Size	Average Rate	Standard Deviation	P-Value*	% Diff.*
110	30	0.43	0.67	0.015	-55.7%
140	17	0.43	0.53	0.093	-41.1%
150	9	0.32	0.54	1.000	0.0%
151	6	0.11	0.06	0.002	-57.7%
170	14	2.25	2.10	0.074	196.1%
254	4	0.49	0.25	No ITE Rate	No ITE Rate
310	6	0.75	0.36	No ITE Rate	No ITE Rate
540	7	1.62	1.84	0.267	-36.2%
565	17	7.84	6.48	0.021	-36.5%
610	6	3.39	5.04	0.465	264.5%
620	4	0.50	0.38	0.398	-32.4%
630	3	3.52	2.34	No ITE Rate	No ITE Rate
640	7	2.14	1.69	0.014	-54.7%
720	16	2.16	1.72	0.020	-39.5%
812	9	0.82	1.39	<0.001	-81.7%
814	9	6.72	3.87	0.941	-1.5%
816	5	0.93	0.69	<0.001	-80.8%
820	7	2.40	7.85	0.709	-35.3%
841	21	3.05	2.88	0.692	16.4%
842	5	0.84	3.95	0.522	-66.9%
843	7	4.81	2.50	0.266	-19.6%
852	3	14.76	7.25	0.055	-57.3%
853	26	39.02	19.94	0.008	-23.4%
881	4	14.71	4.80	0.172	48.4%
890	7	0.56	0.81	0.819	24.4%
912	16	6.61	5.59	<0.001	-72.8%
932	32	8.50	8.66	0.526	-13.7%
933	4	19.39	27.69	0.662	-25.9%
934	26	29.64	14.56	0.350	-9.2%
935	5	39.43	31.28	0.732	-12.4%
943	37	2.16	2.04	No ITE Rate	No ITE Rate
944	7	102.55	162.13	No ITE Rate	No ITE Rate
945	11	54.05	40.62	0.014	-44.5%
946	3	38.60	25.13	No ITE Rate	No ITE Rate
*Comparison of average rate to corresponding ITE trip generation rate. P-Value obtained from weighted T-test.					

Table 11. Trip Generation Rates per 1,000 Sq. Feet Gross Floor Area (Weekday A.M. Peak Hour of Generator)

ITE LUC	Sample Size	Average Rate	Standard Deviation	P-Value*	% Diff.*
110	30	0.71	0.99	0.342	-29.7%
140	17	0.73	0.67	0.783	-7.6%
150	9	0.37	0.60	0.887	-11.9%
151	6	0.15	0.14	0.094	-46.4%
170	14	2.37	2.30	No ITE Rate	No ITE Rate
254	4	0.51	0.31	No ITE Rate	No ITE Rate
310	6	1.05	0.47	No ITE Rate	No ITE Rate
540	7	2.05	2.39	0.327	-33.7%
565	17	18.36	23.70	0.454	36.6%
610	6	4.52	6.07	0.386	370.8%
620	4	0.69	0.66	0.844	15.0%
630	3	4.55	3.13	No ITE Rate	No ITE Rate
640	7	3.72	2.27	No ITE Rate	No ITE Rate
720	16	4.28	3.02	0.426	22.3%
812	9	1.26	1.49	0.002	-69.7%
814	9	5.34	1.81	0.036	40.2%
816	5	1.35	0.66	0.001	-72.5%
820	7	2.26	7.80	No ITE Rate	No ITE Rate
841	21	3.51	3.03	0.266	58.1%
842	5	1.24	4.22	No ITE Rate	No ITE Rate
843	7	5.18	1.97	0.347	17.5%
852	3	9.42	4.22	0.015	-71.1%
853	26	38.93	17.40	0.286	-9.2%
881	4	12.69	7.12	0.357	51.8%
890	7	0.55	0.59	0.671	37.5%
912	16	7.78	6.02	<0.001	-55.7%
932	9	23.14	26.82	<0.001	-82.6%
933	4	37.33	17.92	0.063	-41.2%
934	26	40.74	26.46	0.034	-24.0%
935	5	57.34	46.29	No ITE Rate	No ITE Rate
943	37	2.76	2.45	No ITE Rate	No ITE Rate
944	7	97.44	147.19	No ITE Rate	No ITE Rate
945	11	43.32	27.65	0.006	-44.5%
946	3	39.61	14.44	No ITE Rate	No ITE Rate
*Comparison of average rate to corresponding ITE trip generation rate. P-Value obtained from weighted T-test.					

Table 12. Trip Generation Rates per 1,000 Sq. Feet Gross Floor Area (Weekday P.M. Peak Hour of Generator)

ITE LUC	Sample Size	Average Rate	Standard Deviation	P-Value*	% Diff.*
110	30	0.66	0.87	0.134	-38.9%
140	17	0.91	0.98	0.613	21.3%
150	9	0.34	0.56	0.738	-24.4%
151	6	0.15	0.17	0.130	-48.3%
170	14	2.40	2.07	No ITE Rate	No ITE Rate
254	4	0.60	0.26	No ITE Rate	No ITE Rate
310	6	1.16	0.51	No ITE Rate	No ITE Rate
540	7	2.06	2.49	0.590	-22.0%
565	17	13.72	13.98	0.994	-0.2%
610	6	3.66	5.84	0.520	215.5%
620	4	0.71	0.58	0.477	-29.7%
630	3	4.13	2.93	No ITE Rate	No ITE Rate
640	7	3.77	2.73	No ITE Rate	No ITE Rate
720	16	3.67	2.66	0.485	-14.1%
812	9	1.24	1.61	<0.001	-77.7%
814	9	8.11	4.04	0.432	16.0%
816	5	1.14	0.59	<0.001	-75.9%
820	7	2.72	10.10	No ITE Rate	No ITE Rate
841	21	4.11	3.18	0.280	46.8%
842	5	1.12	4.00	No ITE Rate	No ITE Rate
843	7	6.50	3.37	0.964	0.9%
852	3	14.87	6.94	0.044	-58.9%
853	26	44.94	20.41	<0.001	-28.2%
881	4	15.75	8.09	0.275	62.0%
890	7	0.65	0.80	0.800	22.6%
912	16	8.74	7.06	<0.001	-67.3%
932	32	15.88	13.35	0.428	-14.1%
933	4	50.95	18.55	0.887	-2.8%
934	26	53.61	28.58	0.318	13.3%
935	5	73.14	52.33	No ITE Rate	No ITE Rate
943	37	2.88	2.79	No ITE Rate	No ITE Rate
944	7	137.90	226.04	No ITE Rate	No ITE Rate
945	11	56.09	40.06	0.017	-42.3%
946	3	47.05	21.76	No ITE Rate	No ITE Rate

*Comparison of average rate to corresponding ITE trip generation rate. P-Value obtained from weighted T-test.

Table 13. Trip Generation Rates per Special Independent Variable (Weekday Daily)

ITE LUC	Sample Size	Average Rate	Standard Deviation	P-Value*	% Diff.*
110	30	16.66	21.15	<0.001	-67.8%
140	17	27.74	24.84	0.263	-28.7%
150	9	20.16	84.66	0.453	-64.8%
151	6	11.44	7.40	0.001	-67.7%
310	6	3.07	1.12	<0.001	-62.4%
540	7	1.07	0.85	0.723	-13.0%
816	5	94.17	97.92	0.001	-82.7%
853	26	220.69	132.02	<0.001	-59.3%
912	16	123.30	76.70	0.448	-11.5%
944	7	179.41	134.88	0.847	6.4%
945	11	161.32	87.89	0.959	-0.9%
946	3	260.79	113.81	0.249	70.6%
*Comparison of average rate to corresponding ITE trip generation rate. P-Value obtained from weighted T-test.					
Special independent variables for specific land uses as follows: Acres (110, 140, 150, 151, 816), Rooms (310), Students (540), Fueling Positions (853, 944, 945, 946), and Drive-Through Lanes (912)					

Table 14. Trip Generation Rates per Special Independent Variable (Weekday A.M. Peak Hour of Adjacent Street Traffic)

ITE LUC	Sample Size	Average Rate	Standard Deviation	P-Value*	% Diff.*
110	30	2.15	3.35	<0.001	-249.3%
140	17	2.52	2.82	<0.001	-195.2%
150	9	2.64	8.55	0.158	-279.9%
151	6	1.39	0.92	0.035	-85.6%
310	6	0.21	0.08	<0.001	-152.4%
540	7	0.11	0.10	0.844	-9.1%
816	5	11.13	11.31	0.953	-3.7%
853	26	16.56	9.99	0.996	-0.1%
912	16	9.22	5.93	0.965	-0.8%
944	7	11.02	7.90	0.730	-10.3%
945	11	10.48	5.93	0.868	3.1%
946	3	19.43	9.67	0.314	39.1%
*Comparison of average rate to corresponding ITE trip generation rate. P-Value obtained from weighted T-test.					
Special independent variables for specific land uses as follows: Acres (110, 140, 150, 151, 816), Rooms (310), Students (540), Fueling Positions (853, 944, 945, 946), and Drive-Through Lanes (912)					

Table 15. Trip Generation Rates per Special Independent Variable (Weekday P.M. Peak Hour of Adjacent Street Traffic)

ITE LUC	Sample Size	Average Rate	Standard Deviation	P-Value*	% Diff.*
110	30	1.99	3.09	<0.001	-264.8%
140	17	2.57	3.76	0.001	-224.9%
150	9	2.60	9.21	0.268	-234.2%
151	6	1.67	1.07	0.011	-113.8%
310	6	0.24	0.17	0.005	-150.0%
540	7	0.11	0.07	0.786	-9.1%
816	5	9.50	12.07	0.004	-445.2%
853	26	17.51	10.47	0.507	-8.9%
912	16	12.39	7.12	<0.001	-168.3%
944	7	13.28	8.97	0.875	-4.4%
945	11	14.21	7.16	0.763	4.9%
946	3	19.25	9.67	0.444	28.0%
*Comparison of average rate to corresponding ITE trip generation rate. P-Value obtained from weighted T-test.					
Special independent variables for specific land uses as follows: Acres (110, 140, 150, 151, 816), Rooms (310), Students (540), Fueling Positions (853, 944, 945, 946), and Drive-Through Lanes (912)					

Table 16. Trip Generation Rates per Special Independent Variable (Weekday A.M. Peak Hour of Generator)

ITE LUC	Sample Size	Average Rate	Standard Deviation	P-Value*	% Diff.*
110	30	3.28	4.38	0.001	-142.7%
140	17	4.34	5.13	0.023	-114.3%
150	9	3.02	9.17	0.326	-176.2%
151	6	2.45	2.03	0.174	-59.2%
310	6	0.34	0.15	0.043	-52.9%
540	7	0.13	0.11	0.869	7.7%
816	5	13.84	12.59	0.005	-294.7%
853	26	17.47	9.80	0.841	2.5%
912	16	14.57	10.07	0.019	-48.5%
944	7	12.62	8.87	0.991	0.3%
945	11	11.39	5.57	0.646	7.3%
946	3	19.75	9.61	0.374	32.6%
*Comparison of average rate to corresponding ITE trip generation rate. P-Value obtained from weighted T-test.					
Special independent variables for specific land uses as follows: Acres (110, 140, 150, 151, 816), Rooms (310), Students (540), Fueling Positions (853, 944, 945, 946), and Drive-Through Lanes (912)					

Table 17. Trip Generation Rates per Special Independent Variable (Weekday P.M. Peak Hour of Generator)

ITE LUC	Sample Size	Average Rate	Standard Deviation	P-Value*	% Diff.*
110	30	3.06	3.66	<0.001	-186.6%
140	17	5.43	5.87	0.115	-69.6%
150	9	2.78	9.26	0.277	-215.5%
151	6	2.39	2.23	0.196	-62.8%
310	6	0.37	0.16	0.016	-64.9%
540	7	0.13	0.11	0.867	7.7%
816	5	11.67	12.42	0.003	-376.8%
853	26	20.17	10.39	0.935	0.9%
912	16	16.37	9.14	<0.001	-77.5%
944	7	17.85	12.76	0.682	12.3%
945	11	14.75	7.03	0.606	8.0%
946	3	23.47	10.15	0.273	38.1%
*Comparison of average rate to corresponding ITE trip generation rate. P-Value obtained from weighted T-test.					
Special independent variables for specific land uses as follows: Acres (110, 140, 150, 151, 816), Rooms (310), Students (540), Fueling Positions (853, 944, 945, 946), and Drive-Through Lanes (912)					